2-24-2016 12:00 AM

Investigation And Modeling of Dip-Coating Process for Dispersions

Mahyar Javidi Soufiani
The University of Western Ontario

Supervisor
Andrew N. Hrymak
The University of Western Ontario

Abstract

Dip coating of liquid film deposition on cylindrical substrates is studied using mathematical modeling, numerical simulation and experimental investigation. A mathematical model based on the Landau-Levich approach for dip coating has been developed using the Ellis constitutive equation, for cylindrical geometries, to analyze the effects on the coating thickness of the substrate radius and hydrodynamic behavior for a non-Newtonian fluid. The influence of the viscosity at low shear rates near the surface of the withdrawal film is included in the Ellis model and coating thickness results for Ellis, power law and Newtonian models are compared with experimental data. Good agreement for the measured and predicted coating thickness was obtained with the Ellis model.

Dip coating process is numerically simulated to understand the effects of the proximity of the coating bath wall to the substrate. The free surface position is determined by the volume of fluid technique applying Carreau, power law and Newtonian constitutive models in a three dimensional system, including density, viscosity and surface tension effects. Numerical calculations have been performed in an open source CFD software package of OpenFOAM. Numerical outcomes are validated with experimental data over a range of withdrawal velocities up to $6 \, m/s$, capillary range $Ca \leq 60$ and a dimensionless range of distance, $4 \leq R/r \leq 60$ for bath radius to the substrate radius being withdrawn.

Finally, dip coating of dispersions is examined with particle distribution in the free-surface concentrated suspensions studied by developing a numerical algorithm in a computational fluid dynamic platform based on the particle diffusion-flux model. The numerical predictions are for finite length cylinder being pulled out of a concentrated suspension bath in the unsteady condition. The initial rigid particle volume fraction of 0.1-0.4 and the withdrawal velocity varies in the range of 0.05-0.15 m/s and capillary number range of $Ca \leq 1$. Simulation results are compared against experimental data with good agreement in the predicted coating thickness.

Keywords

Co-Authorship Statement

In the development of this work, three papers are written and co-authored, the extent of the collaboration of the co-authors is stated below.

Chapter 2

Abstract title	Withdrawal of a cylinder from an Ellis fluid
Current Status	Published as a ISCST Conference Abstract

Mahyar Javidi: Theoretical calculations, literature review, writing and corrections of several drafts and final paper

Michael Pope: Experimental design and laboratory work as part of a senior research thesis at McMaster University.

Andrew N. Hrymak: Technical and theoretical advisor and corrections of several drafts and final paper.

Chapter 3

Paper title	Numerical simulation of the dip-coating process with wall effects on the coating film thickness
Current Status	Published in Journal of Coatings Technology & Research; Sep 2015, Vol. 12 Issue 5, p 843

Mahyar Javidi: Experimental investigations, Theoretical study and computational simulations, applying the new parameter in dip coating system and writing paper

Andrew N. Hrymak: Technical and theoretical advisor and corrections of several drafts and final paper.

Chapter 4

Paper title	Simulation of concentrated suspensions in thin film development
Current Status	Submitted to Canadian Journal of Chemical Engineering

Mahyar Javidi: Implementing the new simulation algorithm, simulations, experimental procedure, writing and corrections of several drafts and final paper

Andrew N. Hrymak: Technical and theoretical advisor and corrections of several drafts and final paper.

Acknowledgments

I would like to express my sincere gratitude to my supervisor Professor Andrew Hrymak for his continuous support, advice, patience, and motivation. Thanks for giving me this enriching opportunity and being a stunning role model in both academic and real life.

I also want to thank my PhD advisory committee, Dr. Ajay Ray and Dr. John de Bruyn and Dr. Jesse Zhu for all the guidance and good advice and thanks to all the people/ individuals who have contributed to my professional development.

Thanks to my friends in Dr. Hrymak's research group and Ms. Fate Hashemi, Ms. Mary Jane Walzak at Western surface science and Dr. Kamran Siddiqui for their great help.

Thanks to Mohammad Norouzi for his support, understanding, and caring. It has been great to have someone beside me who shares my passion for chasing dreams.

Thanks with love to my family: My mother, my father, and my sister. You are my strength, my biggest support and motivation.

Table of Contents

List of Tables

List of Figures

Nomenclature

a_c = capillary length

a_c = capillary length

a = particle radius

B_c = constant value

B_η = constant value

C_m = meniscus curvature

Ca = capillary number

C_α = compression factor

Co = Courant number

C_V^P = curvature in the vertical direction

C_R^P = curvature in radial direction

D_1 = dimensionless number

D_2 = dimensionless number

F_b = body force

g = gravitational acceleration

G = radius parameter, $M_0 N_{GO}$

h = film thickness at any point

h_0 = film thickness in constant thickness region

K_1 = dimensionless number

k = curvature of the interface

L = dimensionless coordinates of relative coated radius

m = radius of coated fibre at any point

m_0 = radius of coated fibre in constant film thickness region

M = dimensionless coated radius, (mR^{-1})

M_0 = dimensionless coated radius, $(m_0 R^{-1})$

M_c = particle interaction rate flux

M_η = viscosity varying flux

n_p = power law index

n_c = parameters of Carreau equation

N_{GO} = Goucher number, $(R(\rho g)^{0.5}(2\sigma)^{-0.5})$

P = pressure field

P_0 = atmospheric pressure

P_{rgh} = piezometric pressure

S = power law constant

T_1 = dimensionless coordinate

T_2 = dimensionless coordinate

t = time

u = velocity field

$u_{r\alpha}$ = compression velocity

U = withdrawal velocity

V = settlement velocity of spherical particles

Q_1 = volume flow rate of liquid in region 1

Q_2 = volume flow rate of liquid in region 2

Greek Symbols

α_1 = liquid volume fraction

α = index of Ellis constitutive equation

β = curvature parameter

β_1 = damping factor

β_2 = damping factor

σ = surface tension at gas-liquid interface

λ = small dimensionless number

λ_c = parameter of Carreau equation

τ = stress tensor

$\tau_{1/2}$ = shear stress at $(\mu_0/2)$

μ_0 = zero shear viscosity

μ_∞ = viscosity at the shear rate of infinity

η_r = relative viscosity

η_s = viscosity of suspending medium

φ = volume fraction of particles in flow

φ_m = volume fraction at which η_r tends to infinity for hard spheres

$\dot{\gamma}$ = shear rate

μ = viscosity

ρ = density

ρ_p =density of particles

θ = contact angle

Chapter 1

1 « Introduction»

Dip coating is examined through analytical, numerical and experimental approaches for dispersions. Steady-state (continuous) and unsteady-state (discrete) coating of cylindrical structures, which exhibit significant curvature effects of the coating substrate, are explored. The main goal is to be able to predict the coating film thickness as a function of capillary number and liquid-solid dispersion loadings.

1.1 « Background and Motivation»

1.1.1 « Definition and Applications »

Vertical withdrawal of a substrate from a Newtonian or non-Newtonian reservoir of liquid, known as dip coating or free coating, is an inexpensive method of depositing a thin, even layer of material in the liquid state onto a substrate (Kistler and Schweizer, 1997). Liquid deposition processes are very versatile methods to produce sub-micron homogeneous coatings through spreading of a solution onto a substrate and evaporation of the volatile compounds or other methods of vitrification.

Dip coating is an alternative to dry deposition techniques, such as physical vapor deposition (PVD) chemical vapor deposition (CVD) or plasma-enhanced CVD (PECVD). PVD, uses physical processes (such as heating or sputtering) to produce a vapor of the coating material, which is deposited on the object. CVD is used in the semiconductor industry to produce films. In typical CVD, the wafer (substrate) is exposed to one or more volatile precursors, which react and/or decompose on the substrate surface to produce the desired coating film.

Free withdrawal or dip coating, is the best-known example of a self-metering coating flow, in which the coating thickness is a dependent variable (Ruschak, 1985).

There are similar coating methods to generate a thin film by withdrawing a substrate such as a roller or fiber from a bath of liquid or forcing a bubble into a capillary tube which is initially full of liquid. Various geometries for plate coating, roll coating, fiber coating and coating of the inside of a tube (or a Hele-Shaw cell) are shown in Figure 1-1 and in each case, the relative motion between the solid and the liquid implies the deposition of a thin liquid layer of a liquid on the solid. Roll coating and fiber withdrawal were the topic of early investigation. Cylindrical geometry in tubes such as emptying of a capillary tube was studied as well as a closely related problem leading to similar results is the drainage of a Hele-Shaw cell.
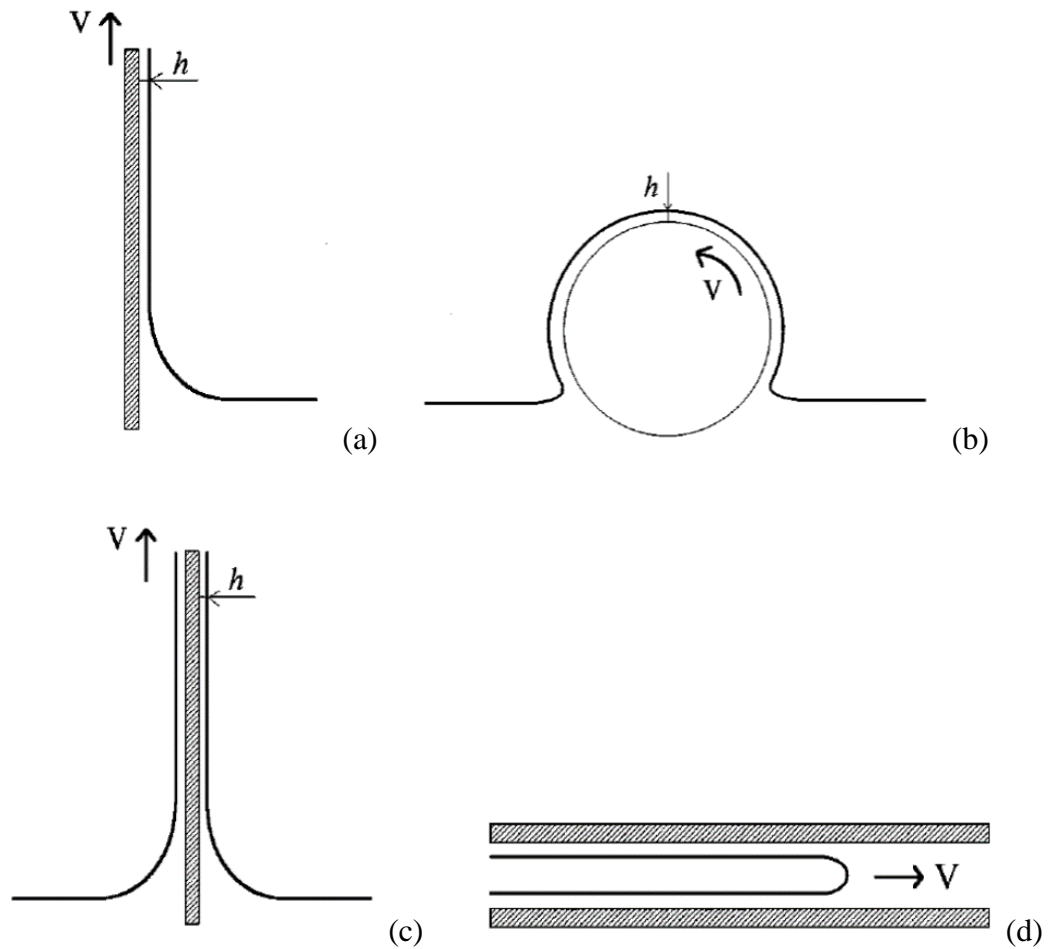
Figure 1-1: Various geometries applied in fluid coating. (*a*) Plate coating; (*b*) roll coating; (*c*) fiber coating; (*d*) coating of the inside of a tube (or a Hele-Shaw cell) (Quere, 1999)

One of the advantages of this process is the ability to coat irregularly shaped substrates (Peralta et al., 2014). Dipping and withdrawal are not only used to apply the coating, but also to control the final microstructure of the coated film in a hydrodynamically driven colloidal assembly (Colosqui et al., 2013). An example of tailored coating is the production and enhancement of screen-printed multi-crystalline silicon solar cells by a dip coating process (Fahim et al., 2012). Dip coating has also been used in sol-gel derived mesoporous titania and silica coating (Soler-lllia et al., 2003), as well as selected value-added coatings such as RuO_2-SiO_2 nanocomposite optical absorber (Ceratti et al., 2015).

Furthermore, free coating is essential for the surface engineering of high quality products and it is one of the better developed methods to enhance and alter the physical and mechanical surface characteristics. For instance, the performance properties of optical fibers, including abrasion resistance and strength, are strongly influenced by adding a coated layer (Yang et al., 2008). A fiber-based polymer light-emitted diode (PLED) is fabricated using dip coating with the high luminance ($> 1000\ cd\ m^{-2}$) and low operating voltages ($< 10\ v$), is safely integrated into electronic textiles. This process allows for low cost mass production by roll-to-roll manufacturing (Kwon et al., 2015).

Therefore, it is useful to be able to predict the dynamics of dip coating, based on the fluid properties and operating conditions, to control the film thickness.

In recent years electro-active polymers have received attention because of their distinct potential as actuators and sensors, and the cylindrical shape may bring explicit advantages to actuator design (Yang et al., 2008; Watanabe et al., 2004). Therefore, cylindrical micro fabrication is of interest, particularly due to the advantages conferred by the geometry of substrate.

Unlike planar substrates, cylindrical substrates offer axisymmetric flexibility, complete surface area utilization, and radial symmetry. These properties offer opportunities such as catheter based electronics in the medical industry, fiber optic modulation for medical devices, or equipment for heat and mass transfer in gas–liquid systems to provide a large interfacial area (Grunig et al., 2010). The thickness of the liquid layer that remains on the surface of the substrate depends on the viscosity, surface tension of the coating fluid,

gravity and the speed of withdrawal. The complicating feature of dip coating problems is the strong role played by the free surface in controlling the coating dynamics, particularly in the region where the object leaves the surface of the coating fluid bath (Middleman, 1977).

1.1.2 « Analytical Estimations of Dip Coating »

An analysis of the problem of estimating the entrainment of a liquid film on a solid substrate, which is continuously withdrawn at a constant speed from a bath of liquid, has been studied with an approximate expression for the thickness of the deposited Newtonian film when the coating velocity is very small (Landau and Levich, 1942). This pioneering work, initiated theoretical and experimental study of the flow of entrained thin liquid film, through withdrawal of a flat sheet from a bath of liquid. Invoking the lubrication concept, they treated the rising film as nearly one-dimensional and the meniscus near the reservoir as static. Using the classical lubrication equations together with the hydrostatic differential equation, a matching condition is applied for the film entrainment and the static meniscus regions. For vertical withdrawal, the Landau-Levich approach provides an expression for the film thickness in terms of the key parameters and physical properties.

$$h_0 = c_1 \frac{(\mu U)^{2/3}}{\sigma^{1/6}} (\rho g)^{1/2} \qquad\qquad (1-1)$$

The dimensionless constant c_1 has been determined to be about 0.944 (Newtonian liquids) and where μ (Pa.s) and σ (N/m) are the liquid viscosity and surface tension respectively (Landau and Levich, 1942). In equation 1-1, h_0 is the coating thickness in meter, U (m/s) is the coating velocity, ρ (kg/m^3) defined as fluid density and gravitational acceleration is g (m/s^2). At about the same time, Deryagin (1943) derived equation 1-1 independently, and then the theory was extended to non-Newtonian liquids (Deryagin and Levi, 1964; Gutfinger and Tallmadge, 1965).

Ruschak (1976) and Wilson (1982) have since shown the equation 1-1 is an asymptotic solution to the film thickness in dip coating and valid as the capillary number, $Ca = \mu U/\sigma$, tends to zero. Experimental data compared with equation 1-1 confirmed the validity for capillary numbers less than 0.01 (Spiers et al., 1974).

Several studies have focused on coating at slow withdrawal speeds (Landau and Levich, 1942; Deryagin, 1943). The solid-liquid interface is responsible for the liquid entrainment and due to the assumption of the no-slip condition, the liquid near the solid must move at the same velocity as the solid substrate. At the same time, the motion of the solid provokes a deformation of the liquid-air interface and controls the deposited thin film. Thus, the capillary number, which is the ratio of viscous and surface tension forces is considered a key parameter.

Many have used the theory of Landau and Levich, although their equation is only applicable at very low capillary numbers, $Ca < 0.01$. Groenveld (1971) applied it to expand Jeffrey's (1930) classical drainage result to include the effects of surface tension. Ruschak (1976; 1985) extended it to explain the relationship between pre-metered and self-metered coating flows at low capillary number. He also compared the low capillary number theory with the data of Morey (1940) and found good agreement at capillary number less that 0.01 (Ruschak, 1976). Many applications of equation 1-1 have been seen for coating of advanced materials, which are normally applied at low Capillary number (Hurd and Brinker 1990, Park 1991).

In the low capillary number limit, a theoretical prediction of the coating thickness was derived using the Ellis constitutive model for a flat plate (Tallmadge, 1966). A model was developed with validation from an experimental study for coating a plate with a power-law fluid, with qualitative but not quantitative agreement (Gutfinger and Tallmadge, 1965). Models based on the Bingham, Ellis and power-law models were developed and compared with experiments for coating a plate by Spiers et al. (1975) and prediction of coating thickness with these models were in good agreement only for some of the of experimental data using different coating liquids.

To bridge the gap between the results at high and low capillary numbers, two-dimensional flow equations and additional parameters were investigated. Due to the limits of applicability of the Landau-Levich approximation, the effect of gravity in the film-entrainment region becomes important. White and Tallmadge (1965) were among the first to attempt the extension of equation 1-1 to higher capillary numbers. The effect of gravity in the film entrainment region has been successfully incorporated into the analysis of the equations of nearly rectilinear flow by Lee and Tallmadge (1975).

Moreover, whenever gravity or other high-order effects are included, Landau and Levich's procedure for matching curvature between regions breaks down (Ruschak, 1985). This was another difficulty in extending the analysis of Landau and Levich to higher capillary numbers which lies in matching the solution to the differential equation given the meniscus shape of the film-entrainment region and the static meniscus associated with the reservoir fluid. The equations defining the meniscus shape were solved by a more accurate numerical procedure (Talmadge, 1969) for the static meniscus to achieve better prediction of the coating layer.

Lee and Tallmadge (1974) solve the complete two dimensional equation with the finite difference method and explored the effect of inertia and bath dimensions for $Ca > 1$. Wilson (1982) used the method of matched asymptotic expansion to obtain a closed form solution for the film profile. Kheshgi et al. (1992) integrated a film profile equation, similar to one derived by Ruschak (1978) and Tekic and Jovanovic (1982), to obtain a first-order approximation of the film profile for a variety of situations geometrically similar to dip coating, and it was also shown that the bath configuration controlled the final film thickness.

Coating with non-Newtonian fluids for flat plates has been recently analytically approached by applying the generalized Newtonian methods without considering the surface tension in the thickness estimation (Peralta et al., 2014).

Development of dip coating theory for cylindrical substrates was getting more attention due to the axisymmetric flexibility and surface area utilization. It is worth noting that

when the radius of the cylinder is large compared to the capillary length $a_c = \sqrt{\sigma/\rho g}$, then the effect of the curvature of the cylinder is very weak and results in only small perturbations to the uniform film thickness on the cylinder. However, considering a film on a highly curved surface, where the radius of curvature of the coated surface is in the order of magnitude of the film thickness, the film flow can no longer be approximated by a planar coating film (White and Tallmadge, 1967). In addition, considering the cylindrical geometries in the development of dip coating theory for non-Newtonian fluids using the cylindrical coordinate for Navier-Stokes equation, increases the complexity of the problem and difficulty of the calculation process.

Fiber withdrawal (White and Tallmadge, 1966) was the topic of early investigations on cylindrical geometries. Fiber coating is of practical importance, since glass and polymeric fibers are, for example, covered with a thin layer of lubricant liquid to prevent them from breaking during further operations. Furthermore, fibers for reinforcing composites, require coating to provide compatibility and the desired degree of bonding with the matrix.

Tubes are also considered as cylindrical geometries, where draining a capillary tube has been studied extensively (Quere, 1999; Bretherton, 1961). The drainage of a Hele-Shaw cell (Ro and Homsy, 1995; Abedijaberi et al., 2011), investigated as a closely related problem to a capillary tube drainage which leads to similar results. Development of the original work and extension to more complicated geometries are described in several review articles (Kistler and Scriven, 1984; Quere, 1999; Ruschak, 1985).

Beside the importance of substrate geometry, non-Newtonian effects merit more attention because many, if not most, of the liquids coated depart significantly from Newtonian behavior. Several studies have adapted the asymptotic analysis to account for non-Newtonian effects.

The review of some results from published studies on Newtonian and non-Newtonian coating flows by providing a summary of the literature, detailing the geometry and the

constitutive equation used, is presented in Table 1-1. This tabular summary is to focus primarily on key developments for the plate, fiber and roller geometries.

All the theories in Table 1-1 are based on the analytical solutions.

Table 1-1: Partial summary of relevant literature on coating with Newtonian and non-Newtonian fluids

Authors	T: theory N: numerical E: experimental	Geometry	Constitutive equation
Landa and Levich (1942)	T	flat plate	Newtonian
Deryagin (1943)	T	fiber	Newtonian
Bretherton (1961)	T	Bubble in tube	Newtonian
Gutfinger and Tallmadge (1965)	T, E	flat plate	power-law
Tallmadge (1966)	T	flat plate	Ellis
Spiers et al. (1974)	T, E	flat plate	Newtonian
Spiers et al. (1975)	T, E	flat plate	Bingham, Ellis & power-law
Middleman(1978)	E	roller	(no theory)
Tharmalingham and Wilkinson (1978)	T, N, E	roller	Newtonian
Cerro and Scriven (1980)	N	flat plate	Newtonian
Wilson (1982)	T	inclined plate	Newtonian
Campanella et al. (1982b)	T, E	roller	power- law
Campanella and Cerro (1982a)	T, N, E	roller	Newtonian

Ro and Homsy (1995)	T	flat plate, fiber, bubble in tube	Oldroyd-B
de Ryck and Quere (1998)	T, E	fiber	Power law
Kizito et al. (1999)	E	roller	Newtonian
Ashmore et al. (2007)	T, E	fiber	Criminale-Ericksen-Filbey (CEF)
Jenny and Souhar (2009)	N	flat plate	Newtonian
Abedijaberi et al. (2011)	N	bubble in tube	Chilton- Ralison (FENE-CR)
Peralta et al. (2014)	T, E	Flat plate	Generalized Newtonian

In the dip coating process, coating film thickness increases with increasing velocity and viscosity, due to inertial. By increasing the shear rate in the system, the viscosity decrease in shear thinning fluids influences the fluid conditions at the withdrawal point in the bath (White and Tallmadge, 1967; Middleman, 1978; Spiers et al., 1974; Tallmadge, 1966).

 Analytical solutions are calculated using techniques that provide exact solutions, but this solution depends on the applied assumptions in the system. Due to complexity of the problem, it may not always be possible to calculate the solution using analytical techniques and also there is a limitation in defining the exact conditions that reflect the system behavior in this kind of solution. Also, the analytical solution is restricted to the simple constitutive equations and even in solution of complicated constitutive equations (Peralta et al., 2014), the dip coating problem is solved without considering the surface tension force in the system and Peralta et al. (2014) applied only viscosity and gravity forces.

1.1.3 « Numerical Calculations of Dip Coating and Free Surface Systems »

The correct representation and solution of this kind of system is not only valuable in coating processes but is key knowledge in a wide range of industrial processes. This is when a solution for the complex dip coating problem can be approximated using numerical techniques. Due to the increase of computational power and the development of Computational Fluid Dynamic (CFD) tools, numerical studies have been replacing some analytical approximations.

Modern computer aided techniques for solving the complete Navier-Stokes system have made full theories of dip coating possible.

Marques et al. (1978) used a finite difference technique to solve the high capillary number limit with the objective of determining the flow profiles in the thin film and it was found that during dip coating at large capillary numbers the inertial force became very important and a delicate balance between viscous, gravitational, and inertial forces was necessary in order to determine the flow profiles.

Tanguy et al. (1984) applied the finite element method for dip coating simulation, where the Galerkin method coupled to a discontinuous pressure element discretization of continuum. Even though they concentrated on $Ca > 0.01$, their analysis was extended to dip coating of wires and cylinders and also to non-Newtonian liquids. The finite element method requires a prior approximate knowledge of the final free surface shape (Reglat et al., 1993). Moreover, the number of iterations to reach convergence in the finite element methods can be quite large and solution depends strongly on the quality of the initial guess (Reglat et al., 1993).

Dip coating is also solved for an asymptotic film thickness using the full steady-state Navier-Stokes equations. The solution to this free surface problem were found using FIDAP, a computational fluid dynamics software for capillary numbers smaller than 0.4 (Jenny and Souhar, 2009) is found to agree with Wilson (1982).

In computational fluid dynamics systems, free surface flow needs to be defined by the presence of well-defined interface, and its position must be determined as part of the solution algorithm (Ferziger and Peric, 1996). The requirements for a good numerical prediction in the free surface flows are the representation of the interface on a discrete grid, movement of interface with time, treatment of partially filled cells and coupling of interface conditions with the equations of motion (Ubbink, 1997). There have been numerous methodologies capable of predicting interfacial flow field, but there are advantages and disadvantages attached to each approach.

Computation of the free surface can be classified into two major groups of *surface methods* (surface fitting techniques) and *volume methods or surface capturing* methods (Ferziger and Peric, 1996). Schematic representation of free surface computational methods is given in Figure 1-2.
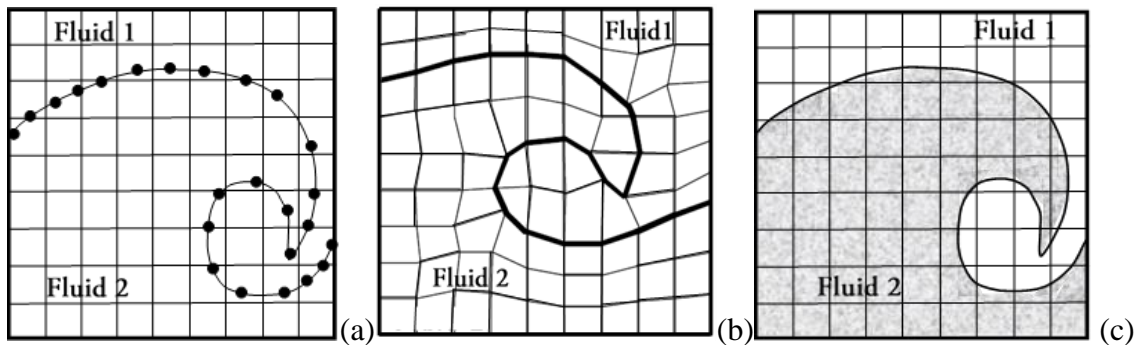
Figure 1-2: Schematic representation of the Surface methods (a) Marker particle on the interface, (b) Interface attached to a mesh surface, and volume methods (c) fluids are marked with indicator function or massless particles

In surface methods, the interface is represented and tracked explicitly either by marking it with special marker points, or by attaching it to a mesh surface which is forced to move with the interface. In the volume capturing methods, the fluids on either side of the interface are marked by either massless particles or an indicator function.

In surface methods, where the interface marked with special points, the positions between these points are approximated by interpolation, usually piecewise polynomial (Hyman, 1984).

11

The advantages of this approach is that the interface position is known throughout the calculation, remains sharp, and eases the computational effort needed for the calculation of the interface curvature for the inclusion of the surface tension force.

Dip coating process has also been evaluated through the level-set method for computing liquid film formation on a moving flat plate (Lee and Son, 2015).

The problem of partially filled cells, is the driving force in the development of most of the interface fitted methods. Various surface fitted techniques to attach the interface to a mesh surface have been developed during the past years (Dervieux and Thomasset, 1979; Takizawa et al., 1992; Li and Zhan, 1993). These methods are implemented mainly to reduce computer storage needed for the interface markers, to ensure a sharp interface and avoiding partially filled cells. These methods are limited to interfaces, which are not subjected to large deformations, because these lead to significant distortion of the mesh.

The other significant category of interface predicting approaches is the volume methods. Volume methods mark the fluids on either side of the interface and gives rise to the main drawback of this technique, as the exact position of the interface is not known explicitly and special techniques need to be applied to capture a well-defined interface (Ubbink, 1997). The calculation of the surface tension forces in volume methods has long been a problem but has been partially overcome by the continuum surface force (CSF) model of Brackbill et al. (1992). Their model has been implemented successfully in various volume based methods (Kothe and Mjolsness, 1992; Lafaurie et al., 1994).

Among the volume methods, predicting the free surface based on volume fraction, is an important technique. In this technique, the presence of one fluid is indicated by zero and the second fluid is specified by one. A scalar indicator function between zero and one, known as the volume fraction, is used to distinguish between two different fluids and define the interface and the value of cell at interface (between 0 and 1), gives an indication of the relative proportions occupying the cell volume (see Figure 1-3).

0	0	0	0	0	0
0	0.4	0.6	0.7	0.5	0
0	0.7	1	1	0.9	0.2
0	0.6	1	1	1	0.4
0	0.5	1	1	1	0.6
0	0.3	1	1	1	0.7

Figure 1-3: Schematic representation of volume of fluid method

Using volume fractions is more economical than marker particles and only a scalar convective equation, like other transport equations, needs to be solved to propagate the volume fractions through the computational domain.

However, the volume fraction approach also has the drawback of smearing the interface over several mesh cells and even with applying convective differencing schemes, such as upwind methods (Ubbink, 1997).

During the past years different researchers proposed various techniques in order to maintain a well-defined interface within the volume fraction framework: line techniques, the donor-acceptor formulation and higher order differencing schemes.

Sample pictures of a smeared interface using a volume method is shown in Figure 1-4.
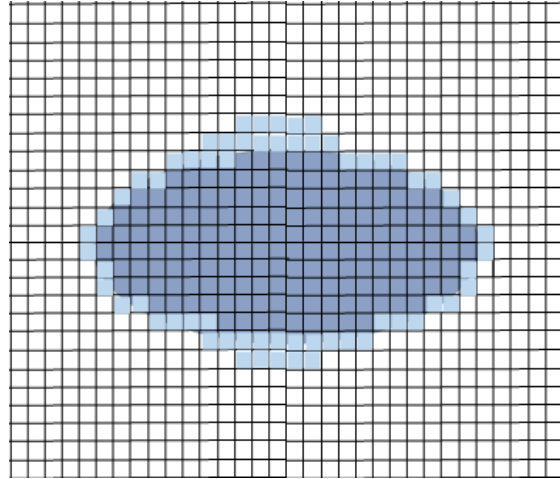
Figure 1-4: Smeared interface (light blue) define the liquid (in dark blue) boundary with surrounding gas (in white)

VOF is perhaps the most widely used method, robust and therefore features in many commercial CFD codes. However, there are a few problems associated with it, such as limitation to the structured meshes. Also instances of non-physical deformation of the interface shape or the numerical diffusion have been reported and restriction in capturing of sharp interfaces. Compressive interface capturing scheme for arbitrary meshes (CICSAM) (Ubbink, 1997) was introduced to overcome the problems experienced previously. (Ubbink, 1999). CICSAM is a highly-resolution differencing scheme based on the idea of the donor-acceptor flux approximation using normalized variable diagram (NVD) of Leonard (1988).

Inter-gamma differencing scheme proposed by Jasak and Weller (1995) wherein the necessary compression of interface is achieved by introducing an artificial compression term into VOF equation. The inter-gamma differencing scheme is also based on donor-acceptor formulation using the normalized variable diagram (Leonard, 1988). The variable and control volume arrangement is similar to ones in CICSAM scheme and the VOF methods implementation in OpenFOAM is close to the Inter-gamma method.

1.1.4 « Dispersions in Dip Coating Process »

Although in this work particle-laden flows are going to be studied in dip coating process, these flows are important in a wide variety of scientific and engineering applications including design and manufacture of composite materials, oil and gas production (Mukhopadhyay et al., 2009) and manufacturing processes in pharmaceutical, biomaterials and paper industries. In many of these industries, uniformity in particle distribution is required and the product quality is strongly dependent upon the consistency of particle distribution (Ritz et al., 2000).
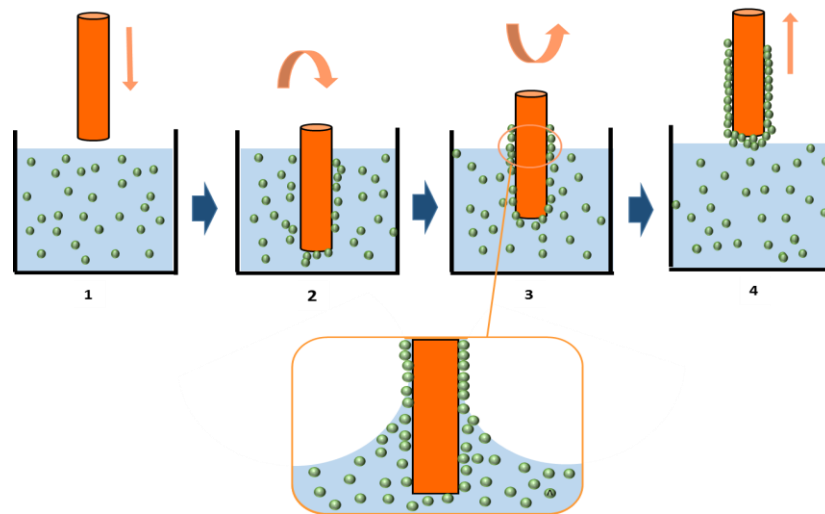
Figure 1-5: Dip coating of a cylindrical substrate though dispersion

A schematic picture of dip coating of a cylindrical substrate though dispersion is shown in Figure 1-5. In view of its varied applications, a number of theoretical and experimental investigations have been carried out and these have explored various aspects of the flow properties and characteristics of suspensions. Most of the investigations on the flow properties of suspensions of spherical particles have focused their attention upon the development of theoretical or empirical formulae relating the bulk rheology to the number of particles, assuming that the concentration of the particles remains uniform in space.

Additionally, the main focus in most of the investigations has been to predict the complex rheological effects on a specific suspension. Aidun and Lu (1995) introduced a

rheological constitutive law to model a filled suspension. They found that the evolution of the viscosity with respect to concentration is in good agreement with Krieger's empirical law (Krieger, 1972).

On the other hand, the modelling of many-body interactions and microstructure configurations of particle suspensions has been made possible in recent years with the aid of simulation methods such as direct simulation (Ritz and Caltagirone, 1999), Stokesian Dynamic Simulation (Brady and Bossis, 1998), lattice Boltzman method (Ladd, 1994; Kromkamp et al., 2006; Brady 1988) and the Completed Double Layer Boundary Element Method (Chen and Doi, 1989; Phan-Thien and Kim, 1994), the number of particles involved in the simulations is still small, of the order 10^2 -10^3 , due to the large computation effort required (Fang and Phan-Thien, 1999). However, the characterization of the interactions appearing at the scale of one particle, can allow understanding the behavior of a suspension flow.

The transport of liquid and solid particlesat a microstructural level, where the interactions between the solid particles and the carrier fluid as well as the interactions among the particles play an important role, strongly influences the global physical properties of suspensions. This shows that the behavior of the flowing suspension must be clearly understood for effectively controlling particle concentrations throughout in a variety of engineering applications such as the polymer processing industry (Cho and Kensey, 1991; Perktold et al., 1991; Sharp et al., 1996; Clifton et al., 1988; Unwin and Hammond, 1990; Barree and Conway, 1994; Husband, 1989; Givler and Crochet, 1983) and the process of proppant (treated sand or man-made ceramic materials) placement within hydraulic fractures that are used in the hydrocarbon extraction industry (Miskin et al., 1996; Unwin and Hammond, 1990; Barree and Conway, 1994).

The most prominent phenomenon observed in solid–fluid suspensions is shear-induced migration, in which initially well-mixed particles in suspensions subjected to inhomogeneous shear migrate from regions of high strain rate to regions of low strain rates and assume a non-uniform concentration distribution (Abbott et al., 1991; Eckstein et al., 1977; Gadala-Maria and Acrivos, 1980; Leighton and Acrivos, 1987; Chow et al.,

1994; Koh et al., 1994). Shear-induced diffusion or migration has been found to be different from conventional Brownian diffusion that arises from molecular motion. This has important implications both in viscometric measurements of concentrated suspensions (particle concentration of 30–60% by volume) and in industrial manufacturing processes where the performances and the appearance of the finished products are greatly affected by the degree of solids dispersion (Ritz et al., 2000; Chow et al., 1994).

The importance and application of dispersions and suspensions in the production procedures, requires the ability to estimate the behavior of the process and predict the performance of dispersed phase in the system.

In the numerical approach for the prediction of solid particles distribution in concentrated systems, the suspension can be considered as a continuum phase modeled through a rheological law which is a function of the local values of macroscopic quantities such as shear rate and particle concentration. From a practical point of view, a constitutive equation is needed, which can reasonably describe the behavior of real suspensions in flowing situations. Constitutive models that take into account the variation of particle concentration are proper choice for the estimation of viscosity in concentrated systems.

Recent theoretical investigations on concentrated suspensions undergoing inhomogeneous shearing flows have shed some light on the mechanics that cause irreversible migration of particles, although the phenomenon is not yet fully understood (Fang and Phan-Thien, 1999). It has been observed that there are a number of mechanisms that exist in the presence of the flow that leads to non-uniform concentration even in the region away from any walls or flow boundaries (Leighton and Acrivos, 1987; Mukhopadhyay, 2009). As a result, concentrated suspensions exhibit apparent non-Newtonian behavior with a viscosity that depends on the local volume fraction of particles (Koh et al., 1994).

There are two noteworthy numerical approaches, one is the particle diffusive model (Leighton and Acrivos, 1987; Phillips et al., 1992), which is based on the effects of a spatially varying inter particle interaction frequency and a spatially varying effective

viscosity. Another is the suspension balance model/suspension temperature model (Morris and Brady, 1998; Nott and Brady, 1994), which is based on the conservation of mass and momentum for both particle and suspension phases. A 'particle temperature' is introduced to associate the particle stress with the strength of particle fluctuations due to multi-body interactions.

Nott and Brady (1994) showed that, for some special cases (e.g. steady state pipe flow), suspension temperature model reduces to a diffusion equation similar to that of Phillip et al. (1992), however, the suspension balance model in its current form is difficult to implement numerically, due to its lack of an explicit convection–diffusion equation for the volume fraction. The diffusive flux model has still been extensively used to predict the concentration profile in many practical applications (Buyevich, 1996; McTigue and Jenkins, 1992; Phan-Thien and Fang, 1995) since the diffusive flux model is relatively simple and its accuracy is comparable with the suspension temperature model.

Development of the diffusive flux model was started with the study of a class of mechanisms, recognized by Leighton and Acrivos (1986, 1987), for the evolution of non-uniform concentration profiles which is a consequence of irreversible hydrodynamic interactions between the neighboring particles. They have used the flow-induced concentration non uniformities caused by the particle interactions to explain transient stresses that have been observed when a concentrated suspension is subjected to a simple Couette flow. They have attributed these transients in the suspension stress to the migration of particles caused by spatial gradients in the particle interaction frequency and the particle concentration. From these arguments and simple dimensional analysis, Leighton and Acrivos (1987) have derived diffusive flux expressions for the particulate phase and have demonstrated that these are consistent with the existence of a fully developed non-uniform particle concentration distribution for flow within a parallel wall channel. Phillips et al. (1992) have adapted the scaling arguments of Leighton and Acrivos (1987) and have derived a constitutive equation for the particle flux.

The model is considered a balance between a contribution due to a spatially varying interaction frequency and an opposite contribution due to a spatially varying viscosity

and has yielded excellent predictions in a circular Couette flow. The numerical simulation of transient circular Couette flow has predicted particle migrations from the rotating inner cylinder to the stationary outer cylinder. Their results for an axisymmetric Poiseuille flow show that the particles migrate towards the centerline, leading to a sharply peaked concentration and a blunt velocity profile in that region. A number of experimental studies have been carried out to study the effects of viscous resuspension in a pipe, a channel and Couette flow geometries (Buyevich, 1996; Phillips et al., 1992; Koh et al, 1994; Hampton et al., 1997; Hookham, 1986; Hampton et al., 1997; Lyon and Leal, 1998).

The results of the experimental study of concentrated suspension motion in a two-dimensional channel flow for mono-disperse systems by Lyon and Leal (1998) show that the particle concentration distributions reach a maximum near the channel centerline and a minimum at the channel walls; however, the concentration profile is not as sharply peaked as predicted by the theory (Koh et al., 1994). Coupled to these concentration distributions are blunted velocity profiles and particle velocity fluctuation distributions that have a sharp maximum at a position approximately 0.8H from the channel axis, where H denotes half the width of the channel (Lyon and Leal, 1998).

Diffusive flux equation allows describing the time evolution of the solid concentration based on the two-body interaction model (Phillips et al. 1992). The suspension stress is modelled as a generalized Newtonian fluid with a particle concentration dependent viscosity. In addition, it is assumed that the shear-induced diffusivity is linearly proportional to the local shear rate.

For determination of particle distribution in concentrated suspensions, a number of numerical calculation codes have been developed, but there are not many prior studies for enhancing the estimation tool to predict the behavior of concentrated suspensions. There are some numerical works based on the Phillips et al. (1992) model, for the liquid phase flow consist of solid particles (Phan-Thien and Fang, 1995). However, for most industrial applications, a reliable model requires for the prediction of concentrated dispersions in the free surface systems, where particles dispersion in the liquid as significant as the

interface behavior and free surface hydrodynamics. Coating systems are examples of processes where the free surface needs to be considered along with the dispersion of rigid particles in the system.

The simulation of the flow of a particle suspension in a dip coating process is one of the objectives of this work. First, the physical model is discussed in detail. Next, the numerical strategy based on the finite volume method is presented and tested on finite length dip coating flow problems.

In the current study the aim is to investigate the free coating flows for suspensions and describing a method to predict the dip coating hydrodynamics, coating film thickness at higher Ca, and predictive methods to describe dispersion flows with free surface.

1.2   « Objectives of the Work »

For numerical calculations, an Open source CFD platform has been chosen where the Finite Volume Method (FVM) used and determination of the free interface is managed by the VOF method. OpenFOAM is employed with the great advantageous of code customization and parallel simulation. The main objectives of the current work are:

- Analytical solution of dip coating process to understand the main processing parameters and considering the combination of substrate curvature and non-Newtonian fluids outcomes on the coating thickness

- Numerical simulation of free coating process for Newtonian and non-Newtonian coating fluids using complex non-Newtonian models for the coating film thickness estimation

- Prediction of coating film thickness at high withdrawal velocities

- Investigation on new effective parameters on developing the coating film layer in dip coating process and the influence of a new factors as the proximity of coating

bath to the coating substrate for the investigation in effective design, scale up, optimal control, and efficient operation of this process.

- Numerical investigation on suspensions hydrodynamics and solid particle distribution in dip coating process with implementing a new simulation algorithm for dense suspensions with the free surface in the OpenFOAM® applications by developing the C++ programming code.

- Implementing a new viscosity model based on the volume fraction of solid particles in the flow, in the OpenFOAM® libraries using the C++ programming code.

- Simulation of dip coating in unsteady-state condition for a finite length substrate by applying a non-structured dynamic mesh

- Validation of simulation results with rheological measurements and determining the coating fluid properties, image analysis for film thickness measurement in the coating layer using a high speed- high resolution camera

1.3 « Thesis Outline »

Chapter 2, starts with an introduction to previous work on the developing of analytical solution and their relation to the solution that is developed for non-Newtonian Ellis fluids. The cylindrical substrate considered as the geometry to study the curvature effects in dip coating where the substrate radii is in the same order as the coating film thickness. The theory developed based on the regional method that divides the coating process into three main regions and solve the Navior-Stokes equation for each region based on the role of major forces in each specific region. This chapter, the first appendix and the related references provides a strong reason for the use of Ellis constitutive equation for the development of theory that predicts the deposited film thickness for different pull out velocities. The experimental data belong to two different grades of TiO_2 particles

suspended in a commercial polymeric resin, Dymax 1186-MT which is being used in the medical sensors fabrication.

In Chapter 3, the simulation procedure is discussed starting with the discretization process of the geometry, boundary condition setting and VOF interface tracking technique that used for the free surface calculations. In this chapter, the Navier-Stokes equations is presented, the solution of which is managed by the PIMPLE method. Chapter 3 describes the use of OpenFOAM® as the tool for Finite Volume Method discretization selected for dip coating numerical calculations and the solver implementation. The simulation results validated with the Middleman experimental data for Newtonian and non-Newtonian fluids in the prediction of the process performance at high capillary numbers up to 60 for non-Newtonian fluids and capillary number of about 1.1 for Newtonian liquids. Also the results compared with the analytical solution of Roy and Dutt (1981) for a non-Newtonian fluid. Chapter 3 also presents the wall effect as a new parameter that needs to be taken into account in dip coating process. This factor studied using the two-phase flow with a free surface for both Newtonian and non-Newtonian fluids. Carreau and power law constitutive equations are used for the calculation of non-Newtonian fluids. For considering the low shear rate effects, the Ellis constitutive equation is applied in the analytical solution, where good prediction of coating thickness achieved at low withdrawal velocities (up to 0.8 cm/s). The Carreau model is used in the simulation process for predicting the coating layer thickness at high withdrawal speeds (up to 6 m/s) and higher capillary number range up to 60.

The Carreau model could not be used in the analytical solution due to the complexity of the equations for the Carreau constitutive equation with four parameters. The Ellis constitutive equation was not available in the OpenFOAM package and due to time constraints a model was not implemented thus numerical simulations were not performed using the Ellis model.

Dip coating is investigated numerically and experimentally including coating bath wall proximity to the substrate. Experiments were performed by taking the images of coating substrate over a range of withdrawal velocities and different bath diameters. Physical

properties of fluids were measured and implemented in the numerical calculations for the prediction of the process behavior.

Chapter 4, is devoted to the methods for the solution of the dispersed solid particles in the coating fluids. In this study, a new algorithm is developed for simulating the systems of dense suspensions with a free surface. Investigation of the dip coating process for the dense suspensions is performed by implementing a new OpenFOAM solver with a constitutive equation for handling the particles effects and interface-capturing technique of VOF in the system. A viscosity model based on the particle volume fraction is implemented in the OpenFOAM libraries. The new solver has the capability of solving the liquid-solid particle dispersions with the capability of interface tracking in in a fully multidimensional framework. Also the solver has the capability of performing the simulation for dynamic mesh, which has been applied for the coating of a finite length cylinder in the current study. The simulations developed in three dimensions to be able to capture the all effects of dip coating process. An experimental study has been performed for studying the coating of finite length geometries in presence of distributed solid particles in the coating liquid.

Finally, Chapter 5 presents the conclusions and recommendations for future work regarding research in this area.

Analytical solution

Experimental data using coating resin + fiber optics

Ellis constitutive equation

Navier-Stokes equation + three region method

Withdrawal velocity and film thickness relationship

Numerical Solution

Navier-Stokes equation + Grid generation+ Boundary conditions

CFD platform (OpenFOAM)

Prediction of coating thickness at high withdrawal speeds (Ca < 6) for Newtonian & non-Newtonian

Experimental data of S. Middleman

New parameters effect

CFD platform (OpenFOAM)

Experimental procedure + coating images

New parameters effect, (wall proximity effect) on the coating film thickness for Newtonian and non-Newtonian

Concentrated suspensions in thin film

Flux diffusion of solid Particles

Volume of Fluid methods for free

Mineral oil suspensions

Numerical simulation+ new code for particle distribution in free surface problems+ new viscosity model suspensions

Experimental procedure with image processing by high speed, high resolution

Particle distribution & film thickness prediction in coating film and concentrated

Figure 1-6: General scheme of thesis structure

24

1.4 « References »

Abbott J. R., Tetlow N., Graham A. L., Altobelli S. A., Fukushima E., Mondy L. A., Stephens T. A., Experimental observations of particle migration in concentrated suspensions: Couette flow, Journal of Rheology, Vol. 35, pp. 773, 1991

Abedijaberi A., Bhatara G., Shaqfeh E. S. G., Khomami B., Computational study of the influence of viscoelasticity on the interfacial dynamics of dip coating, Journal of Non-Newtonian Fluid Mechanics, Vol. 166, pp. 614, 2011

Ashmore J., Shen A. Q., Kavehpour H. P., Stone H. A., McKinley G. H., Coating flows of non-Newtonian fluids: Weakly and strongly elastic limits, Kluwer Academic Publishers, Netherlands, 2007

Aidun C., Lu Y., A method for rheological analysis of coating suspensions at high shear, Coating fundamentals symposium, 1995

Barree R. D., Conway, M. W., Experimental and numerical modeling of convective proppant transport, paper SPE 28564 presented at the SPE ATCE; New Orleans, LA, USA; 26-28 Sep 1994; later published in Journal of Petroleum Technology, 1995

Brady J. F., Phillips R. J., Lester J. C., Bossis G., Dynamic simulation of hydrodynamically interacting suspensions, J. Fluid Mech, Vol. 195, pp. 257-280, 1988

Brady J. F., Bossis, G., Stokesian dynamics, Annual Review of Fluid Mechanics, Vol. 20, pp. 111, 1998

Bretherton F. P., The motion of long bubbles in tubes, Journal of Fluid Mechanic, Vol. 10, pp. 166, 1961

Buyevich I. A. Particle distribution in suspension shear flow, Chemical Engineering Science, Vol. 51, pp. 635, 1996

Campanella O. H., Cerro R. L., Viscous flow on the outside of a horizontal rotating cylinder: the roll coating regime with a single fluid, Chemical Engineering Science, Vol. 39, pp. 1443, 1982

Campanella O. H., Galazzo J. L., Cerro R. L., Viscous flow on the outside of a horizontal rotating cylinder-II. Dip coating with a non-Newtonian fluid, Chemical Engineering Science, Vol. 41, pp. 2707, 1982

Ceratti D. R., Louis B., Paquez X., Faustini M. Grosso D., A New dip coating method to obtain large-surface coatings with a minimum of solution, Advanced Materials, Vol 27, pp. 4958, 2015

Cerro R. L., Scriven, L.E. Rapid free surface film flows. An integral approach, Industrial and Engineering Chemistry Fundamentals, Vol. 19, pp. 40, 1980

Chen D., Doi M., Simulation of aggregating colloids in shear flow, Journal of Chemical Physics, Vol. 91, pp. 2656, 1989

Cho Y. I., Kensey K. R., Effects of the non-Newtonian viscosity of blood on flows in a diseased arterial vessel: part 1: steady flows, Biorheology, Vol. 28, pp. 241, 1991

Chow A. W., Sinton S. W., Iwamiya J. H., Stephens T. S., Shear-induced particle migration in Couette and parallel-plate viscometers: NMR imaging and stress measurements, Physics of Fluids, Vol. 6, pp. 2561, 1994

Clifton R. J., Brown U., Wang J. J., Multiple fluids, proppant transport, and thermal effects in three-dimensional simulation of hydraulic fracturing, Society of Petroleum Engineers Journal, pp. 1819, 1988

Colosqui C. E., Morris J. F., Stone H. A., Hydrodynamically driven colloidal assembly in dip coating, Physical Review Letters, Vol. 110, pp. 188302-1, 2013

Derjaguin B., On the thickness of the liquid film adhering to the walls of a vessel after emptying, Acta Physicochem, USSR, Vol. 39, pp. 13, 1943

Dervieux, A. and Thomasset, F., A finite element method for the simulation of a Rayleigh-Taylor instability, IRIA-LABORIA report, F-78150 Le Chesnay, 1979

Deryagin B. V., Levi S. M., Film coating theory, Focal press limited, 1964

de Ryck A., Quere D., Fluid coating from a polymer solution, Langmuir, 1998, Vol.14, pp. 1911, 1998

Eckstein E. C., Bailey D. G., Shapiro A. H., Self-diffusion of particles in shear flow of a suspension, Journal of Fluid Mechanics, Vol. 79, pp. 191, 1977

Fahim N., Ouyang Z., Zhang Y., Jia B., Shi Z., Gu M., Efficiency enhancement of screen-printed multicrystalline silicon solar cells by integrating gold nanoparticles via a dip coating process, Optical Materials Express., Vol. 2, pp. 190, 2012

Fang Z., Phan-Thien N., Numerical simulation of particle migration in concentrated suspensions by a finite volume method, Journal of Non-Newtonian Fluid Mechanics, Vol. 58, pp. 67, 1995

Fang Z., Phan-Thien N., A particle suspension model: an unstructured finite-volume Implementation, Journal of Non-Newtonian Fluid Mechanics, Vol. 80, pp. 135, 1999

Ferziger J. H., Peric M., Computational methods for fluid dynamics, Springer-Verlag, Berlin, 1996

Gadala-Maria F., Acrivos A., Shear-induced structure in a concentrated suspension of solid spheres, Journal of Rheology, Vol. 24, pp. 799, 1980

Givler R. C., Crochet M. J., Pipes R. B., Numerical predictions of fiber orientation in dilute suspensions, Journal of Composite Materials, Vol. 17, pp. 330, 1983

Groenveld P., Drainage and withdrawal of liquid films, American Institute of Chemical Engineering journal, Vol. 17, pp. 489, 1971

Grunig J., Skale T., Kraume M., Liquid flow on a vertical wire in a countercurrent gas flow, Chemical Engineering Journal, Vol. 164, pp. 121, 2010

Guttfinger C., Tallmadge J. A., Films of non-Newtonian fluids adhering to flat plates, American Institute of Chemical Engineering Journal, Vol. 11, pp. 403, 1965

Hampton R. E., Mammoli A. A., Graham A. L., Tetlow N., Altobelli S. A., Migration of particles undergoing pressuredriven flow in a circular conduit, Journal of Rheology, Vol. 41, pp. 621, 1997

Hookham P. A., Concentration and velocity measurements in suspensions flowing through a rectangular channel, Ph.D. Thesis, California Institute of Technology, New York, 1986

Hurd A. J., Brinker C. J., Sol-gel film formation by dip coating, MRS Proceedings, Cambridge University Press, 1990

Husband D. M. Continuous processing of composite solid propellants, Chemical Engineering Progress, Vol. 85, pp. 55, 1989

Hyman, J. M., Numerical methods for tracking interfaces, Physica, Vol. 12D, pp. 396, 1984

Jenny M., Souhar M., Numerical simulation of a film coating flow at low capillary numbers, Computers and Fluids, Vol. 38, pp. 1823, 2009

Jasak H., Weller H. G., Interface-Tracking capabilities of InterGamma differencing scheme, Technical report, Imperial Collage, University of London, 1995

Kheshgi K. S., Kistler S. F., Scriven L. E., Rising and falling film flows: viewed from a first-order approximation, Chemical Engineering Science, Vol. 47, pp. 683, 1992

Kistler S. F., Scriven, L. E., Coating flow theory by finite element and asymptotic analysis of the Navier-Stokes system, International Journal of Numerical Methods in Fluids, Vol. 4, pp. 207, 1984

Kistler S. F., Schweizer P. M., Liquid Film Coating, Chapman and Hill, London, 1997

Kizito J. P., Kamotani Y., Ostrach S., Experimental free coating flows at high capillary and Reynolds number, Experiments in Fluids, Vol. 27, pp. 235, 1999

Krieger I. M., Rheology of monodisperse lattices, Advances in Colloid and Interface Science, Vol. 3, pp. 111, 1972

Kromkamp J., van den Ende D., Kandhai D., van der Sman R., Boom R., Lattice Boltzmann simulation of 2D and 3D non-Brownian suspensions in Couette flow, Chemical Engineering Science, Vol. 61, pp. 858, 2006

Koh C. J., Hookham P., Leal L. G., An experimental investigation of concentrated suspension flows in a rectangular channel, Journal of Fluid Mechanics, Vol. 266, pp. 1-32, 1994

Kothe, D.B., Mjolsness, R.C., RIPPLE: A new method for incompressible flows with free surfaces, American Institute of Aeronautics and Astronautics Journal, Vol. 30, pp. 2694, 1992

Kwon S., Kim W., Kim H., Choi S., Park B. C., Kang S., Choi K. C., High luminance fiber-based polymer light-emitting devices by a dip-coating method, Advanced electronic materials, Vol. 1, pp. 2015

Ladd A. J., Numerical simulation of particulate suspensions via a discretized Boltzmann equation, Journal of Fluid Mechanics, Part 1, Vol. 271, pp. 285, 1994

Lafaurie, B., Nardone, C., Scardovelli, R., Zaleski, S., Zanetti, G., Modelling merging and fragmentation in multiphase flows with SURFER, Journal of Computational Physics, Vol. 113, pp. 134, 1994

Landau L., Levich B., Dragging of a liquid by a moving plate, Acta physicochem. URSS, Vol. 17, pp. 42, 1942

Lee J., Son G., Numerical simulation of two-phase flows in dip coating, European coating symposium, Eindhoven, Netherlands, 2015

Lee C. Y., Tallmadge J. A., Dynamic meniscus profiles in free coating III predictions based on two-dimensional flow fields, American Institute of Chemical Engineering Journal, Vol. 20, pp. 1079, 1974

Lee C. Y., Tallmadge J. A., Meniscus shapes in withdrawal of flat sheets from liquid baths. II. A Quasi-one-dimensional flow model for low capillary number, Industrial and Engineering Chemistry Research Fundamentals, Vol. 14, pp 120, 1975

Leighton D., Acrivos A., Viscous resuspension, Chemical Engineering Science, Vol. 41, pp. 1377, 1986

Leighton D., Acrivos A., Measurement of shear-induced self-diffusion in concentrated suspensions of spheres, Journal of Fluid Mechanics, Vol. 177, pp. 109, 1987

Leighton D., Acrivos A., The shear-induced migration of particles in concentrated suspensions, Journal of Fluid Mechanics, Vol. 181, pp. 415, 1987

Leonard B. P., Simple high-accuracy resolution program for convective modeling of discontinuities, International Journal of Numerical Methods in Fluids, Vol 8, pp. 1291, 1988

Li, Y. S., Zhan, J. M., An efficient three-dimensional semi-implicit finite element scheme for simulation of free surface flows, International Journal of Numerical Methods in Fluids, Vol. 16, pp. 187, 1993

Lyon M. K., Leal L. G., An experimental study of the motion of concentrated suspensions in two-dimensional channel flow. Part 1. Monodisperse systems, Journal of Fluid Mechanics, Vol. 363, pp.25, 1998

Marques D., Costanza V., Cerro R. L., Dip coating at large capillary numbers: an initial value problem, Chemical Engineering Science, Vol. 33, pp. 87, 1978

McTigue D. F., Jenkins J. T., Channel flow of a concentrated suspension, In Advances in Micromechanics of Granular Materials, Shen H. H., Satake M., Mehrabadi M., Chang C. S., Campbell C. S. (eds). Elsevier: Amsterdam, pp. 381, 1992

Middleman S., Fundamentals of polymer processing, McGraw-Hill, New York, 1977

Middleman S., Free coating of viscous and viscoelastic liquids onto a partially submerged rotating roll, Polymer Engineering and Science, Vol. 18, pp. 734, 1978

Miskin I., Elliott L., Ingham D. B., Hammond P. S., Steady suspension flows into two-dimensional horizontal and inclined channels, International Journal of Multiphase Flow, Vol. 22, pp. 1223, 1996

Morey F., Thickness of a liquid film adhering to a surface slowly withdrawn from the Liquid, Journal of Research of the National Bureau of Standards, Volume 25, 1940

Morris J. F., Brady J. F., Pressure-driven flow of a suspension: buoyancy effects, International Journal of Multiphase Flow, Vol. 24, pp. 105, 1998

Mukhopadhyay S., Usha R., Tulapurkara E. G., Numerical study of concentrated fluid–particle suspension flow in a wavy channel, International Journal of Numerical Methods in Fluids, Vol. 59, pp. 1125, 2009

Nott P. R., Brady J. F., Pressure-driven flow of suspensions: simulation and theory, Journal of Fluid Mechanics, Vol. 275, pp. 157, 1994

Park C. W., Effects of insoluble surfactants on dip coating, Journal of colloid and interface science, Vol. 146, pp. 382, 1991

Peralta J. M., Meza B. E., Zorrilla S. E., Mathematical modeling of a dip-coating process using a generalized Newtonian fluid 1. Model development, Industry and Engineering Chemistry Research, Vol. 53, pp. 6521, 2014

Perktold K., Resch M., Florian H., Pulsatile non-Newtonian flow characteristics in a three-dimensional human carotidartery bifurcation model, Journal of Biomechanical Engineering-Transactions of the ASME, Vol. 113, pp. 464, 1991

Phan-Thien N., Kim S., Microstructures in elastic media: Principles and computational methods, Oxford University Press, London, 1994

Phillips R. J., Armstrong R. C., Brown R. A., Graham A. L., Abbott J. R., A constitutive equation for concentrated suspension that accounts for shear-induced particle migration, Physics of Fluids A, Vol. 4, pp. 30, 1992

Quere D., Fluid coating on a fiber, Annual Review of Fluid Mechanics, Vol. 31, pp. 347, 1999

Ritz J. B., Caltagirone J. P., A numerical continuous model for hydrodynamics of the fluid particle systems, International Journal of Numerical Methods in Fluids, 1999

Ritz J. B., Bertrand F., Thibault F., Tanguy P. A., Shear-induced particle migration in a short-dwell coater, Chemical Engineering Science, Vol 55, pp. 4857, 2000

Ro J. S., Homsy G. M., "Viscoelastic free surface flows: thin film hydrodynamics of Hele-Shaw and dip coating flows", Journal of Non-Newtonian Fluid Mechanics, Vol. 57, pp. 203, 1995

Ruschak K. J., Limiting flow in a pre-metered coating device, Chemical Engineer Science, Vol. 31, pp. 1057, 1976

Ruschak K. J., Coating flows, Annual Review of Fluid Mechanics, Vol. 17, pp. 65, 1985

Sharp M. K., Thurston G. B., Moore J. E., The effect of blood viscoelasticity on pulsatile flow in stationary and axially moving tubes, Biorheology, Vol. 33, pp. 185, 1996

Soler-Illia G. J., Crepaldi E. L., Grosso D., Sanchez C., Block copolymer-templated mesoporous oxides, Current Opinion in Colloid and Interface Science, Vol. 8 , pp. 109, 200

Spiers R. P., Subbaraman C. V., Wilkinson W. L., Free coating of a Newtonian liquid onto a vertical surface, Chemical Engineering Science, Vol. 29, pp. 389–396, 1974

Spiers R. P., Subbaraman C. V., Wilkinson W. L., Free coating of non-Newtonian liquids onto a vertical surface, Chemical Engineering Science, Vol. 30, pp. 379, 1975

Tallmadge, J. A., A Withdrawal Theory for Ellis Model Fluids, American Institute of Chemical Engineering Journal, Vol. 12, 1011, 1966

Tallmadge J. A., Improved withdrawal theories for cylinders by a more accurate description of curvatures of static menisci, American Institute of Chemical Engineering Journal, Vol. 15, pp. 941, 1969

Tanguy P., Fortin M., Choplin L., Finite element simulation of dip coating, I: Newtonian Fluids, International Journal for Numerical Methods in Fluids, Vol. 4, pp. 441, 1984

Takizawa A., Koshizuka S., Kondo S., Generalization of physical component boundary fitted co-ordinate (PCBFC) method for the analysis of free-surface flow, International Journal for Numerical Methods in Fluids, Vol. 15, pp. 1213, 1992

Tekic M. N., Jovanovic S., Liquid coating onto a rotating roll, Chemical Engineering Science, Vol. 37, pp. 1815, 1982

The OpenFOAM® Foundation (www.OpenFOAM.org)

Ubbink O., Numerical prediction of two fluid systems with sharp interfaces, PhD thesis Imperial College, 1997

Ubbink O., Issa R., A method for capturing sharp fluid interfaces on arbitrary meshes, J. Comp. Phys., Vol. 153(1), pp. 26-50, 1999

Unwin A. T., Hammond P. S., Computer simulations of proppant transport in a hydraulic fracture, Society of Petroleum Engineers Journal, pp. 29649, 1990

Watanabe M., Wakimoto N., Hirai T., Yokoyama M., Thermal switching of the actuation ability of an electroactive polymer actuator, Journal of Applied Polymer Science, Vol. 95, pp. 1566, 2004

White D. A., Tallmadge J. A., A gravity corrected theory for cylinder withdrawal, American Institute of Chemical Engineering Journal, Vol. 13, pp. 745, 1967

Wilson S. D. R., The drag-out problem in film coating theory, Journal of Engineering Mathematics, Vol. 16, pp. 209, 1982

Yang A., Tao X. M., Cheng X. Y., Prediction of fiber coating thickness via liquid-phase process, Journal Materials Processing Technology, Vol. 202, pp. 365, 2008

Chapter 2

2   « Analytical Solution »

The chapter addresses the hydrodynamics of dip coating process using Ellis fluids and cylindrical substrates. Chapter 2 is an expanded version of "Investigation on Dip Coating Process by Mathematical Modeling of non-Newtonian Fluids on Cylindrical Substrates", presented at International Society of Coating Science and Technology Conference (ISCST), Atlanta, USA, 2012.

2.1   « Abstract »

A mathematical model for the dip coating process has been developed for cylindrical geometries with non-Newtonian fluids. This investigation explores the effects of the substrate radius and hydrodynamic behavior of the non-Newtonian fluid on the resulting thin film on the substrate. The coating fluid studied, Dymax 1186-MT, is a resin for fiber optics and used as a matrix to suspend 1 vol% titanium dioxide particles. The coating substrate is a 100 μm diameter fiber optic diffuser. The Ellis constitutive equation is applied for the non-Newtonian model for coating thickness prediction, including the influence of viscosity at low shear rates that occur near the surface of the withdrawal film. In addition, results of Newtonian and power law models are compared with the Ellis model outcomes. The rheological properties and surface tension of fluids were analyzed and applied in the models and good agreement between experimental and analytical solution obtained for Ellis model.

2.2   « Introduction »

One of the common and low cost industrial methods of depositing a thin, uniform layer of liquid onto an object is dip coating (or free withdrawal coating) for planar, cylindrical and irregularly shaped substrates (Middleman, 1977). Thin films of Newtonian and non-Newtonian fluids play a major role in several industrial applications such as solar cell

manufacturing, rust proof protection, gas assisted injection molding and enhanced oil recovery (Adedijaberi et al., 2011). In the recent surge of research on advanced materials, dipping and withdrawal are used to apply the coating and also to control the final microstructure; for example, fiber optic modulation has attracted substantial attention because of the great potential for sensors and medical devices (Kostanski et al., 2009). Cylindrical substrates provide axisymmetric flexibility, complete surface area utilization, and radial symmetry.

In the dip coating process, the surface to be coated is initially immersed in the coating fluid and then withdrawn (Peralta et al., 2014). An analysis of the problem started with the pioneering work of Landau and Levich (1942). Significant development in the problem formulation was achieved by White and Tallmadge investigating withdrawal of flat plates and derivation of the film thickness for small capillary numbers (White and Tallmadge, 1965; Tallmadge, 1970). However, a film on a highly curved surface, where the radius of curvature of the coated surface is in the order of magnitude of the film thickness, the film flow can no longer be approximated by a planar liquid film (Grunig, 2010). Studies on cylindrical substrates are much less common than for flat plate geometries due to curvature treatment difficulties in analytical solutions. White and Tallmadge included gravity effects in an improved theory for driving a relation between the deposited film thickness, withdrawal velocity and fluid properties for cylindrical substrates (White and Tallmadge, 1966). Non-Newtonian fluid rheology, in addition to the curvature effects in calculations, extremely complicates the analytical solution. A model presented by Roy and Dutt for withdrawal of cylinders included a power law fluid (Roy and Dutt, 1981). However, a deficiency of the power law constitutive form is neglecting the low shear plateau commonly found in non-Newtonian fluids, especially as low shear rates occur near the surface of withdrawal films. Therefore, it seems reasonable to expect better agreement with a model using a constitutive equation that includes rheological behavior near zero shear rates as well as intermediate shear rates, such as the Ellis constitutive equation (Tallmadge, 1966; 1968; Gutfinger and Tallmadge, 1965).

2.3 «Theory Development »

Coating thickness depends on the fluid properties and withdrawal speed. The coating flow is considered in steady state. The common methodology developed by Landau and Levich to carry out the coating thickness prediction and describe the dynamics of this process is based on considering the flow in three sections above the bath free surface, as shown in Figure 2-1.
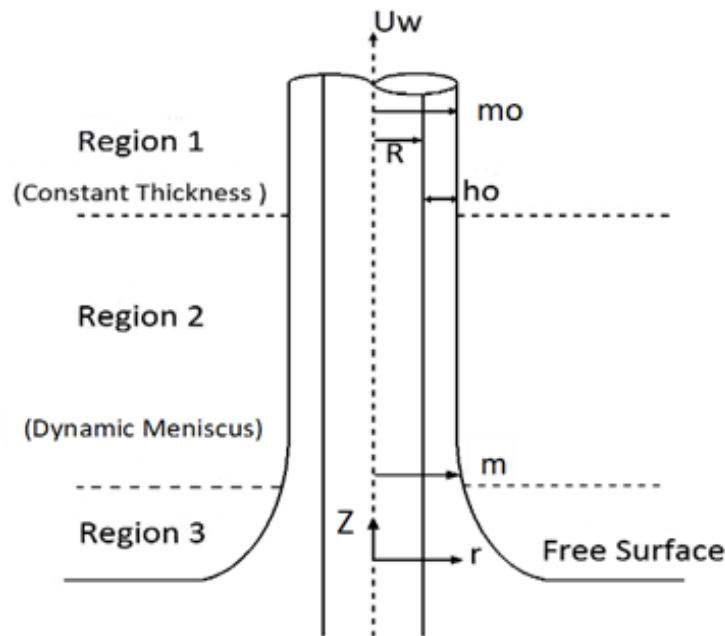
Figure 2-1: The coating flow regions for a cylindrical substrate

The Navier-Stokes equations are used to describe the momentum balance in each section and appropriate boundary conditions applied to define the flow in adjoining regions.

Region 1 is relatively far from the surface of coating fluid bath and due to the uniformity of this region all the derivatives of coating film disappear with respect to substrate height. Consequently, surface tension effects, which are a function of the surface curvature, are not taken into account in the flow equation for region 1. In region 2, which is called the dynamic meniscus region, all forces contribute significantly to the underlying flow and the coating film thickness changes with vertical distance. In region 3, which is the static

meniscus region, and closest to the coating bath surface, gravity and surface tension forces play a significant role in the flow development.

2.3.1 « Equations of Motion »

Flow is considered as one dimensional in cylindrical coordinates and the Navier-Stokes equation be used as shown in equation 1 to describe the flow in all three regions (Landau and Levich, 1942; White and Tallmadge, 1966).

$$\sigma \frac{d}{dz}(C_V^P - C_R^P) - \rho g - \frac{1}{r}\frac{d}{dr}(r\tau_{rz}) = 0 \qquad (2-1)$$

C_V^P is the principal curvature in the vertical direction and C_R^P is the curvature in radial direction.

Ellis fluids (Tallmadge, 1966), characterized by equation 2-1, in which, μ_0 is zero shear viscosity, α is the dimensionless Ellis index and $\tau_{1/2}$ is the shear stress at a shear viscosity of $\mu_0/2$.

$$\mu = \frac{\mu_0}{1 + \left(\frac{\tau_{rz}}{\tau_{\frac{1}{2}}}\right)^{\alpha-1}} \qquad (2-2)$$

Thus, shear rate is expressed by equation 2-3, will be applied in flow rate estimation of region 1 and 2.

$$\tau_{rz}(A + B|\tau_{rz}|^{\alpha-1}) = -\frac{du}{dr} \qquad (2-3)$$

In equation 2-3, $A = 1/\mu_0$ is the inverse of the zero shear viscosity and $B = 1/\mu_0(\tau_{1/2})^{\alpha-1}$ then simplifying equation 2-1 for each region and replacing the corresponding values for shear stress, the velocity can be calculated.

The flow equations for the specific region can be obtained from the general equation of motion with respect to essential assumptions applicable to the corresponding region.

2.3.2 « Constant Thickness Region »

In this region, which is shown in Figure 2-1 as region 1, surface tension effects are not significant and the following equation is obtained.

$$\rho g + \frac{1}{r}\frac{d}{dr}(r\tau_{rz}) = 0 \qquad (2-4)$$

The boundary conditions are $u = U_w$ at $r = R$ where U_w is the withdrawal velocity for the moving cylinder and $\tau_{rz} = 0$ at $r = m_0$ in which τ_{rz} is the shear stress at the coating film interface m_0 and applying these boundary conditions, τ_{rz} can be defined in the region.

$$\tau_{rz} = \frac{-\dfrac{\rho g}{2(r^2 - m_0^2)}}{r} \qquad (2-5)$$

The velocity profile can be obtained by integrating on equation 2-3 after replacing the value of τ_{rz} from equation 2-5, and a another integration leads to the flow rate Q_1 as,

$$Q_1 = \pi U_w m_0^2 - \pi U_w R^2$$
$$+ A\rho g\pi \left[\frac{(m_0)^4 - R^4}{8} - \frac{(m_0)^4 - R^4}{4} \right.$$
$$\left. - m_0^2 \left(m_0^2 ln m_0 - R^2 lnR - \left(\frac{m_0^2 - R^2}{2} \right)(1 + lnR) \right) \right]$$
$$- B \left(\frac{\rho g}{2} \right)^{\alpha} 2\pi \int_R^{m_0} r dr \int_R^r \left(\frac{r^2 - m_0^2}{r} \right)^{\alpha} dr \qquad (2-6)$$

In calculating Q_1 the repeated integral in the last term is replaced by a function of dimensionless coating radius M_0 and results in

$$F(M_0) = \int_1^{M_0} \left(1 - \frac{1}{r^2}\right)^{(1+\alpha)} r^{\alpha-2} dr \qquad (2-7)$$

And $E(M_0)$ is estimated as;

$$E(M_0) = \left[\frac{(M_0 R)^4 - R^4}{8} - \frac{(M_0 R)^4 - R^4}{4}\right.$$

$$\left. - M_0^2 R^2 \left(M_0^2 R^2 \ln M_0 R - R^2 \ln R - \left(\frac{M_0^2 R^2 - R^2}{2}\right)(1 + \ln R)\right)\right] \quad (2-8)$$

To simplify the notation in equation 2-6, $F(M_0)$ and $E(M_0)$ are introduced and consequently, the flow rate in region 1 can be rearranged as

$$Q_1 = \pi U_w M_0^2 R^2 - \pi U_w R^2 + A\rho g\pi E(M_0) - B\left(\frac{\rho g}{2}\right)^\alpha \pi (M_0 R)^{\alpha+3} F(M_0) \quad (2-9)$$

2.3.3 « Dynamic Meniscus Region »

The hydrodynamic behavior of flow in region 2 (shown in Figure2-1) is described by considering all the terms from equation 2-1.

The first term of equation 2-1 on the left can be replaced by (Tallmadge and Gutfinger, 1967)

$$\sigma\frac{d}{dz}(C_V^P - C_R^P) = \sigma\frac{d}{dz}\left\{\frac{d^2m/dz^2}{\left[1 + \left(dm/dz\right)^2\right]^{\frac{3}{2}}} + \frac{1}{m\left[1 + \left(dm/dz\right)^2\right]^{\frac{1}{2}}}\right\} \quad (2-10)$$

where m is the film thickness plus the substrate radius. Equation 2-10 has been solved using the boundary conditions for a static meniscus, where the first derivative for film thickness is zero at the top of the meniscus and the second derivative is taken as infinite at the free surface (Tallmadge and Gutfinger, 1967).

Thus, equation 2-10 will be simplified to

$$\sigma \frac{d}{dz}(C_V^P - C_R^P) = \sigma \frac{d}{dz}\left(\frac{d^2 m}{dz^2}\right) \qquad (2-11)$$

For region 2, equation 2-1 can be written as

$$\sigma \frac{d^3 m}{dz^3} - \rho g - \frac{1}{r}\frac{d}{dr}(r\tau_{rz}) = 0 \qquad (2-12)$$

Surface tension can be defined by the pressure difference across the fluid interface and $u = U_w$ at $r = R$ where U_w is the withdrawal velocity of cylindrical substrate and $\tau_{rz} = 0$ at $r = m$ in which shear stress is zero at m the interfacial area of film.

Similar to region 1, appropriate integration by applying the boundary conditions for the momentum equation in region 2, the velocity profile and flow rate can be defined respectively.

$$F(M) = \int_1^M \left(1 - \frac{1}{r^2}\right)^{(1+\alpha)} r^{\alpha-2} dr \qquad (2-13)$$

$$E(M) = \left[\frac{M^4 R^4}{8}\left(1 + \frac{1}{M^4} - \frac{2}{M^2} - 8 lnRM + \frac{lnR}{M^2} + (1 + lnR)\left(4 - \frac{4}{M^2}\right)\right)\right] \qquad (2-14)$$

Rearranging the expression for the flow rate of second region by replacing $N = \rho g - \sigma \frac{d^3 m}{dz}$ yields

$$Q_2 = \pi U_w M^2 R^2 - \pi U_w R^2 + AN\pi E(M) - B\left(\frac{N}{2}\right)^\alpha \pi (MR)^{\alpha+3} F(M) \qquad (2-15)$$

Matching flow rate of region 1 and region 2, $Q_1 = Q_2$, in equation 2-16 will be the appropriate estimation of flow behavior in corresponding regions.

$$ANE(M) - B\left(\frac{N}{2}\right)^{\alpha} \pi(m)^{\alpha+3} F(M) = U_w(m_0^2 - m^2) + A\rho g E(M_0)$$

$$- B\left(\frac{\rho g}{2}\right)^{\alpha} \pi(m_0)^{\alpha+3} F(M_0) \qquad (2-16)$$

Equation 2-16 is converted into a dimensionless form, where T_1, K_1, D_1 and D_2 are the dimensionless numbers defined as

$$T_1 = -(\frac{\rho g}{\sigma m_0})^{\frac{1}{3}} z \qquad (2-17)$$

$$K_1 = \frac{m_0^{\alpha+1} \rho^{\alpha} g^{\alpha}}{2^{\alpha} \mu_0 U_w (\tau_{\frac{1}{2}})^{\alpha-1}} \qquad (2-18)$$

$$D_1 = \frac{\rho g m^4}{\mu_0 U_w m_0^2} \qquad (2-19)$$

$$D_2 = \frac{\rho g m_0^2}{\mu_0 U_w} \qquad (2-20)$$

Thus,

$$\frac{d^3 L}{dT_1^3} = \left(\frac{(L^2 - 1) + K_1\left(L^{(\alpha+3)} F(M) - F(M_0)\right) - D_1 E(M) + D_2 E(M_0)}{-D_1 E(M) + \alpha K_1 L^{(\alpha+3)} F(M)}\right) \qquad (2-21)$$

Equation 2-21 is a third order non-linear differential equation in L with the appropriate initial conditions at $T_1 = 0$,

$$L = \frac{m}{m_0} = 1 \quad , \quad \frac{dL}{dT_1} = 0 \quad , \quad \frac{d^2 L}{dT_1^2} = 0 \qquad (2-22)$$

In matching boundary conditions between region 1 and region 2, the thickness, slope and curvature dynamic meniscus conditions are captured in (2-22).

2.3.4 « Static Meniscus Region »

For region 3, the Navier-stokes equation declines to the surface tension and gravitational forces

$$\sigma \frac{d}{dz}\left(\frac{d^2m}{dz^2}\right) - \rho g = 0 \qquad\qquad (2-23)$$

The schematic picture of region 3 is presented in Figure 2-1. The viscous term is excluded in the momentum balance of region 3. Tallmadge calculated the curvature at the upper part of static meniscus (Tallmadge, 1969). In their calculation, the Laplace equation for the pressure drop across curved liquid-gas interfaces is applied to the solution of the profile of a static liquid meniscus on the outside of a fiber with a circular cross section.

Considering the practical range for this estimation, the static curvature is expressed by equation 2-24 and equation 2-25.

$$\lim_{z \to m_0} \frac{d^2m}{dz^2} = \frac{2}{a_c} Cm \qquad\qquad (2-24)$$

$$Cm = \frac{3.36G}{1 + 3.36G} + \frac{0.5}{G} \qquad\qquad (2-25)$$

Capillary Length, a_c in equation 2-24 is defined as $(2\sigma/\rho g)^{1/2}$ for the static meniscus and G is the radius parameter defined as $M_0 N_{GO}$ where M_0 is the dimensionless coated radius and N_{GO} is the dimensionless Goucher number, $R(\rho g/2\sigma)^{1/2}$.

In equation 2-24, the Cm values obtained using empirical equation 2-25, were compared with theoretical values for a range of $0.003 < G < 30$, and the curvature values from equation 2-25 were found to be accurate within 0.5% for all G and to be accurate within 0.1 for $G < 0.02$ and $G > 2$ (Tallmadge, 1969).

Connecting the static meniscus and dynamic meniscus regions has been completed using the dimensionless form of the curvatures of region 2 and region 3 where it is given by

$$\lim_{L \to 1} \frac{d^2L}{dT_1^2} = \lim_{L \to \infty} \frac{d^2L}{dT_1^2} \qquad\qquad (2-26)$$

Integrating equation 2-21 results in the solution of the right hand side of equation 2-26, where the left and right side of equatio 2-26 can be obtained by the estimation for the static curvature in equation 2-24.

Solving equation 2-21 with corresponding initial conditions will be extremely complicated. Therefore, an approximate solution for equation 2-21 can be reached by substituting $L = 1 + \lambda$, and ignoring term of $O(\lambda^2)$ and above. In addition, the functions $F(M)$ and $E(M)$ can be written as

$$F(M) = F(M_0 L) = F(M_0 + \lambda M_0) \qquad\qquad (2-27)$$

$$E(M) = E(M_0 L) = E(M_0 + \lambda M_0) \qquad\qquad (2-28)$$

The above functions can be rearranged based on dimensionless coated radius M_0 applying the Taylor series

$$F(M) = F(M_0) + \lambda M_0 F'(M_0) \qquad\qquad (2-29)$$

$$E(M) = E(M_0) + \lambda M_0 E'(M_0) \qquad\qquad (2-30)$$

Then, defining the derivatives of these functions yield

$$E'(M_0) = \frac{d}{dM_0}\left\{ \frac{1}{8}\left(1 + \frac{1}{M_0^4} - \frac{2}{M_0^2} - 8lnRM_0 + \frac{8lnR}{M_0^2} + (1 + lnR)\left(4 - \frac{4}{M_0^2} \right) \right) \right\}$$

$$= -\frac{1}{2M_0^5} + \frac{1}{2M_0^3} - \frac{1}{M_0} + \frac{1}{M_0^3} - \frac{lnR}{M_0^3} \qquad\qquad (2-31)$$

$$F'(M_0) = \frac{d}{dM_0}\left\{ \int_1^{M_0} \left(1 - \frac{1}{r^2} \right)^{(1+\alpha)} r^{\alpha-2} dr \right\} = \left(1 - \frac{1}{M_0^2} \right)^{(1+\alpha)} M_0^{\alpha-2} \qquad\qquad (2-32)$$

Thus, equation 2-21 may be expressed as

$$\frac{d^3 L}{dT_1{}^3}$$

$$= \left(\frac{(L^2 - 1) + K_1 \left(L^{(\alpha+3)} F(M) - F(M_0) \right) - D_1 \left(E(M_0) + \lambda M_0 E'(M_0) \right) + D_2 E(M_0)}{-D_1 E(M) + \alpha K_1 L^{(\alpha+3)} F(M)} \right) \quad (2$$

$$- 33)$$

Considering $D_2 = D_1$ based on their definition and dropping very small value of

$-D_1 E(M)$ comparing to the value of term $\alpha K L^{(\alpha+3)} F(M)$ gives;

$$\frac{d^3 L}{dT_1{}^3} = \left(\frac{(L^2 - 1) + K_1 \left(L^{(\alpha+3)} F(M) - F(M_0) \right) - D_1 \left(\lambda M_0 E'(M_0) \right)}{\alpha K_1 L^{(\alpha+3)} F(M)} \right) \quad (2 - 34)$$

Furthermore, employing the binomial series, $(1 + \lambda)^z = 1 + z\lambda$ provides;

$$\frac{d^3 \lambda}{dT_1{}^3} = \left(\frac{2 + K_1(\alpha + 3) F(M_0) - D_1 E'(M_0)}{\alpha K_1 F(M_0)} \right) \left(\frac{\lambda}{(1 + \lambda)^{\alpha+3}} \right) \quad (2 - 35)$$

Introducing T_2 as a new variable reduce the number of terms involved in the related

equation.

$$T_2 = \left(\frac{2 + K_1(\alpha + 3) F(M_0) - D_1 E'(M_0)}{\alpha K_1 F(M_0)} \right)^{\frac{1}{3}} T_1 \quad (2 - 36)$$

Implementing C using equation 2-37 in the equation 2-36 returns equation 2-38, for

calculating T_2 based on T_1

$$C = \left(\frac{K_1(\alpha + 3) F(M_0) - D_2 E'(M_0)}{\alpha K_1 F(M_0)} \right) \quad (2 - 37)$$

$$T_2 = \left(\frac{2^{\alpha+1} \mu_0 U_w (\tau_1)^{\alpha-1}}{\alpha m_0^{\alpha+1} \rho^\alpha g^\alpha F(M_0)} + C \right)^{\frac{1}{3}} T_1 \quad (2 - 38)$$

Changing the notation of equation 2-35 for L, employing T_2 instead of T_1 and $\lambda = L - 1$, results in

$$\frac{d^3 L}{dT_2{}^3} = \frac{L - 1}{L^{\alpha+3}} \qquad (2 - 39)$$

Equation 2-34 was solved numerically where the parameter β, is a function of α and the relation between them calculated by integrating of the equation 2-39.

$$\beta = \lim_{L \to \infty} \frac{d^2 L}{dT_2{}^2} \qquad (2 - 40)$$

An analogous computer code developed by Gutfinger is used to obtain the value of β for the Ellis model and modified Euler method used for the numerical solution (Gutfinger, 1965). The relationship between β and the power law index is similar to the relationship between β and the index in the Ellis model. The Ellis model reduces to the power law model when the power law constitutive equation is represented by;

$$\mu = S\dot{\gamma}^{n_p - 1} \qquad (2 - 41)$$

$$A = 0 \quad , \quad B = \frac{1}{S^\alpha} \quad , \quad \alpha = \frac{1}{n_p} \qquad (2 - 42)$$

In equation 2-41, $\dot{\gamma}$ is the shear rate, S is the viscosity at shear rate of one reciprocal of second and n, is the power law index. Based on equations 2-42, the values of parameter β relating to the Ellis index, α, can be estimated based on the power law values of parameter β. The semi empirical parameter β is given in Table 1 relating to the Ellis index α while the corresponding data of β for the power law index n_p is shown in Table 2.

Table 2-1: Semi empirical parameter β as function of Ellis index α

Ellis index α	β	Ellis index α	β
1	0.4166	3	0.1068
1.5	0.2567	3.5	0.08784
2	0.1755	4	0.07620
2.5	0.1329	4.5	0.0647

Table 2-2: Semi empirical parameter β as function of power law index n_p (Roy and Dutt, 1981)

Power law index n_p	β	Power law index n_p	β
0.3	1.8619	0.7	0.6174
0.4	1.2194	0.8	0.5317
0.5	0.9165	0.9	0.4671
0.6	0.7371	1.0	0.4166

The data for the Ellis index α is given in Table 2-1, and corresponding data for the power law index n is shown in Table 2-2.

The withdrawal velocity can be obtained from equations 2-24, 2-26 and 2-40.

$$\frac{\rho g^{\frac{2}{3}}}{\sigma m_0} \frac{2}{a_c} \left[\frac{3.36(M_0 N_{GO})}{1+3.36(M_0 N_{GO})} + \frac{0.5}{M_0 N_{GO}} \right] = \beta \left(\frac{2^{\alpha+1}\mu_0 U_w(\tau_{\frac{1}{2}})^{\alpha-1}}{\alpha m_0^{\alpha+1}\rho^\alpha g^\alpha F(M_0)} + C \right)^{\frac{2}{3}} \qquad (2-43)$$

The velocity for the withdrawal of cylinders from Ellis fluids can be predicted by equation 2-44.

$$U_w = \left[\left(\frac{2C_m}{a_c \beta} \right)^{\frac{3}{2}} \frac{\rho g}{\sigma m_0} - C \right] \frac{\alpha m_0^{\alpha+1}\rho^\alpha g^\alpha F(M_0)}{2^{\alpha+1}\mu_0(\tau_{\frac{1}{2}})^{\alpha-1}} \qquad (2-44)$$

The film thickness, cylinder radius, and physical properties of coating liquid are required to calculate the speed at which the cylinder substrate must be withdrawn to achieve the constant coating film thickness.

If the actual coating velocity is $< U_w$, the film thickness will be less than the estimated value.

2.4 « Experimental Procedure »

The material used in the coating of fiber optic diffusers is a formulation to provide capability of light scattering using titanium dioxide dispersed in a UV curable resin (1186-MT, Dymax Corp.) for the application in photodynamic cancer therapy.

The resin cures via photo initiated free-radical crosslinking polymerization. This resin is a complex mixture of multiple components, but is primarily composed of acrylated polyurethane oligomers and acrylic acid. The TiO_2 grades differ in terms of their surface treatment, mean particle diameter and dispersability in the polymer resin (Kostanski et al., 2009).

The experiments were done by Pope (2007) and the experimental data belong to two different grades of TiO_2 particles (RCA, Kalamazoo paper chemicals and Kronos1014, Kronos Worldwide) suspended in the resin. This resin is a complex mixture of multiple components but is primarily composed of acrylated polyurethane oligomers and acrylic acid. The TiO_2 grades differ in terms of their surface treatment, mean particle diameter and dispersability in the polymer resin (Kostanski et al., 2009). The coating of fiber optic with Dymax1186-MT resin, is shown in Figure 2-2.
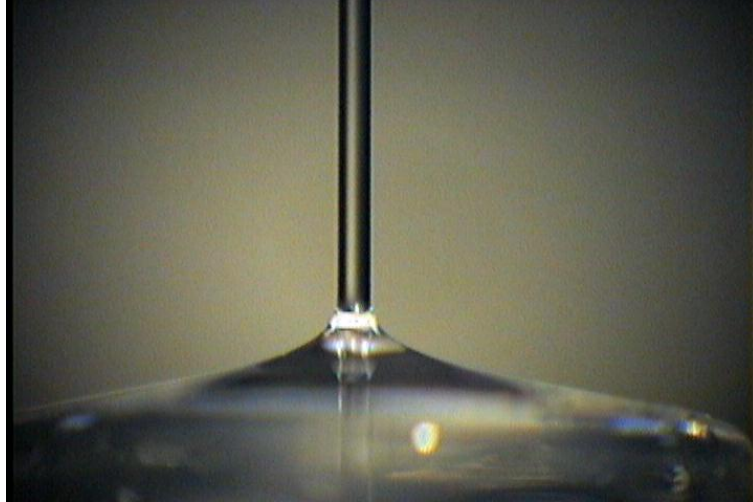
Figure 2-2: Dip coating of optical fiber with Dymax1186-MT resin (without titanium dioxide)

The rheological properties and surface tension of these suspensions were analyzed and corresponding values are represented in Table 2-3 and 2-4. The values displayed in Table 2-3 and 2-4 input as parameters into models of free withdrawal coating for the comparison of the models prediction and experimental data. Rheological measurement was carried out using a controlled stress ATS rheometer using a cone and plate geometry and the pendant drop method was applied to estimate the surface tension of the different suspensions. Shear viscosity as a function of shear rate for Dymax1186-MT resin with RCA and Kronos grade of TiO_2 particles are shown in Figure 2-3 and 2-4 respectively. The rheology measurements have been performed at 22 $°C$ as room temperature.

The coating procedure is performed using 15 cm samples of 100 μm diameter optical fibers. Fibers were stripped by soaking in acetone and pretreated by boiling in sulfuric acid. The coating resin was introduced into a liquid reservoir and the required withdrawal speed was programmed for an Instron 3366 tensile testing machine, which is used to withdraw the fiber at constant speed.
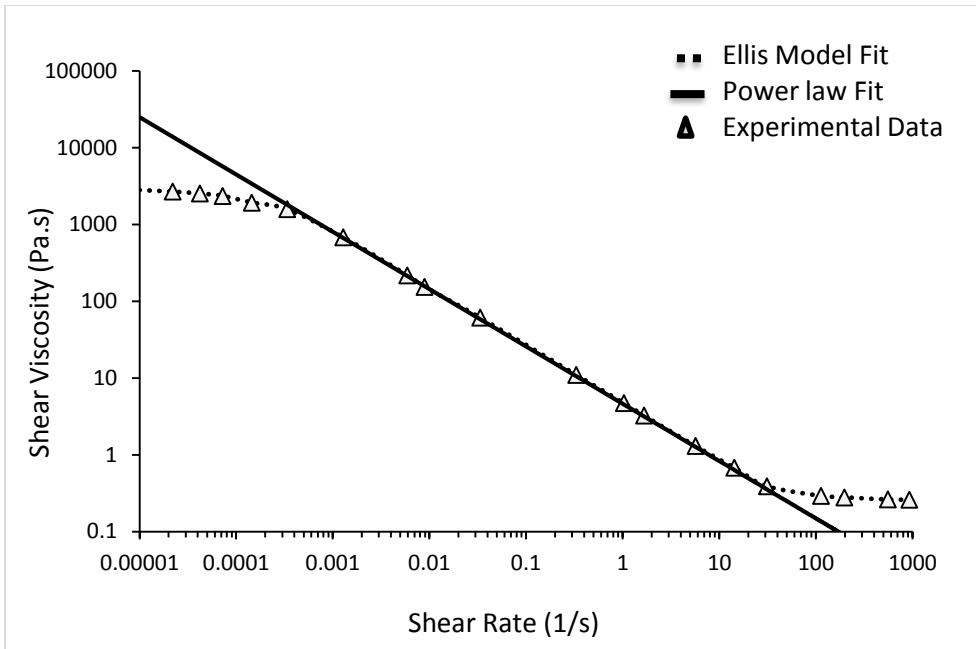
Figure 2-3: Shear viscosity as a function of shear rate for Dymax1186-MT resin with RCA grade of TiO$_2$ particles (Pope, 2007)
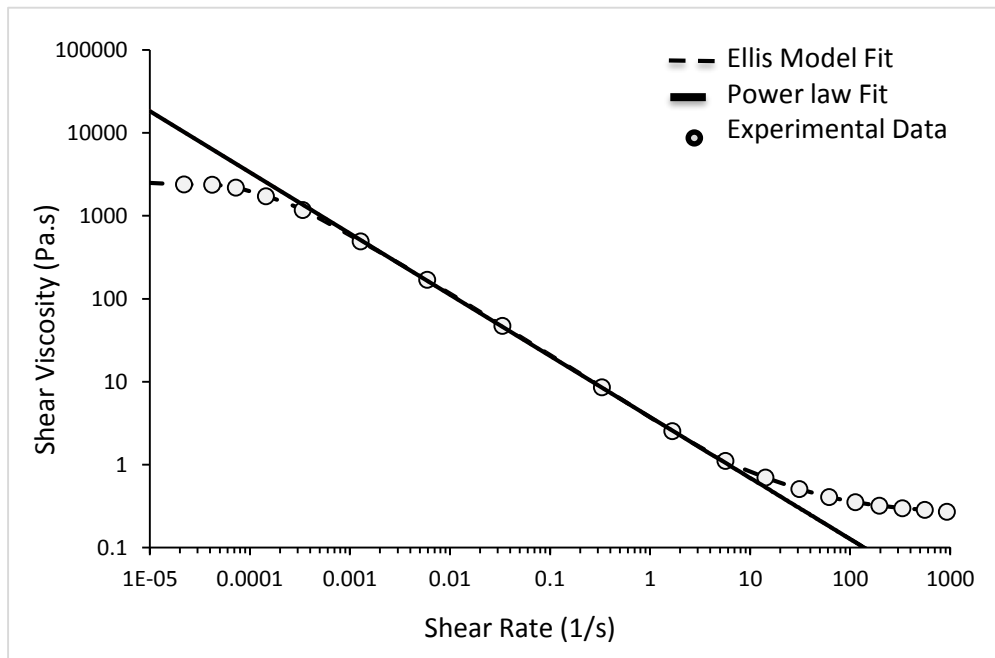
Figure 2-4: Shear viscosity as a function of shear rate for Dymax1186-MT resin with Kronos grade of TiO$_2$ particles (Pope, 2007)

All TiO$_2$ grades showed similar shear thinning behavior with a Newtonian plateau in low shear rates. Ellis model and power law parameters were regressed to the experimental data for each TiO$_2$ suspension.

The power law equation applied in this study is denoted in equation 2-43, where S is the constant value of power law, $\dot{\gamma}$ is the shear rate and n is the power law index.

$$\mu = S\dot{\gamma}^{n_p - 1} \qquad\qquad (2-43)$$

The power law parameters for each suspension are given in Table 2-3, and the Ellis parameters are given in Table 2-4.

Table 2-3: Power law parameters fitted to experimental data obtained for suspensions of different grades of TiO$_2$

TiO_2 Grade	Power law parameters		
	$S(\text{pa s}^n)$	n_p	σ (N m^{-1})
RCA	5.7	0.29	0.027
Kronos	4.9	0.35	0.022

Table 2-4: Ellis parameters fitted to experimental data attained for suspensions of different grades of TiO$_2$

TiO_2 Grade	Ellis parameters			
	$\mu_0(\text{Pa s})$	α	$\tau_{\frac{1}{2}}(\text{Pa})$	$\sigma(\text{N m}^{-1})$
RCA	2782	3.44	0.44	0.027
Kronos	2563	2.87	0.18	0.022

2.5   « Results and Discussion »

The White and Tallmadge solution for the case of cylinder withdrawal from a Newtonian fluid (1966), and the Roy and Dutt derived relationship for power law fluids (1981) were used as comparator cases. In Figures 2-5, 2-6 and 2-7 the prediction results of Ellis (this work), power law and Newtonian models are compared with experimental data of the coating thickness for the two different titanium dioxide dispersions on optical fiber. The addition of 1 vol% of TiO_2 to this resin was expected to slightly increase the viscosity and power law index of the suspension.

It is found that good agreement between coating thickness data and the Ellis model, compared to the power law and Newtonian model solutions.
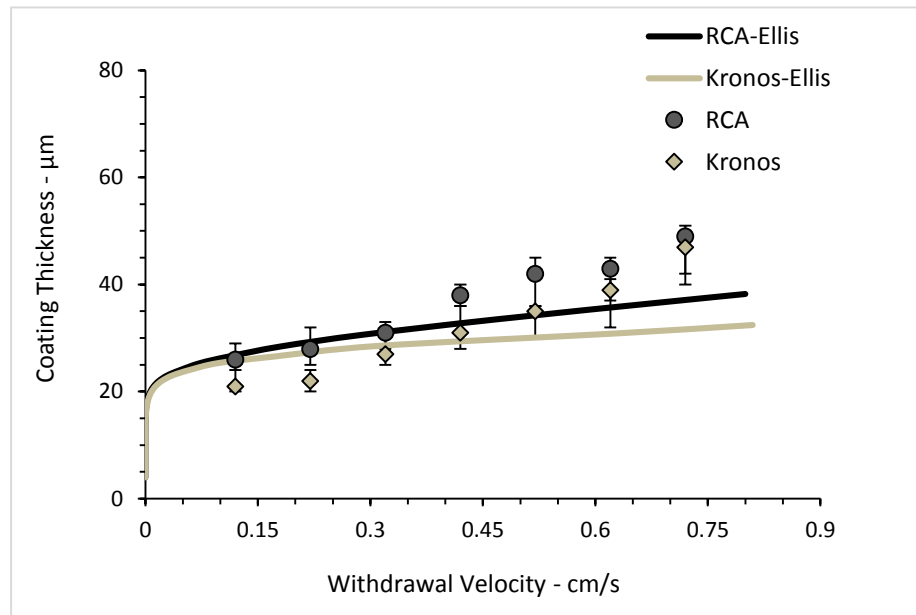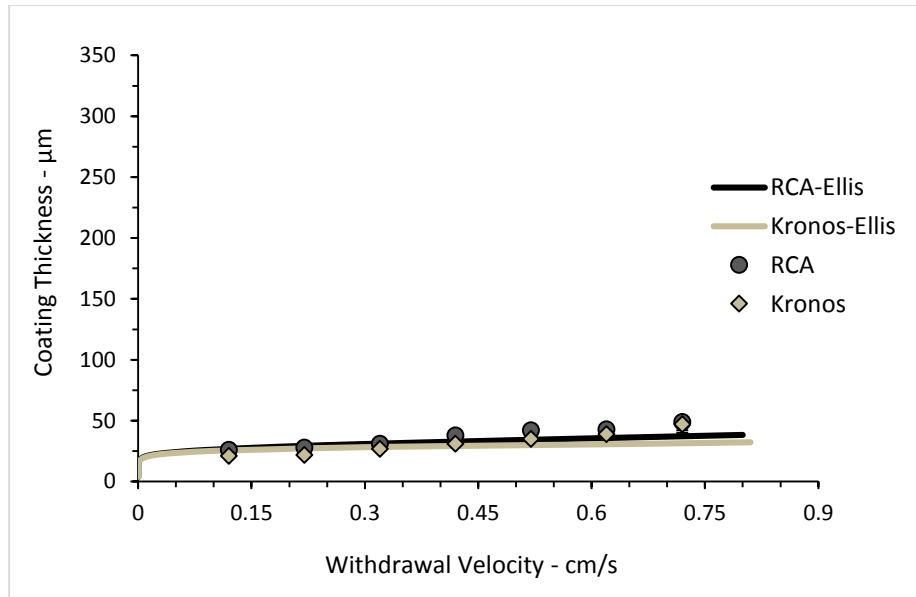
Figure 2-5 a,b: Ellis predictions of coating thickness (lines) compared to experimental data (symbols) of two different grades of TiO_2 (RCA and Kronos)
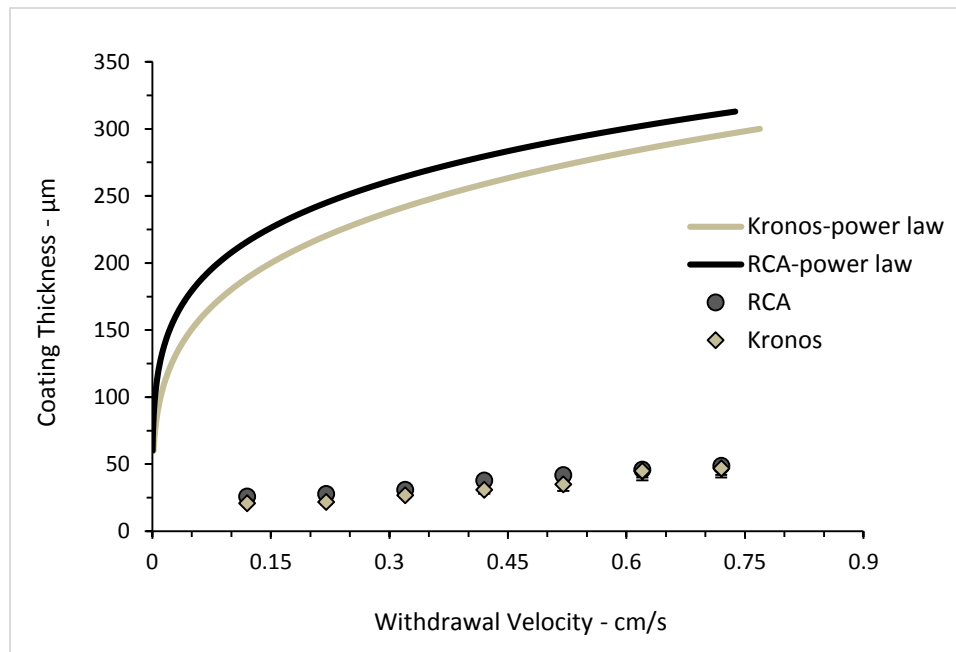
Figure 2-6: Power law predictions of coating thickness (lines) compared to experimental data (symbols) of two different grades of TiO_2 (RCA and Kronos)
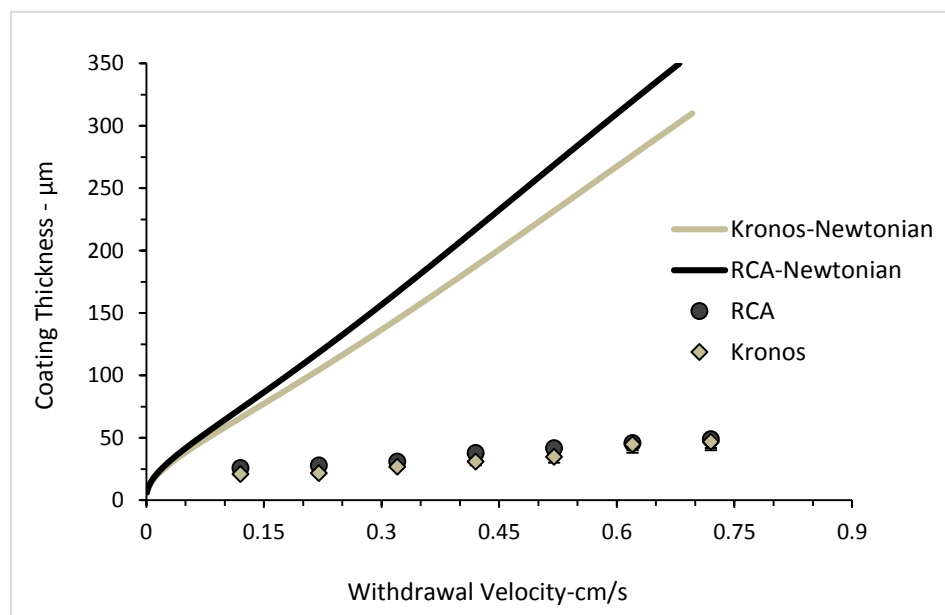
Figure 2-7: Newtonian prediction of coating thickness (lines) compared to experimental data (symbols) of two different grades of TiO_2 (RCA and Kronos)

In the case of analytical solution for Newtonian fluid, the power law index n is set to 1 and power law constant value S is considered as μ for the viscosity of Newtonian fluid. The viscosity value at shear rate of 1 sec^{-1} is the same for all three constitutive models, i.e. Newtonian, Ellis and power law. The particle interaction effect has not been taken into account.

2.6 « Conclusion »

A new model has been developed for the prediction of deposited coating thickness in dip coating of cylindrical substrates by withdrawal from a bath of an Ellis fluid extending previous work for Newtonian and power law fluids.

Experimental investigation has been performed for the coating of fiber optic diffusers used in photodynamic cancer therapy and the coating layer thickness compared with the results of the theories.

Good agreement between the model developed using Ellis constitutive equation with experimental data, indicates the significant role that the low shear rate viscosities play in predicting coating thickness for dip coating.

2.7 « References »

Adedijaberi A., Bhatara G., Shagfeh E. S. G., Khomami B., A computational study of the influence of viscoelasticity on the interfacial dynamics of dip coating flow, Journal of Non-Newtonian Fluid Mechanics, Vol. 166, pp. 614, 2011

Grunig J., Skale T., Kraume M., Liquid flow on a vertical wire in a countercurrent gas flow, Chemical Engineering Journal, Vol. 164, pp. 121, 2010

Gutfmger C., Ph.D. Thesis, Yale University, US, 1965

Gutfinger, C., Tallmadge, J. A., Films of non-Newtonian fluids adhering to flat plates, American Institute of Chemical Engineering Journal, Vol. 11, pp. 403, 1965

Kostanski L.K., Pope M. A., Hrymak A. N., Gallant M., Whittington W. L., Vesselov L., Development of novel tunable light scattering coating materials for fiber optic diffusers in photodynamic cancer therapy, Journal of Applied Polymer Science, Vol. 112, pp. 1516, 2009

Landau L., Levich B., Dragging of a liquid by a moving plate, Acta physicochim, URSS, Vol. 17, pp. 42, 1942

Middleman S., Fundamentals of Polymer Processing, McGraw-Hill, New York, 1977

Peralta J. M., Meza B. E., Zorrilla S. E., Mathematical modeling of a dip-coating process using a generalized newtonian fluid. 1. Model Development, Industrial Engineering and Chemistry Research, Vol. 53, pp. 6521, 2014

Pope M, Free-Withdrawal coating with UV-curing titania filled resins – Modeling and die design, Undergraduate Thesis, Department of Chemical Engineering, McMaster University, 2007

Roy S. C., Dutt D. K., Wire coating by withdrawal from a bath of power law fluid, Chemical Engineering Journal, Vol. 36, pp. 1933, 1981

Tallmadge J. A., A Withdrawal theory for Ellis model fluids, American Institute of Chemical Engineering Journal, Vol. 12, pp. 1011, 1966

Tallmadge J. A., Gutfinger C., Entrainment of liquid films drainage, Withdrawal and Removal, Industrial Engineering and Chemistry Research, Vol. 59, pp. 19, 1967

Tallmadge J. A., The method of addition for deriving continuous withdrawal equation, American Institute of Chemical Engineering Journal, Vol. 14, pp. 837, 1968

Tallmadge J. A., Improved withdrawal theories for cylinders by a more accurate description of curvature of static menisci, American Institute of Chemical Engineering Journal, Vol. 15, pp. 941, 1969

Tallmadge J. A., Withdrawal of flat plates from power law fluids, American Institute of Chemical Engineering Journal, Vol. 16, pp. 925, 1970

White D. A., Tallmadge J. A., Theory of drag out of liquids on flat plates, Chemical Engineering Science, Vol. 20, pp. 33, 1965

White D. A., Tallmadge J. A., A gravity corrected theory for cylinder withdrawal, American Institute of Chemical Engineering Journal, Vol. 13, pp. 745, 1966

Chapter 3

3 « Numerical Simulation and Wall Effect »

This chapter is based on the paper "Numerical simulation of the dip coating process with wall effects on the coating film thickness" Published in the Journal of Coatings Technology and Research, September 2015, Volume 12, Issue 5, pp 843-853, and presented at the European Coating Symposium (ECS), Mons, Belgium, 2013 and presented at the International Symposium of Coating Science and Technology (ISCST) annual meeting, San Diego, USA, 2014.

3.1 « Abstract »

The dip coating process for liquid film deposition on cylindrical substrates is numerically simulated and the effects of the coating bath walls proximity to the substrate are investigated for the deposited film thickness. In the present work, the hydrodynamics of non-Newtonian liquid films are studied, applying Carreau and power law models. The free surface position is determined by the Volume of Fluid (VOF) technique in a three dimensional system while the impacts of density, viscosity and surface tension are taken into account. The momentum and mass balance, alongside the constitutive equations were solved for dip coating process using numerical simulations in an open source CFD software package of OpenFOAM. Numerical outcomes are validated with experimental data over a large range of withdrawal velocities up to $6\ m/s$. Also good agreement is obtained for numerical simulation results with experimental data for coating thickness, considering the proximity effects of bath walls to the cylindrical substrate being withdrawn from a coating bath.

3.2 « Introduction »

Vertical withdrawal of a substrate from a Newtonian or non-Newtonian pool of liquid, known as dip coating or free coating, is an inexpensive method of depositing a thin,

58

uniform layer of materials in the liquid state onto a substrate (Kistler and Schweizer, 1997). In this process, the surface to be coated is initially immersed in the coating fluid and then withdrawn. One of the advantages of this process is the ability to coat irregularly shaped substrates (Kistler and Schweizer, 1997; Peralta et al., 2014). Dip coating, is a popular post-metered coating method, and nowadays dipping and withdrawal is not only used to apply the coating, but also to control the final microstructure of the coated film (Colosqui et al., 2013).

Free coating is essential for the surface engineering of high quality products and it is one of the better developed ways to enhance and alter the physical and mechanical surface characteristics. For instance, the performance properties of optical fibers, including abrasion resistance and strength, are strongly influenced by adding a coated layer (Yang et al., 2008). In recent years electro-active polymers have received attention because of their distinct potential as actuators and sensors, and the cylindrical shape may bring explicit advantages to actuator design (Yang et al., 2008; Watanabe et al., 2004).

Therefore, cylindrical micro fabrication is of interest, particularly due to the advantages conferred by the geometry of the substrate. Unlike planar substrates, cylindrical substrates offer axisymmetric flexibility, complete surface area utilization, and radial symmetry. These exclusive properties offer opportunities such as catheter based electronics in the medical industry, fiber optic modulation for medical devices, or equipment for heat and mass transfer in gas-liquid systems to provide a large interfacial area (Grunig et al., 2010).

The thickness of the liquid layer that remains on the surface of substrate depends on the viscosity, surface tension of the coating fluid, gravity and the speed of withdrawal. The principle complicating feature of dip coating problems, is the strong role played by the free surface in controlling the coating dynamics, particularly in the region, where the object leaves the surface of the coating fluid bath (Middleman, 1977).

The calculation of coating film thickness started with the work of Landau and Levich (1942) and Derjaguin (1943). Guttfinger and Tallmadge (1965) estimated coating film thickness for Non-Newtonian fluids on flat plates. However, in considering a film on a

highly curved surface, where the radius of curvature of the coated surface is in the order of magnitude of the film thickness, the film flow can no longer be approximated by a planar coating film.

A significant improvement in film thickness assessment was attained by White and Tallmadge (1967) with the gravity corrected model for cylindrical substrates. There is smaller number of studies on cylindrical substrates compared to flat plate substrates due to the difficulties in solving the final equation. Furthermore, handling both curvature effects and non-Newtonian coating fluids, which are more realistic in the industries, makes analytical calculation very complicated for dip coating process of cylindrical geometries. Accordingly, for handling the substrate geometries and interfacial phenomena, sound knowledge regarding the relationship between the final coating thickness, withdrawal speed and fluid properties is essential for effective design, scale up, optimal control, and efficient operation of the free coating process.

3.3   « Theoretical Procedure »

Dip coating process is characterized by the physical conditions of liquid and gas and the topology of the interface (Rusche, 2002). Development of an approach that predicts substantial details with sufficient accuracy in the entire flow field is essential for free coating system. In this study, dip coating process numerically studied by an open source computational fluid dynamics package (*OpenFOAM - Open Source Field Operation and Manipulation*) and three dimensional simulations are developed in order to capture all of the physically important features of the free surface flows. In addition, the volume of fluid method (VOF) is applied with the benefit of handling the evolution of free surface (Hirt and Nicholls, 1981). Discretization of equations are obtained by the Finite Volume methods (FVM) applying a collocated variable arrangement (www.openfoam.org, 2013; Ferziger and Peric, 1996).

In a VOF method, the free surface is identified by a marker function such as the volume fraction of a tracking variable, unlike surface-fitting methods, which treat the free surface

as a moving boundary of the computational domain. Surface-fitting methods are very efficient for free surface problems, but the validity is tested by the skewness of the resulting grid. If the free surface becomes highly distorted a new mesh may have to be generated to maintain the accuracy of the solution. There are other limitations in the cases of wave breaking and fluid–fluid interactions, such as the trapping of one fluid within another, as in this case no explicit boundary conditions can be specified at the interface (Farm et al, 1994; Qian, 2006).

An advantage of the VOF technique and FVM applied in this study, is the ease of code implementation and working with parallel simulation of three dimensional systems in OpenFOAM. The main disadvantage of the VOF technique is the limited accuracy of results in numerical simulation with large mesh elements. Therefore, to overcome the disadvantage of VOF method, the mesh is densified with reasonably small elements around the cylindrical substrate surface.

3.3.1 « Mathematical Formulation »

Incompressible flows in free coating process, governed by the Navier-Stokes and continuity equations. In OpenFOAM, the individual terms of the transport equation are treated separately.

The approach used here, is to consider the density and viscosity as variables over the entire domain, but constant in each specific fluid. The conservation of momentum (equation 3-1) and the conservation of mass (equation 3-2) govern the fluid flow over the whole domain, where u and ρ represents the velocity field and density respectively, shared by the two fluids throughout the flow domain, τ is the stress tensor and F_b denotes the body force.

$$\frac{\partial \rho u}{\partial t} + \nabla.(\rho uu) = -\nabla P + \rho g + \nabla.(\tau) + F_b \qquad (3-1)$$

$$\nabla.(u) = 0 \qquad (3-2)$$

In the solution process, piezometric pressure $P_{rgh} = P - \rho g.x$ is implemented instead of the pressure P, where x is the coordinate vector and g is the gravitational acceleration. Accordingly, $-\nabla P + \rho g$ has to be rearranged as $-\nabla P_{rgh} - (g.x)\nabla\rho$ and the momentum equation developed into equation 3-3.

$$\frac{\partial \rho u}{\partial t} + \nabla.(\rho u u) = -\nabla P_{rgh} - (g.x)\nabla\rho + \nabla.(\tau) + F_b \qquad (3-3)$$

The momentum equation, is modified in order to account for the surface tension effects. At the liquid-gas interface, surface tension generates an additional pressure gradient resulting in a force, which is evaluated per unit volume using the continuum surface force (CSF) model of Brackbill et al (1992). The numerical solution procedure for the two fluid methodology is based on the PIMPLE (Pressure Implicit- method for pressure-linked equations) algorithm, which is a combination of PISO (Pressure Implicit Split Operator) algorithm proposed by Issa (1986) and SIMPLE (Semi Implicit Methods Pressure Linked Equations) algorithm to handle the pressure-velocity coupling (Patankar, 1980; Patankar and Spalding, 1972).

3.3.2 « Free Surface Implementation»

The volume of fluid method is a technique to capture the interface, proposed by Hirt and Nicholls (1981).

The VOF method accommodates free surfaces by an indicator function with large deformation on a non-uniform fixed grid system. The phase fraction α_1 can take values within the range $0 \leq \alpha_1 \leq 1$, with the values of zero and one corresponding to regions accommodating only one phase and for the interface where the value of α_1 lies between 0 and 1.

Movement of the free surface is accomplished by calculating net mass flux through control surfaces and by updating the fluid volume fraction in each control volume. The

free surface position can be predicted by solving the continuity equation for the indicator function, represented in equation 3-4.

$$\frac{\partial \alpha_1}{\partial t} + \nabla \cdot (\alpha_1 u) = 0 \qquad\qquad (3-4)$$

Conservation of the phase fraction is a critical issue in numerical simulation of free surface flows using the VOF model. This is especially the case in flows with high density ratios, where small errors in volume fraction may lead to significant errors in the calculations of physical properties. Moreover, accurate calculation of the phase fraction distribution is crucial for a proper evaluation of surface curvature, which is required for the determination of surface tension forces and the corresponding pressure gradient across the free surface (Ubbink and Issa, 1999). An artificial surface compression term is added to the interface continuity equation to overcome the problem of a smeared free surface. This technique developed by Rusche (2002) and defined in equation 3-5.

$$\frac{\partial \alpha_1}{\partial t} + \nabla \cdot (\alpha_1 u) - \nabla \cdot (\alpha_1(1 - \alpha_1)u_{r\alpha}) = 0 \qquad\qquad (3-5)$$

An artificial surface compression term leads to a sharper interface between the two different fluids, where $u_{r\alpha}$, is the compression velocity expressed by equation 3-6. C_α is the compression factor, which yields a conservative compression if the value is one and enhances compression for values greater than one. The compression factor provides no contribution if it is set to zero.

$$u_{r\alpha} = \min\left(C_\alpha |u|, max_G |u| \frac{\partial \alpha_1}{|\partial \alpha_1|}\right) \qquad\qquad (3-6)$$

The artificial surface compression term affects only the liquid surface due to $\alpha_1(1 - \alpha_1)$, whereby $max_G |u|$ is the global maximum value of the velocity field.

According to the VOF method, calculation of physical properties illustrated in equations 3-7 and 3-8 as a weighted average, based on the distribution of the liquid volume fraction, where ρ_l and ρ_g are densities of liquid and gas, respectively. The average

viscosity is represented by μ, that shared by the two fluids throughout the flow domain. Correspondingly μ_l and μ_g are the viscosities of liquid and gas.

$$\rho = \alpha_1 \rho_l + (1 - \alpha_1)\rho_g \qquad (3-7)$$

$$\mu = \alpha_1 \mu_l + (1 - \alpha_1)\mu_g \qquad (3-8)$$

Hence, the momentum continuity, equation 3-1 for the mixture of the two phases remains the same, but is treated with the mixture velocity and surface tension considered as an additional body force, which is developed as equation 3-9.

$$\frac{\partial \rho u}{\partial t} + \nabla.(\rho u u) = -\nabla P_{rgh} - (g.x)\nabla \rho + \nabla.(\tau) + \sigma k \frac{\partial \alpha_1}{|\partial \alpha_1|} \qquad (3-9)$$

Whereby $k = -\nabla.(\frac{\partial \alpha_1}{|\partial \alpha_1|})$ is the curvature of the interface and σ is the surface tension (Brackbill, 1992).

3.3.3 « Constitutive equations »

Numerical simulation of free coating process for non-Newtonian fluids has been prepared by implementing the power law and Carreau models in the calculations. In this system, for Newtonian fluids the rate of strain tensor is linearly related to the stress tensor, τ, given by equations 3-10 and 3-11. The viscosity of fluid is characterized by μ which is a constant value for Newtonian fluids.

$$\dot{\gamma} = (u + (\nabla u)^T) \qquad (3-10)$$

$$\tau = -\mu \dot{\gamma} \qquad (3-11)$$

The viscosity and shear rate expression for power law fluids is defined by equation 3-12. In this equation, $\dot{\gamma}$ is the shear rate, S is the viscosity at shear rate of one reciprocal of second and n_p, is the power law index.

$$\mu = S\dot{\gamma}^{n_p - 1} \qquad (3-12)$$

For Carreau fluids, the viscosity and shear rate relationship is given by equation 3-13, in which, μ_0 is the zero shear rate viscosity and μ_∞ is the viscosity at the shear rate of infinity. λ and n_c are two other parameters of Carreau constitutive equation.

$$\mu = \mu_\infty + (\mu_0 - \mu_\infty)\left[1 + (\lambda\dot{\gamma})^2\right]^{(n_c-1)/2} \qquad (3-13)$$

Parameters of the power law and Carreau models are calculated by fitting the experimental data of rheological measurements.

3.4 « Numerical Procedure »

In the current study, OpenFOAM is employed with parallel computing using 2 dual core processors. In order to ensure stability of the solution procedure, the calculations are performed using a self-adapting time step which is adjusted at the beginning of the time iteration loop based on the Courant number, defined as $Co = (u/\Delta x)\Delta t$, where Δt is the time step and Δx is the cell size in the direction of the velocity.

Using values for velocity and Δt^0 from previous time step, a maximum local Courant number Co^0, is calculated and the new time step is evaluated from equation 3-14.

$$\Delta t^n = \min\left\{\frac{Co^{max}}{Co^0}\Delta t^0, \left(1 + \beta_1\frac{Co^{max}}{Co^0}\right)\Delta t^0, \beta_2\Delta t^0, \Delta t_{max}\right\} \qquad (3-14)$$

Where Δt_{max} and Co^{max} are corresponding prescribed values for the time step and Courant number at the run time and for this study the Co^{max} is set to 0.5 and the value of Δt_{max} is 1. To avoid time step oscillations that may lead to instability, the increase of the time step is restrained using β_1 and β_2 as damping factors according to the conditions in equation 3-14. The time step that is estimated using equation 3-14 is the global time step for the system calculated at every step of calculation process.

Considering the impact of the meshing on Courant number, it can be concluded that for small grid sizes, small time steps are needed to keep the Courant number below its maximum value of 0.5.

In numerical simulation, the discretization process is usually carried out as a first step toward numerical evaluation and it proceeds by defining the boundary conditions of the simulation domain.

3.4.1 « Grid Generation »

CFD problems usually require discretization of the problem into a large number of cells/grid points. In this work, simulation domains for cylindrical coating baths, considered with radius of 4 to 65 times the radius of substrate and height of 20 to 80 times the substrate radius. The cylindrical substrate was centered in the coating bath. Three dimensional meshes have been created for finite volume analysis as a discrete representation of the flow domain.

Mesh quality is an essential factor for an accurate solution. Therefore, the mesh around the cylindrical substrate is refined by adding 40 to 60 layers of mesh to increase the mesh density in the zone of interest around the substrate. In order to optimize the simulation time, a coarse mesh is used for areas far from the substrate. In the densified mesh region around the cylinder, the first layer of mesh is approximately 1 μm and to ensure smoothness in mesh, a 2 to 5 percent increase in subsequent mesh layer thickness has been applied relative to the first layer. This percentage of increase in element size, provides a smooth transition to the coarse mesh area. Figure 3-1, shows the cross section of grid with densified mesh layers around the cylindrical substrate. All meshes consist of hexahedral elements around the cylinder to generate body fitted grids.
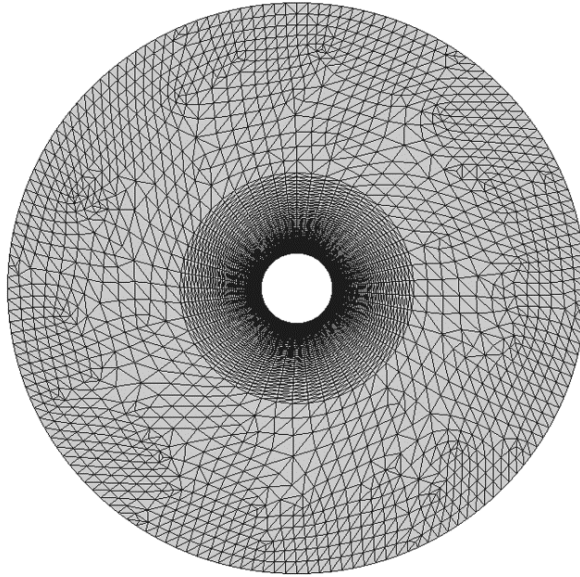
Figure 3-1: Cross section of grid in the coating bath

For the mesh independence study, the simulation was run on the initial mesh and residual was below 10^{-8} for variables, which was acceptable in the defined tolerance. When the convergence criteria were met for the first simulation, the mesh was refined globally and finer cells were generated throughout the domain with 1.5 times the initial mesh size. The simulation was carried out with globally refined mesh and residual error dropped below 10^{-8} with 2% difference with the first mesh results. Achieving relatively the same results for the film thickness and residual errors with the refined mesh, indicated the described mesh resolution was accurate enough to capture the coating film thickness on different cylindrical substrate sizes.

Three dimensional meshes were used to capture the flow effects in the dip coating process. The calculations could be performed on an axisymmetric grid to save simulation time by reducing the number of elements in the mesh, but the axisymmetric mesh requires ultra-small elements around the axis. These small elements decrease the time step due to the Courant number limit in the calculations and consequently with very small time steps the simulation time increases even more that what is required in the three dimensional case.

3.4.2 « Boundary Condition »

Boundary conditions need to be specified following the discretization of the simulation domain. Boundary conditions are defined for boundaries of coating bath and the cylindrical substrate as shown in Figure 3-2. In these simulations, boundaries are set as coating bath wall, bath base, coating bath top and cylindrical substrate. For each boundary the pressure, velocity and volume faction of α_1 are defined.
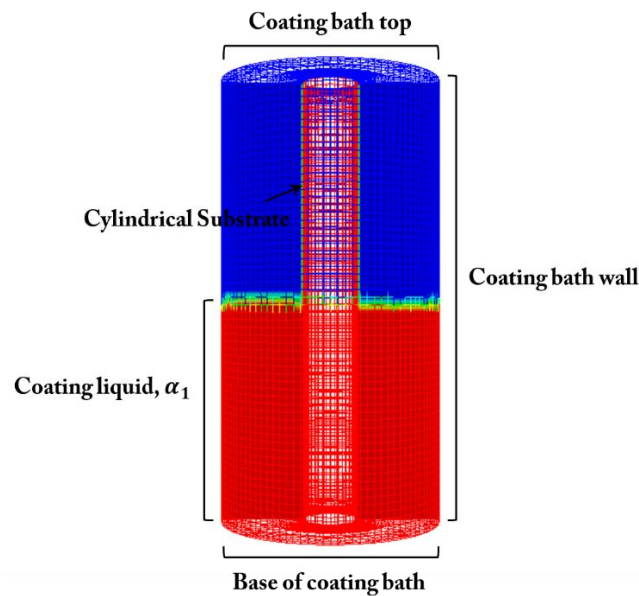
Figure 3-2: Boundary condition in continuous dip coating process

a. Coating bath wall

A zero gradient is set for pressure on the coating bath wall. The volume fraction of α_1 with a constant value for contact angle and zero value for velocity are set for this boundary

b. Base of coating bath

For the base region of the flow domain, the symmetry plane boundary has been set for velocity, pressure and volume fraction of α_1. In OpenFOAM this boundary condition is different from that of a zero gradient condition. Zero gradient sets the boundary value to the near-wall cell value whereas a symmetry plane has the same values for scalars but for

vectors all components parallel to the patch are mirrored while the normal components of vectors are set to zero

c. Coating bath top

Upper part of the simulation domain, which contains the gas phase, is open to the atmosphere. For this region, total pressure condition with the value of zero, is set for the pressure. Total pressure boundary condition is defined as $P = P_0 + \frac{1}{2}\rho|u|^2$ where P_0 is the atmospheric pressure and when u changes, P is adjusted accordingly.

Pressure-inlet-outlet-velocity, is the velocity boundary condition, applied for this region. This boundary condition can be employed, where the pressure is specified and reverse flow is possible or expected. When the flow is inward, the inflow velocity is set as a fixed value of zero and for the outflow, it is a zero gradient velocity condition.

For volume fraction of α_1, the inlet-outlet boundary condition is set in this region, which switches u and P between fixed value and zero gradient, depending on the direction of velocity. This boundary condition provides a generic outflow situation by apply zero gradient condition and specific inflow for the case of return flow with setting specified value for velocity, which has been set to zero in this study.

d. Cylindrical substrate

Boundary conditions for cylindrical substrate is considered as, fixed value velocity of the withdrawal speed, zero gradient for pressure and volume fraction of α_1.In the simulation of dip coating process, coating liquid adheres the substrate and leaves the flow domain by withdrawal of cylindrical substrate. The amount of liquid that leaving the system can be estimated by measuring the liquid level drop in the coating bath during the process.

There was a finite amount of liquid in the domain and during the simulation bath level decreases, as the liquid leaves the domain as a coated layer on the substrate.

3.5 « Results and Discussion »

3.5.1 « Validation of Simulation with previous experimental data »

Middleman (1978) reported film thickness data of 0.75% Polyox 301 solution as non-Newtonian coating fluid and a cylinder with radius of 262 μm was used for coating substrate. In addition, rheological properties of Polyox 301 solution presented by Middleman (1978) in the shear range of 1-1000 s^{-1}. In the present work, non-Newtonian effects on the coating film thickness, have been investigated by power law and Carreau constitutive equations in the simulations. The power law and Carreau models, are fitted to the reported rheological data of Middleman (1978) as illustrated in Figure 3-3.
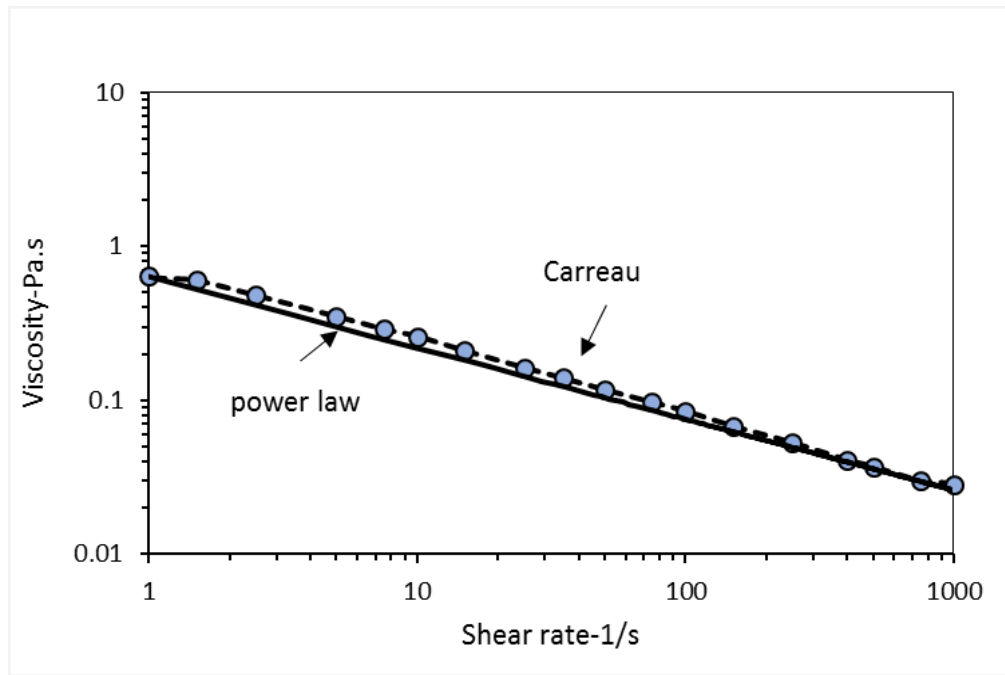
Figure 3-3: Rheological data (blue circles) of 0.75% Polyox 301 solution as non-Newtonian liquid (Middleman, 1978)

In addition, according to the rheological data of viscosity as a function of shear rate for 0.75% solution of Polyox 301 in water, associated parameters of power law and Carreau models are correlated to the reported rheological data (the fitted parameters are included based on all the experimental rheology data) and values are presented in Tables 3-1 and 3-2 respectively.

Table 3-1: Parameters of power law model

σ	ρ	n_p	K
0.062 N/m	1000 kg/m^3	0.64	0.66 (kg/m.s).s^{n-1}

Table 3-2: Parameters of Carreau model

σ	ρ	n_c	λ	μ_0	μ_∞
0.062 N/m	1000 kg/m^3	0.47	1.04	0.92 kg/m.s	0.01 kg/m.s

The results presented in Figure 3-4, are the numerical solution for coated film thickness for a wide range of withdrawal velocities for the cylindrical substrate with the radius of 262 μm in the non-Newtonian fluid.
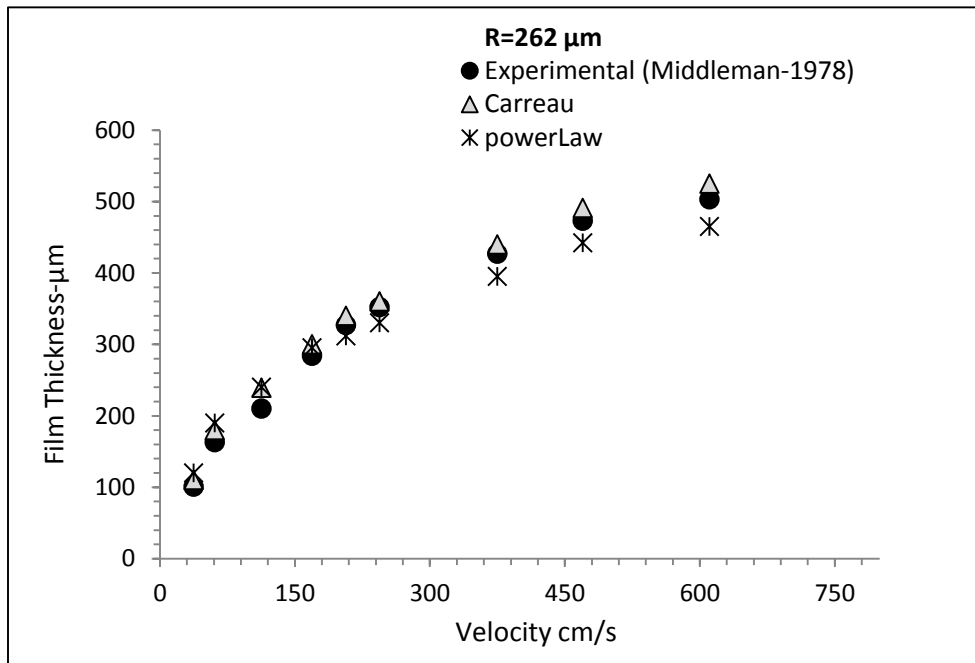
Figure 3-4: The numerical solution for coated film thickness by non-Newtonian fluid for a wide range of withdrawal velocities for the cylindrical substrate (R= 262 μm)

Carreau model has the capability of coating film thickness prediction in withdrawal velocities up to around $6 \ m/s$ when the coating layer is in the same order of substrate diameter and close agreement achieved between simulation results and experimental data.

Roy and Dutt (1981) reported film thickness data for mineral oil as Newtonian fluid and data are presented for two cylindrical substrates with radii of 317 and 445 μm. Physical properties of mineral oil are presented in Table 3-3, which was specified by Roy and Dutt (1981).

**Table 3-3:** Physical properties of mineral oil (Roy and Dutt, 1981)

σ	ρ	μ
0.028 N/m	876 kg/m^3	0.025 kg/m.s

Simulation data obtained for the final film thickness through numerical solution, compared with both experimental data and analytical solution of Roy and Dutt (1981).

Figure 3-5 illustrates the results of coating mineral oil as a Newtonian fluid onto the cylinders of radius 317 μm and the analytical solution is the simplified version of Roy and Dutt (1981) solution which reduces to White and Tallmadge solution for Newtonian fluids (1966). Similar to Figure 3-5, Figure 3-6 represents the coating results for mineral oil for a cylinder of radius 445 μm.

Capillary number is defined as $Ca = \mu u / \sigma$ and as a dimension less number, plays an important role in dip coating processes. Increasing the capillary number can be associated with high withdrawal speed or high viscosity of coating fluid increasing the film thickness. These results are expected and film thickness growth with increasing the withdrawal velocity is shown in Figure 3-4, Figure 3-5 and Figure 3-6. The power-law analytical solution of Roy and Dutt (1981) is restricted to small capillary numbers, which for mineral oil is valid up to a capillary number of 0.7 and limited to withdrawal velocities less than 0.8 m/s as shown in Figure 3-5 and Figure 3-6. The simulation results of the mineral oil coating film thickness, approach $Ca \sim 1.1$. Considering the

viscosity at a shear rate of $1\ s^{-1}$ for the solution of Polyox 301, the capillary number can be up to 60 for non-Newtonian simulations.
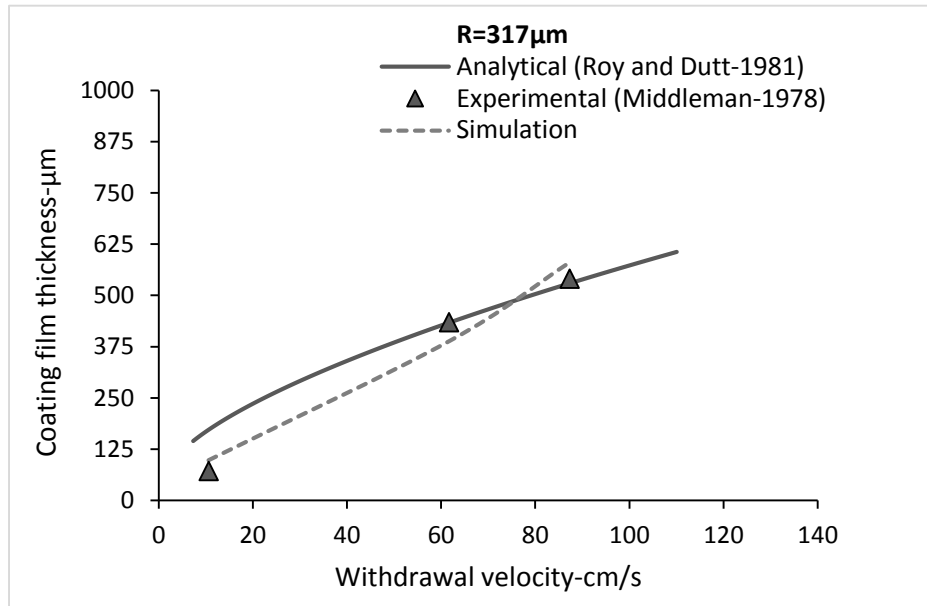

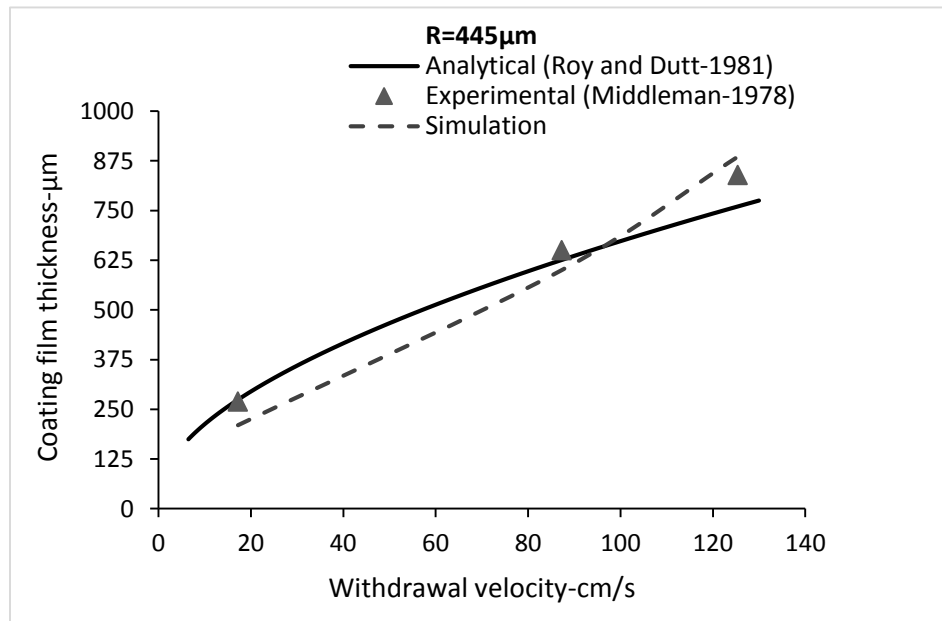**Figure 3-5:** Coating the cylinders of radius 317 μm with mineral oil

Figure 3-6: Coating the cylinders of radius 445 μm with mineral oil

3.6 « Wall Effect »

Wall effects in dip coating process are considered as additional factors for studying the deposited film thickness.

3.6.1 « Experimental »

Coated film thickness is measured above the coating bath surface at the point that the film thickness reaches a constant value and this point considered to be far from the coating meniscus. Images are captured using a high speed, high resolution camera, adjusted to capture 15 frames per second (IO industries camera model Flare 4M180-CL with resolution of 2048x2048 pixels). The camera is positioned about 30 cm above the bath surface and perpendicular to the cylindrical substrate. A black piece of paper was placed in the background and light sources provided around the coated film, which helped to ensure a clear view of the deposited film. Film thickness images have been captured by repeating the measurements eight times for each velocity and individual coating bath size. The precision of the measurements of film thickness is estimated to be within ± 10 μm over most of the range, without taking the parallax effect into account.

Different velocities applied by changing the speed of dip coater apparatus motor, with velocities limited to 15 cm/s. Acrylic tubes with different radius size are used as the coating baths for measuring the wall effects in the system.

Food grade mineral oil (FG WO 35 White Mineral Oil, Petro-Canada) is selected as the Newtonian fluid and 0.75% solution of polyethylene oxide (POLYOX WSR-301, Dow Chemical) with the molecular weight of 4,000,000 has been chosen as the non-Newtonian fluid for wall effects study. The cylindrical substrates used in this work have radii of 785 μm and 1590 μm, chosen based on the radii to be small enough for considering the substrate curvature in the same order of magnitude of coating film thickness and yet large enough to be able to capture the deposited film thickness in a photograph.

Figure 3-7, illustrates a schematic of the dip coating apparatus used in experiments and an actual picture of the coated substrate used for the film thickness measurement is shown as a subfigure.
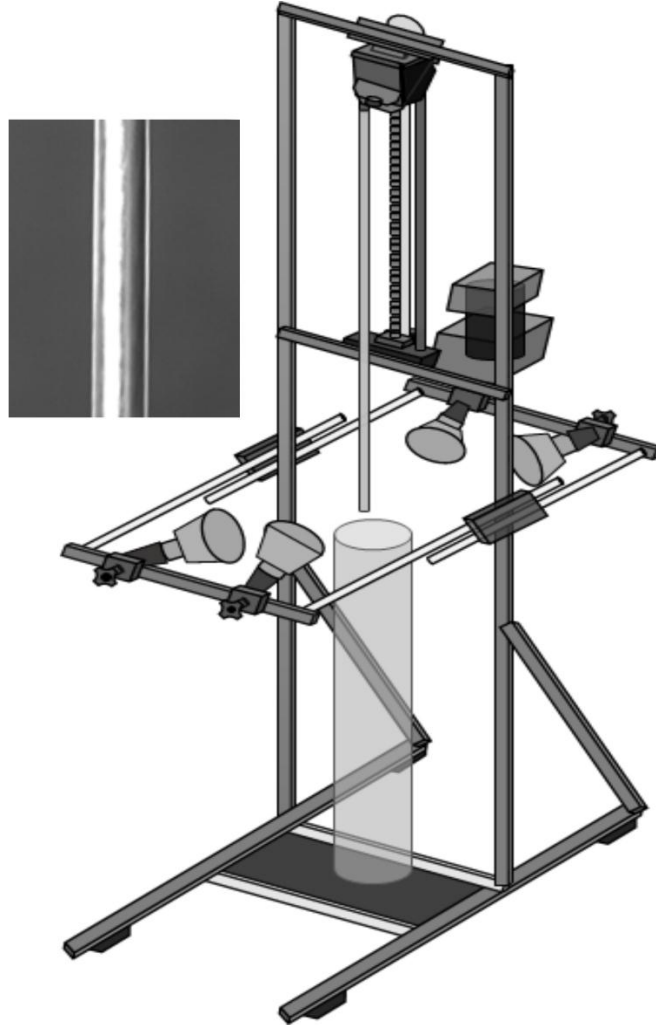
Figure 3-7: Schematic of the dip coating apparatus used in experiments and an actual picture of the coated substrate used for the film thickness measurement

Rheological data of polyethylene oxide solution differs based on the preparation method of solution and some of the effective factors are mixing time and intensity of mixing in producing the solution. Therefore, the rheological data attained using a rheometer (Rheometrics model RDS-II) for 0.75% POLYOX WSR-301 solution. Rheological tests have been conducted in a parallel plate geometry (diameter of $25\ mm$) and five samples

are taken from various parts of the solution to ensure the homogeneity of the prepared solution.

The rheological tests have been performed for the measurement of dynamic viscosity in a range of shear rate of 0.1 to 10000 s^{-1}.
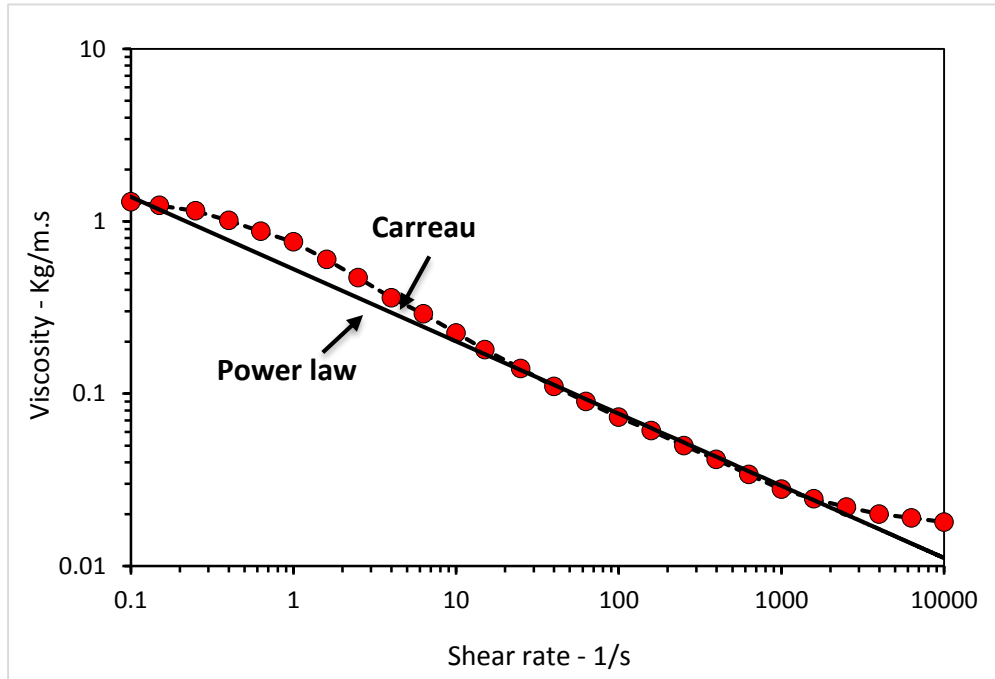
Figure 3-8: Rheological data (red circles) for 0.75% POLYOX WSR-301 solution and the power law and Carreau models are fitted to the measured data

Measurements for each sample were repeated three times to ensure the accuracy of the rheological quantifications.

All rheological measurements conducted at $22°C$, through setting the temperature of the rheometer at $22°C$ and homogeneity of the samples temperature was confirmed by measuring it before the rheological tests. In addition, total time of rheological tests for each sample arranged from 2 to 4 minutes thus the effect of drying of the sample at the edges was not observed for 0.75% POLYOX WSR-301 solution. Measured rheological data for 0.75% POLYOX WSR-301 solution is presented in Figure 3-8 and the power

law and Carreau models are fitted to the measured rheological data, similar to what has been employed for the rheological data of Middleman (1978).

Parameters of the power law and Carreau models are calculated based on the rheological data of Figure 3-8 and corresponding values are reported in Tables 3-4 and 3-5 respectively. In addition, physical properties of food grade mineral oil are presented in Table 3-6. Mineral oil is a Newtonian fluid and dynamic viscosity is the only rheological parameter is measured for this fluid.

Table 3-4: Parameters of the power law model are calculated based on the rheological data of polyox 301 solution and the contact angle value for polyox 301 solution and acrylic bath

σ	ρ	n_p	K	Θ
0.062 N/m	1003 kg/m^3	0.62	0.76 (kg/m.s).s^{n1}	65°

Table 3-5: Parameters of the Carreau model are calculated based on the rheological data of polyox 301 solution and the contact angle value for polyox 301 solution and acrylic bath

σ	ρ	n_c	λ	μ_0	μ_∞	Θ
0.062 N/m	1003 kg/m^3	0.44	1.224	1.03 kg/m.s	0.012 kg/m.s	65°

Table 3-6: Physical properties of mineral oil and contact angle value for mineral oil and acrylic bath

σ	ρ	μ	Θ
0.028 N/m	864 kg/m^3	0.036 kg/m.s	11°

The contact angle must be applied in the numerical calculations to recognize the effects of the coating bath wall proximity to the substrate, on the film thickness. In particular, the angle formed by the free surface with the solid substrate when the three phase contact line is moving is described as the dynamic contact angle.

The dynamic contact angle depends on the contact line speed and the entire flow field in the vicinity of the moving contact line (Blake and Shikhmurzaev, 2002). Based on the images taken from the contact angle during the experimental measurements, the contact angle remains relatively constant, while the substrate is being withdrawn and coating liquid level declines gradually in the coating bath. The relatively constant value of the contact angle can be due to the low withdrawal velocities applied in the experimental process and the steady state condition that develops in the flow field in the surrounding area of the contact angle, in which the contact line is moving, but the angle does not change significantly.

The bath-wall angle is considered as constant contact angle and the reason it is moving is because constant bath level was not maintained during the coating process. The bath level drop is assumed relatively slow, so the assumption of a constant contact angle is sufficient.

A constant value assumed for the dynamic contact angle and behavior of the dynamic contact angle approximated with a static contact angle (θ) between the fluids and an acrylic surface which measured with a contact angle goniometer (Rame-hart model 100).

The equilibrium static contact angle is implemented in the numerical calculations, to recognize its effects in the coating process and final coating film thickness. In the study of wall effects in dip coating process, the ratio of bath radius over cylinder substrate radius (R/r) is considered in the range of 4 to 60. The experimental practical minimum value for R/r is 4 to avoid oscillation of the cylindrical substrate during withdrawal and maintain the concentric position of the substrate in the coating bath.

3.6.2 « Simulation »

Food grade mineral oil and 0.75% solution of POLYOX WSR-301 in water selected for the investigation of Newtonian and non-Newtonian fluids respectively. The coating film thickness was measured at various withdrawal velocities and wall effects considered as a function of (R/r) which is coating bath radius over the cylindrical substrate radius. The simulation domain, bath radius (R) and cylinder substrate radius (r) are illustrated in Figure 3-9.

In the simulation of dip coating, the level of coating fluid in the bath decreases gradually by withdrawing the substrate from bath and contact angle at the bath wall remains constant similar to the images captured through the experimental measurements.
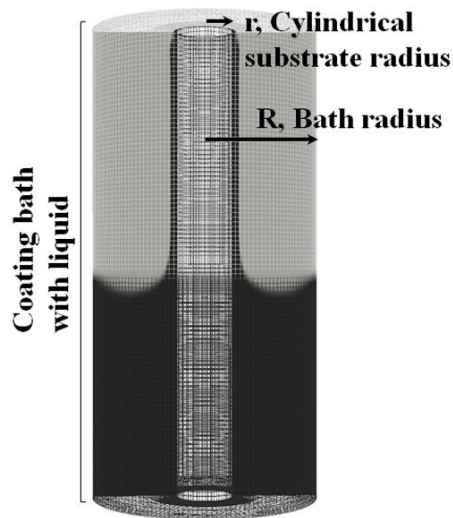
Figure 3-9: The simulation domain, (R) is the bath radius and (r) is the cylinder substrate radius

The film thickness is calculated for infinite bath depth by applying the symmetry plane boundary condition at the base of the bath in the simulation. In Figure 3-10, simulation results with wall effect are presented in different proximity of bath to the coating substrate.
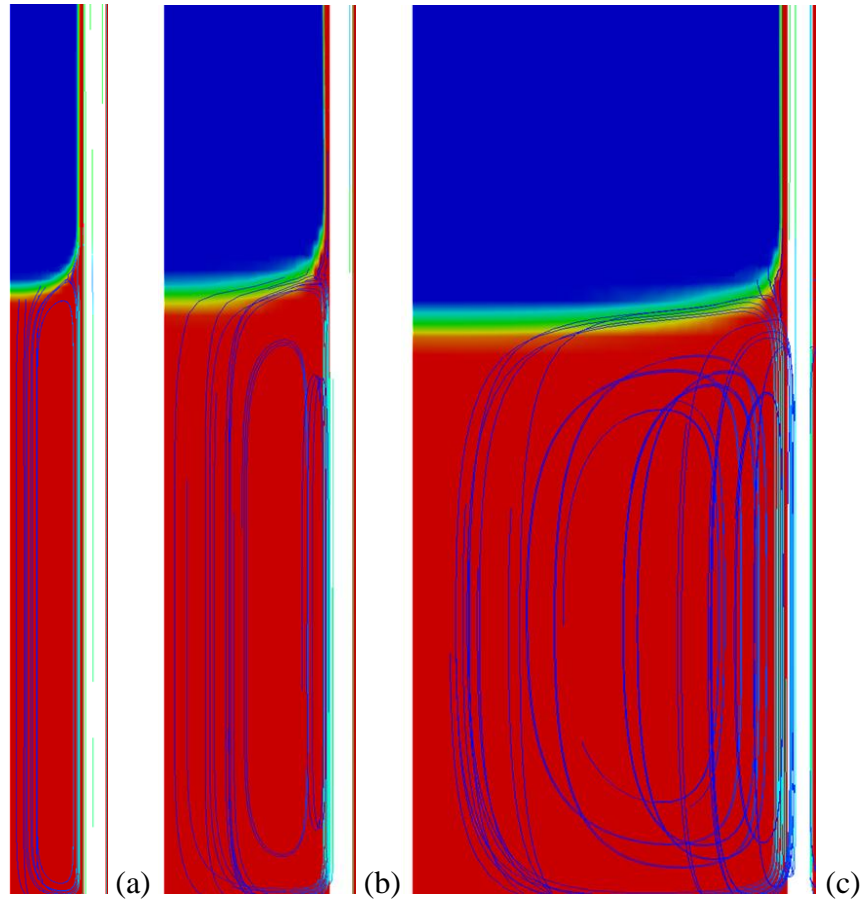
Figure 3-10: Simulation of wall effect is presented in different proximity of bath to the coating substrate, (a) $R/r = 4$, (b) $R/r = 16$, (c) $R/r = 32$

A range of diameters for the coating bath were used to study the influence of the proximity of the bath wall on the coating thickness. Numerical results are shown in Figures 3-11, 3-12 and 3-13 for Newtonian, power law and Carreau models respectively, and compared to the experimental measurements.

Figure 3-11: Numerical and experimental results for wall effect considering mineral oil as a Newtonian fluid with cylindrical substrate radius of 785 μm

Figure 3-12: Numerical and experimental results for wall effect for the 0.75 % Polyox water system applying power-law model and cylindrical substrate radius of 785 μm

Figure 3-13: Numerical and experimental results for wall effect applying for the 0.75 % Polyox water system and the Carreau model with cylindrical substrate radius of 785 μm

The numerical simulation and experimental data for the prediction of coating layer thickness is presented in Figures 3-14, 3-15 and 3-16 for Newtonian, power law and Carreau models respectively using the cylindrical substrate of radius 1590 μm.

In all simulation and experimental results, enhancing the R/r ratio, increases the deposited film thickness on the cylindrical substrate. The increasing the coating thickness with increasing the coating bath radius is also mentioned by Ahn et al. (2015) in their investigation on the transparent conductive silver nanowire films from dip coating flow.
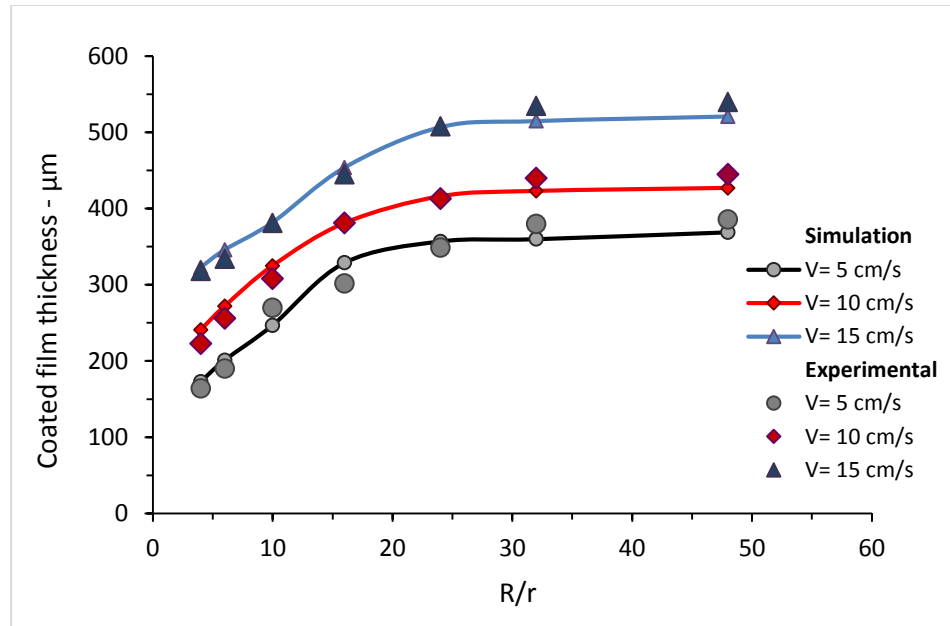
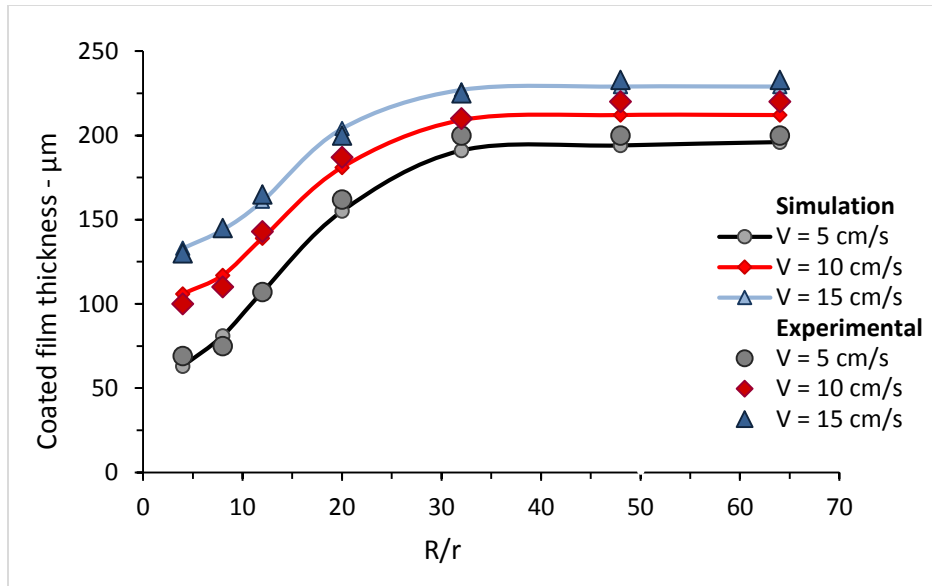**Figure 3-14:** Numerical and experimental results for wall effect considering mineral oil as a Newtonian fluid with cylindrical substrate radius of 1590 μm
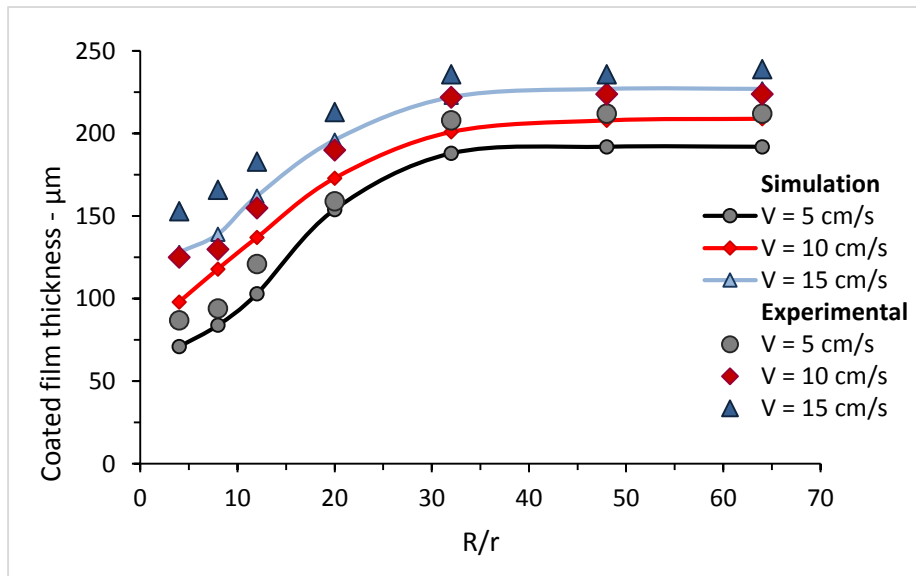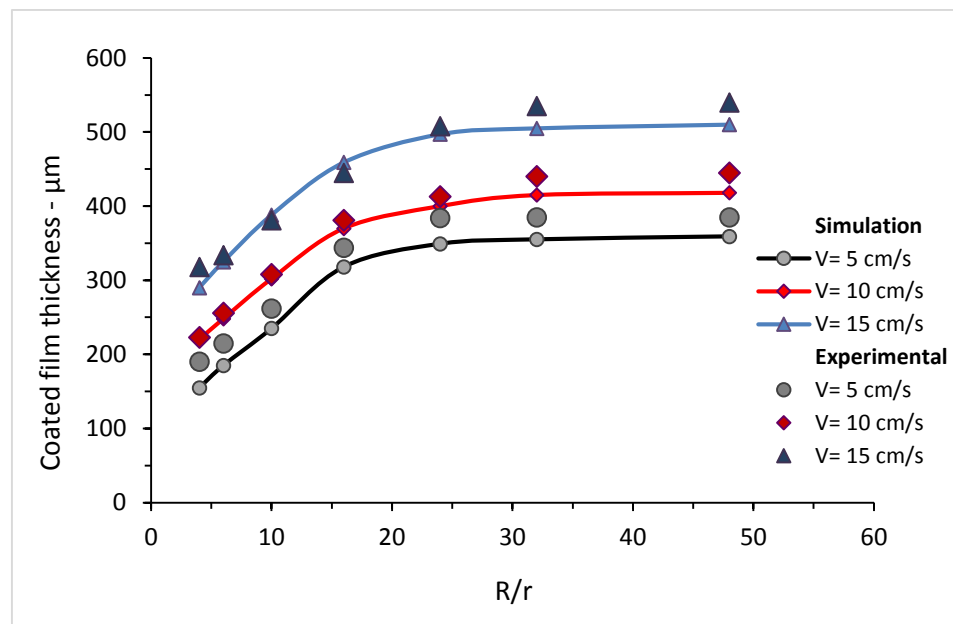

Figure 3-15: Numerical and experimental results for wall effect for 0.75% Polyox-water system and applying power-law model and cylindrical substrate radius of 1590 μm
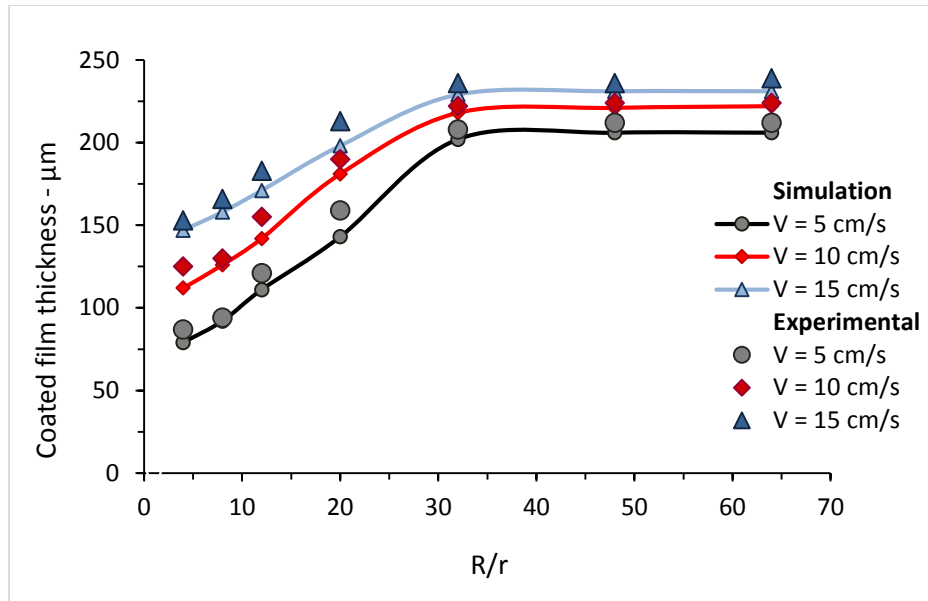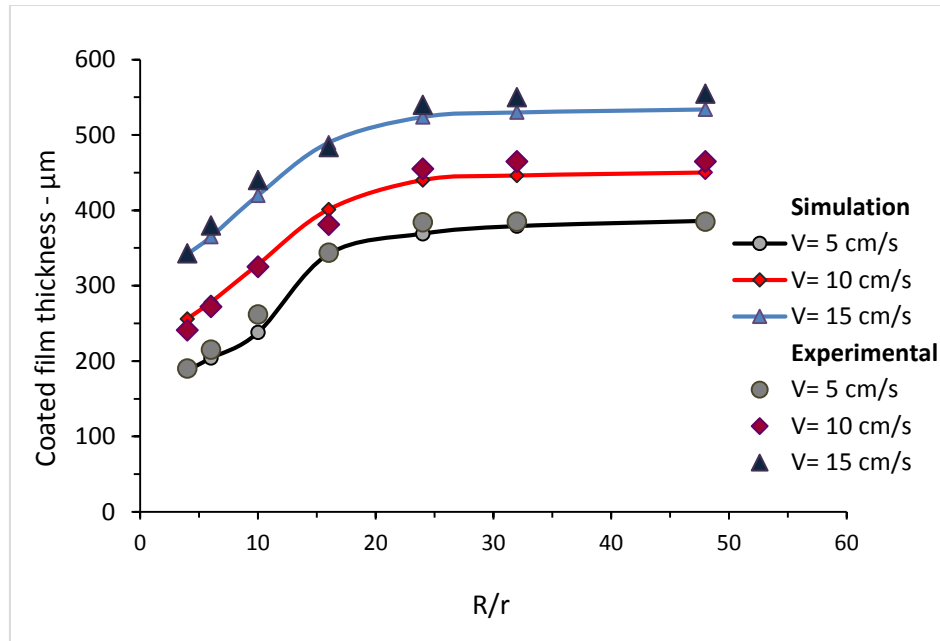
Figure 3-16: Numerical and experimental results for wall effect for 0.75% Polyox-water system and applying the Carreau model with cylindrical substrate radius of 1590 μm

The Carreau constitutive equation has been applied in the numerical calculations for the coating thickness prediction, with results presented in Figures 3-13 and 3-16 indicating good agreement between simulations and experiments.

The numerical and experimental results reveal that there is a plateau value for the coating thickness as a function of the ratio of bath radius over cylinder radius. Below this value of R/r, the deposited film thickness increases with increasing R/r at a constant withdrawal velocity. The results for the substrate with the radius of 785 μm, demonstrates for R/r less than 30, wall effects need to be considered in the coating process and for $R/r > 30$ a plateau coating thickness is reached for film thickness values at constant withdrawal velocity. Similarly, for a substrate radius of 1590 μm, coating thickness increases with increasing R/r up to approximately 25.

Analysis of the flow field of the zone beneath the bath surface helped to understand the wall effects of the coating bath proximity on the development of flow streams and consequently on the coating film thickness.

Flow streams reveal the coating liquid circulation in the bath and by reducing the proximity of the coating bath wall to the substrate, the coating liquid circulation in the bath is confined to a narrow zone. The circulation of flow in a more constricted region affects the location of the stagnation point. The stagnation point is near the meniscus region, where part of the flow engages in the coating and adheres to the substrate and part of it returns back to the coating bath. Results verify that the stagnation point moves closer to the substrate surface with decreasing distance of the bath wall to the cylindrical substrate, resulting in decreasing coating film thickness. In Figure 3-17 the flow field in the free coating bath is displayed and flow streams indicate the coating liquid circulation and the stagnation points.
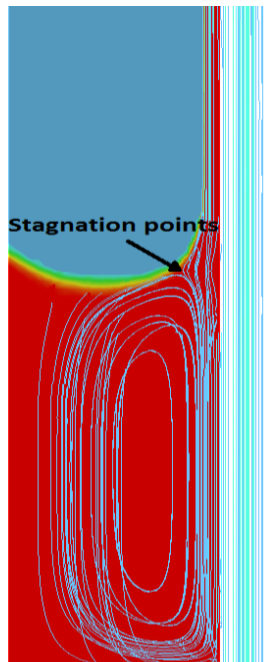
Figure 3-17: Flow streams and stagnation point in a free coating process (0.75% Polyox-water solution, $r = 1590\ \mu m$, and $R/r = 4$)

The stagnation point distance values from the substrate is shown in Figures 3-18, 3-19 and 3-20 for Newtonian, power law and Carreau respectively. The stagnation point distance values are for the cylindrical substrate radius of 1590 μm. Decreasing the values of R/r decreases the distance between the stagnation point and the substrate and this can

be one of the reasons for decreasing the coating film thickness by decreasing the R/r values.
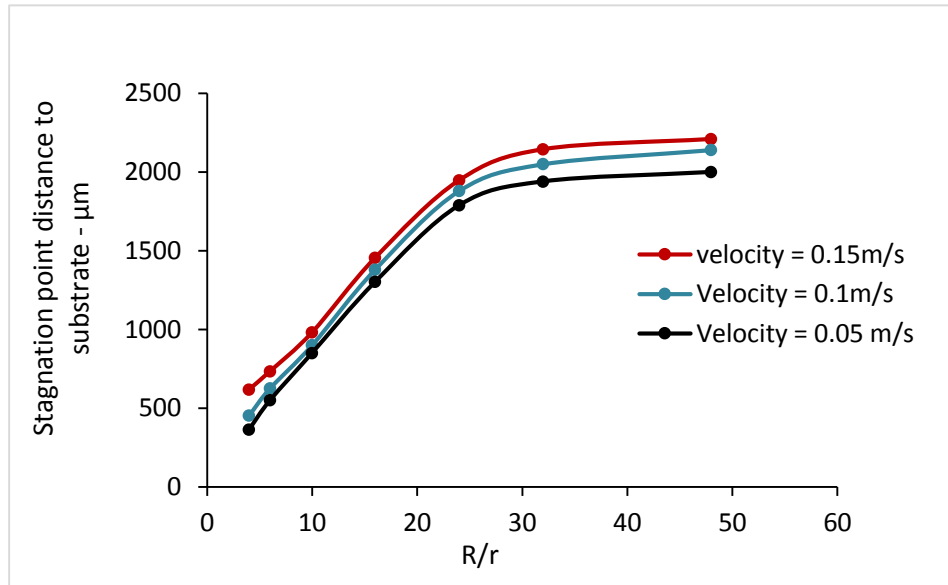
Figure 3-18: Stagnation point distance from substrate at different R/r values for Newtonian fluids (mineral oil)
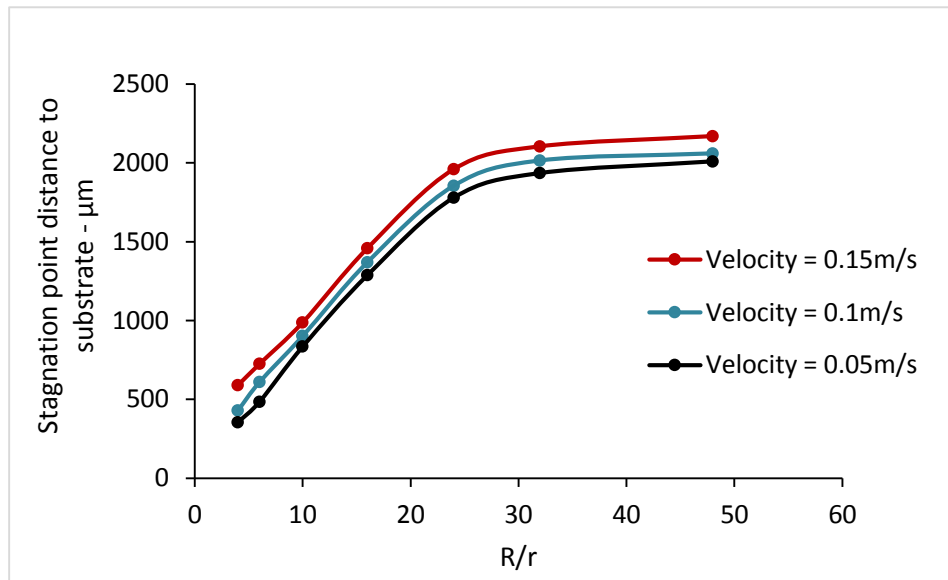
Figure 3-19: Stagnation point distance from substrate at different R/r values for powerlaw fluids (0.75% Polyox-water system)
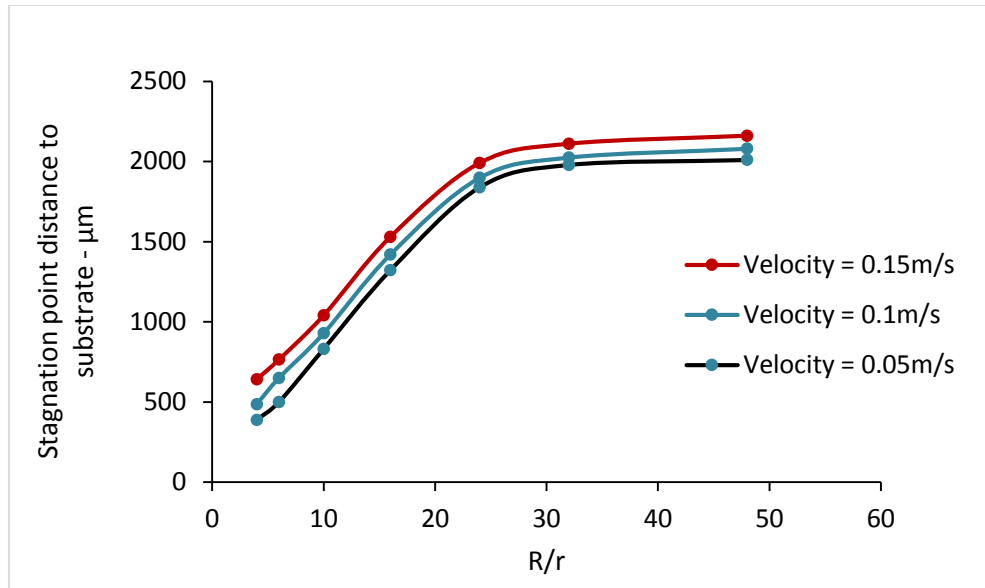
Figure 3-20: Stagnation point distance from substrate at different R/r values for Carreau fluids (0.75% Polyox-water system)

The stagnation point distance results are similar to the coating thickness results regarding to the R/r values.

3.7 « Conclusion »

Numerical solution for two phase flow in dip coating process is investigated and the simulation results indicate significantly better estimation of the coated film thickness compared to analytical models over a wide range of withdrawal velocities.

Three constitutive equations have been considered for numerical solution of both Newtonian and non-Newtonian fluids and compared to experimental data in the literature. Wall effects in dip coating show that the coating film thickness depends on the coating bath dimension.

The rheological behavior of fluid and calculation of coating film thickness for non-Newtonian fluids indicate very good agreement using the Carreau model as compared with experimental data. Based on experimental and simulation results, the wall effect

needs to be considered as an extra factor when R/r is less than a plateau value and this value decreases with increasing cylindrical substrate radius. For both Newtonian and non-Newtonian fluids, the final film thickness increases with raising the ratio of R/r, before achieving a plateau. The desired final thickness is affected by controlling the withdrawal velocity, physical properties of coating fluid, substrate geometry and wall proximity. Simulation of dip coating process, regarding the wall effects has been completed in this work and confirms that the wall influences the deposited film thickness and stagnation point.

3.8 « References »

Ahn K., Kim D., Kim O., Nam J., Analysis of transparent conductive silver nanowire films from dip coating flow, Journal of Coating Technology Research, Vol. 12, pp. 855, 2015

Blake T. D., Shikhmurzaev Y. D., Dynamic wetting by liquids of different viscosity, Journal of Colloid Interface Science, Vol. 253, pp. 196, 2002

Brackbill J. U., Kothe D. B., Zemach C., A continuum method for modeling surface tension, Journal of Computational Physics, Vol. 100, pp. 335, 1992

Colosqui C. E., Morris J. F., Stone H. A., Hydrodynamically driven colloidal assembly in dip coating, Physical Review Letters, Vol. 110, pp. 188302-1, 2013

Deryagin B., On the thickness of the liquid film adhering to the walls of a vessel after emptying. Acta Physicochem, USSR, Vol. 39, pp. 13, 1943

Farm J., Martinelli L., Jameson A., Fast multigrid method for solving incompressible hydrodynamic problems with free surfaces, American Institute of Aeronautics and Astronautics Journal, Vol. 32, pp. 1175, 1994

Ferziger J. H., Peric M., Computational methods for fluid dynamics, Springer-Verlag, Berlin, 1996

Grunig J., Skale T., Kraume M., Liquid flow on a vertical wire in a countercurrent gas flow, Chemical Engineering Journal, Vol. 164, pp. 121, 2010

Guttfinger C., Tallmadge J. A., Films of non-Newtonian fluids adhering to flat plates, American Institute of Chemical Engineering Journal, Vol. 11, pp. 403, 1965

Hirt C., Nicholls B., Volume of Fluid (VOF) method for dynamics of Free boundaries, Journal of Computational Physics, Vol. 39, pp. 201, 1981

Issa R. I., Solution of the implicitly discretized fluid flow equations by operator splitting, Journal of Computational Physics, Vol. 62, pp. 40, 1986

Kistler S. F., Schweizer P. M., Liquid film coating, Chapman and Hill, London, 1997

Landau L., Levich B., Dragging of a liquid by a moving plate, Acta physicochim, URSS, Vol. 17, pp. 42, 1942

Middleman S., Fundamentals of polymer processing, McGraw-Hill, New York, 1977

Middleman S., High speed wire coating from a bath of viscoelastic liquids, Polymer Engineering Science, Vol. 18, pp. 335, 1978

Patankar S. V., Spalding D. B., A calculation procedure for heat, mass and momentum transfer in 3D parabolic flow, International Journal of Heat and Mass Transfer, Vol. 15, pp. 1787, 1972

Patankar S. V., Numerical heat and mass transfer, Hemisphere Publication Corp., Washington, 1980

Peralta J. M., Meza B. E., Zorrilla S. E., Mathematical modeling of a dip-coating process using a generalized newtonian fluid. 1. Model Development, Industrial Engineering and Chemistry Research, Vol. 53, pp. 6521, 2014

Qian L., Causon D. M., Mingham C. G., Ingram D. M., A free-surface capturing method for two fluid flows with moving bodies, Proceeding of the Royal Society London A, Vol. 462, pp. 21, 2006

Roy S. C., Dutt D. K., Wire coating by withdrawal from a bath of power law fluid, Chemical Engineering Science, Vol. 36, pp. 1933, 1981

Rusche H., Computational fluid dynamics of dispersed two phase flows at high phase fractions. Ph.D. thesis, University of London, 2002

The OpenFOAM® Foundation (www.OpenFOAM.org)

Ubbink O., Issa R., A method for capturing sharp fluid interfaces on arbitrary meshes, Journal of Computational Physics, Vol. 153, pp. 26, 1999

Watanabe M., Wakimoto N., Hirai T., Yokoyama M., Thermal switching of the actuation ability of an electroactive polymer actuator, Journal of Applied Polymer Science, Vol. 95, pp. 1566, 2004

White D. A., Tallmadge J. A., A gravity corrected theory for cylinder withdrawal, American Institute of Chemical Engineering Journal, Vol. 13, pp. 745, 1967

Yang A., Tao X. M., Cheng X. Y., Prediction of fiber coating thickness via liquid-phase process, Journal Materials Processing Technology, Vol. 202, pp. 365, 2008

Chapter 4

4 « Concentrated Suspensions »

The materials presented in this Chapter will be a manuscript "Numerical simulation of concentrated suspensions in thin film process" submitted to the Canadian Journal of Chemical Engineering, with results presented at the European Coating Symposium (ECS), Eindhoven, Netherlands, 2015, Canadian Society for Chemical Engineering (CSCHE), Calgary, Canada, 2015 and American Institute for Chemical Engineering (AICHE), Salt Lake City, USA 2015. The sections in Chapter 4 present the results towards the completion of objectives regarding to the simulation of concentrated suspensions with free surface and the developed algorithm tested for dip coating of dispersions.

4.1 « Abstract »

This study is dealing with the numerical simulation of particle distribution and fluid-particle interactions in free-surface concentrated suspensions using the finite volume method. The numerical procedure, based on the particle diffusion-flux model, is implemented in computational fluid dynamic platform for estimating the particle volume fraction in three-dimensional flows with arbitrary geometry and boundary conditions. The Volume of Fluid (VOF) method has been applied to track the flow interface between liquid and gas, with the solid particles dispersed in the liquid phase, in the free coating process. A finite length cylinder is dip coated, where the substrate is pulled out of a concentrated suspension bath. In the current work, the initial solid particle volume fraction range is 0.1-0.4 and the withdrawal velocity varies in the range of 0.05-0.15 m/s. Comparisons are made between numerical simulation predictions and experimental results for coating layer thickness with good agreement achieved.

4.2 « Introduction »

Thin film deposition on a substrate is of great interest in industry and academia. The main challenge in coating processes is to obtain a uniform and smooth coating layer, free of defects, a task that turns out to be more and more problematic as the processing speed and the solid content in the formulation are increased (Ritz et al., 2000). Among the coating techniques, dip coating is an inexpensive method with the capability to coat irregularly shaped substrates (Kistler and Schweizer, 1997). Nowadays, dipping and withdrawal are not only used to apply the coating, but also to control the final microstructure of the coated film (Colosqui et al., 2013). Free coating of dispersions, where the coating liquid includes solid particles, is essential for the surface engineering of high quality products and it is one of the better developed ways to enhance and alter the physical and mechanical surface characteristics.

Analysis of entrainment of a liquid film on a solid substrate, which is continuously withdrawn at a constant speed from a bath of liquid, has been studied since the pioneering work performed by Landau and Levich (1942). Guttfinger and Tallmadge (1965) estimated coating film thickness for Non-Newtonian fluids on flat plates and a significant improvement in film thickness assessment was attained by White and Tallmadge (1967) with the gravity corrected model for cylindrical substrates. The assessment of dip coating process continued with the work of Spiers et al. (1975) for a flat plate, Ro and Homsy (1995) for fiber and flat plate geometries and Ashmore et al. (2007) on the inclined plate and fiber. All these investigations are based on analytical solutions to a problem formulation that takes a partitioned view of the flow domain. Due to the geometric and rheological complexity of the problem, it may not always be possible to calculate the solution using analytical techniques. Numerical techniques are a practical approach to overcome the restrictions of the analytical solutions. The study of the dip coating process with numerical methods requires consideration of the free surface problem. VOF method (Hirt and Nicholls, 1981) has been applied for the current study, which enable tracking of the interface in the three dimensional unsteady-state system. Investigation of the dip coating process for dispersed systems is even more complicated and migration of solid particles affects the hydrodynamics of this free surface system. The migration of particles

93

in the flowing suspension influences velocity and particle concentration distributions thereby affecting the local characteristics of the flow to become different from that known for a homogeneous fluid (Averbakh et al., 1997).

Solid-liquid dispersion flows are important in a wide variety of scientific and engineering applications including design and manufacture of composite materials, oil and gas production (Mukhopadhyay et al., 2009), and manufacturing processes in pharmaceutical, biomaterials and paper industries. In many of these industries, uniformity in particle distribution is required and the product quality is strongly dependent upon the consistency of particle distribution (Ritz et al., 2000). In view of its varied applications, a number of theoretical and experimental investigations have been carried out and these have explored various aspects of the flow properties and characteristics of suspensions. Most of the investigations on the flow properties of suspensions of rigid particles have focused their attention on the development of theoretical or empirical formulae relating to the bulk rheology assuming that the concentration of the particles remains uniform in space (Mukhopadhyay et al., 2009; Mewis and Wagner, 2012).

The assumption of uniform distribution of particles is not applicable in many industrial applications as non-uniform particle distribution can be detected and the relationship between hydrodynamics and the homogeneity of the suspension as well as the impact of the particle distribution on the overall process cannot be ignored (Ritz et al., 2000).

An important phenomenon observed in solid-fluid suspensions is shear-induced migration, in which initially well-mixed particles in suspensions subjected to inhomogeneous shear, migrate from regions of high strain rate to regions of low strain rates and result in a non-uniform concentration distribution (Mukhopadhyay et al., 2009; Mewis and Wagner, 2012; Leighton and Acrivos, 1986; Abbott et al, 1991; Arp and Mason, 1977, Gadala-Maria and Acrivos, 1980). This has important implications both in viscometric measurements of concentrated suspensions and in industrial manufacturing processes where the performances and the appearance of the finished products are greatly affected by the degree of solids dispersion. A small number of theoretical investigations (Mewis and Wagner, 2012; Sierou and Brady, 2004; Marchiaro and Acrivos, 2001) on

94

concentrated suspensions undergoing inhomogeneous shearing flows have thrown light on the mechanics that cause irreversible migration of particles. It has been observed that there are a number of mechanisms that exist in the presence of the flow that leads to non-uniform concentration even in the region away from any walls or flow boundaries (Leighton and Acrivos, 1987).

Shear-induced migration can be studied from a microscopic or macroscopic point of view. In the microscopic point of view, the modelling of many-body interactions and microstructure configurations of particle suspensions has been made possible, but it is presently of limited use because of the huge amount of computing resources that would be needed to calculate the motion of a suspension in an industrial process (Ritz et al., 2000). However, the characterization of the interactions appearing at the scale of one particle can allow one to prescribe macroscopic values, which can then be applied to better describe flow behavior at the scale of the suspension. Direct simulation (Ritz and Caltagirone, 1999), Stokesian dynamics (Brad and Bossis, 1998) and the lattice Boltzman method (Ladd, 1994) are three different numerical strategies that can be used to describe the hydrodynamics of a suspension. Another numerical approach considers the suspension as a continuum phase, a practical point of view to overcome the high computational cost and reasonably describe the behavior of a real suspension in a flow situation. In this method, the suspension as a continuum phase is modeled through a constitutive equation, which is a function of the local values of macroscopic quantities such as shear rate and concentration.

In the evolution of continuum phase models, the development of the diffusive flux model by Leighton and Acrivos (1987) is important for the calculation of non-uniform concentration profiles, which is a consequence of irreversible hydrodynamic interactions between the neighboring particles. Phillips et al. (1992) have adapted the scaling arguments of Leighton and Acrivos (1987) and have derived a constitutive equation for the particle flux. The model is considered a balance between a contribution due to a spatially varying interaction frequency and an opposite contribution due to a spatially varying viscosity and has yielded excellent predictions in a circular Couette flow and

many other applications (Buyevich, 1996; McTigue and Jenkins, 1992; Cho and Kensey, 1991; Perktold, 1992).

Fang and Phan-Thien (1995) developed a simulation procedure based on the Phillips et al. (1992) model and finite volume method for calculating the particle distribution in one phase and free surface prediction was not included in the procedure.
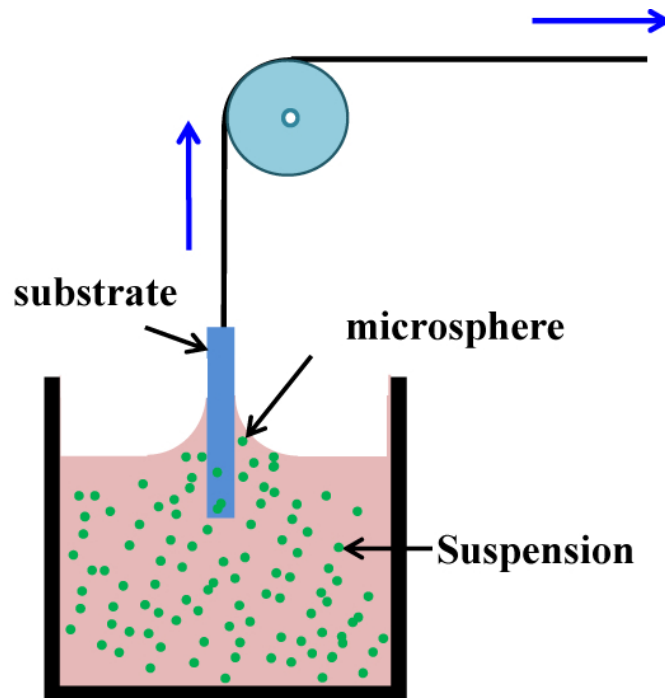
Figure 4-1: Schematic diagram of dip coating of a finite cylinder though a dispersion

Little prior attention has been given to modeling the development of the solid particle concentration profile and film thickness in coating processes of dispersions. Accordingly, the dip coating process is investigated including the interface phenomena and solid particles distribution along with the impact of the unsteady processing condition and substrate curvature in the system. In Figure 4-1, a schematic diagram of dip coating with dispersion is shown.

It is useful to be able to predict the dynamics of dip coating process based on the fluid properties and operational conditions and it is usually desired to be able to control the coating film thickness. The objective of this work consists of simulating the flow of a

concentrated suspension in a dip coating process in order to obtain coating film thickness and concentration profiles in such a process.

4.3 « Modeling Procedure »

In this study, the open source computational fluid dynamics platform (*OpenFOAM - Open Source Field Operation and Manipulation*) was used, including the free surface. The evolution of the free surface is calculated by VOF techniques. Equations are discretized by the Finite Volume method (FVM) applying a collocated variable arrangement. The VOF method is used in problems where surface capturing is crucial, with the important role of surface tension where the free surface position prediction is essential.

The distribution of solid particles in concentrated suspensions is investigated as a continuum phase. For concentrated systems, where there are millions of particles in the system, tracking the individual particles using the microscopic techniques is extremely costly. Thus, a constitutive equation is implemented in the OpenFOAM platform, which can reasonably define the suspension behavior in dip coating. The diffusive flux model (Phillips et al., 1992) has been used for the study of non-uniform concentration profiles. The governing equations are established for the gas-liquid interface and flow of the suspension of rigid, spherical particles in a Newtonian liquid in the next section.

4.3.1 « Governing Equations »

Description of the flow for a concentrated suspension requires mass and momentum balances for the bulk suspension and a particle concentration equation for the particle migration in the flow. The equations are developed by assuming the rigid particles in the fluid can be approximated as a continuum phase. Incompressible flows in free coating process, governed by the Navier-Stokes, equation 4-1 and the conservation of mass, equation 4-2.

$$\frac{\partial \rho u}{\partial t} + \nabla.(\rho uu) = -\nabla P + \rho g + \nabla.(\tau) + F_b \qquad (4-1)$$

$$\nabla.(u) = 0 \qquad (4-2)$$

In OpenFOAM, the momentum equation is modified in order to account for the pressure and surface tension effects and the momentum equation developed into equation 4-3.

$$\frac{\partial \rho u}{\partial t} + \nabla.(\rho uu) = -\nabla P_{rgh} - (g.x)\nabla \rho + \nabla.(\tau) + F_b \qquad (4-3)$$

In the VOF method, the phase fraction, α_1, can take values within the range of 0 and 1 corresponding to regions accommodating only one phase and values between 0 and 1 containing the interface. The free surface position is captured using the interface continuity equation applying the phase fraction α_1, represented in equation 4-4.

$$\frac{\partial \alpha_1}{\partial t} + \nabla.(\alpha_1 u) = 0 \qquad (4-4)$$

Adding an artificial surface compression term to the interface continuity equation assists capture of a sharp interface. The interface continuity equation utilized in OpenFOAM is defined in equation 4-5 and $u_{r\alpha}$, is the compression velocity (Ubbink and Issa, 1999; Rusche, 2002).

$$\frac{\partial \alpha_1}{\partial t} + \nabla.(\alpha_1 u) - \nabla.(\alpha_1(1-\alpha_1)u_{r\alpha}) = 0 \qquad (4-5)$$

Equation 4-1 is treated with the mixture velocity and surface tension considered as an additional body force which develops as equation 4-6.

$$\frac{\partial \rho u}{\partial t} + \nabla.(\rho uu) = -\nabla P_{rgh} - (g.x)\nabla \rho + \nabla.(\tau) + \sigma k \frac{\partial \alpha_1}{|\partial \alpha_1|} \qquad (4-6)$$

Where $k = -\nabla.(\frac{\partial \alpha_1}{|\partial \alpha_1|})$ is the curvature of the interface, and σ is the surface tension (Brackbill et al., 1992).

4.3.1.1 « Viscosity model implementation »

In the momentum equation, the stress tensor τ is given as a Newtonian fluid.

$$\tau = -\eta(\varphi)\dot{\gamma} \qquad\qquad (4-7)$$

Where $\dot{\gamma} = \nabla u + \nabla u^T$ is the rate of strain tensor in equation 4-7 and this equation was originally obtained by fitting data for suspensions with volume fractions in the range $0.01 < \varphi < 0.5$.

The viscosity and particle concentration relationship is attained using a semi-empirical equation proposed by Krieger (1972). This formulation describes the viscosity concentration relations of suspensions and the viscosity $\eta = \eta(\varphi)$ depends on the volume fraction of particles.

$$\eta_r = (1 - \varphi/\varphi_m)^{-n} \qquad\qquad (4-8)$$

$\eta_r = \eta/\eta_s$ is the relative viscosity, and φ_m is the volume fraction at which η_r tends to infinity which is $\varphi_m = 0.68$ for hard spheres. The parameter n in equation 4-8, has been determined through rheological measurements (see Figure 4-5) of the suspensions in this study and an estimated value of $n = 1.86$.

The Krieger-Dougherty model has the exponent $n = -2.5\varphi_m$ at low particle concentrations reduces to the Einstein equation.

4.3.1.2   « Implementing the Diffusion Equation for Particles »

The local particle concentration in the flow depends on the shear rate variation and will result in a viscosity change as given by equation 4-8.

In laminar flow of dilute suspensions, no diffusional or migratory effects of particles occur (Mewis and Wagner, 2012); however, in concentrated suspensions of solid particles, which we deal with in this study, there are interactions between particles (Cho and Kensey, 1991). Self-diffusion is one of the significant interactions, which describes the random motion of a particle in the flow and occurs due to the simultaneous interactions with two or more neighboring particles. In dense systems, diffusion can be calculated using the $\dot{\gamma}a^2$ parameter, as $\dot{\gamma}^{-1}$ and a are the time and radius of particles (Philips et al., 1992). Hydrodynamic diffusion increases in proportion to φ^2 at low volume fractions, but at higher volume fractions the values seem to flatten out or even decrease (Philips et al., 1992). This may be associated with the high shear rate structural changes (Leshansky and Brady, 2005). Shear rate gradients impose the migration of particles to regions of lower shear rate, which is of practical importance in processing of suspensions (Gadala-Maria and Acrivos, 1980; Leighton and Acrivos, 1987). A simplified approach, useful for numerical simulation of these interactions in flow fields, is used here that enables to capture the most important effects of particle concentration.

4.3.1.2.1   « Particle interaction rate flux »

An impact occurs when two particles placed between adjacent shearing surfaces move past one another so it is appropriate to assume a shear flow as shearing surfaces sliding relative to one another (Bird et al, 1987). A schematic diagram of an irreversible two-body interaction is displayed in Figure 4-2(a). A particle can be irreversibly relocated from its original streamline due to the impacts. The reason for this relocation, is the higher rate of collisions from one direction than from the opposing direction and a particle will transfer normal to its shearing surface in the direction of the lower

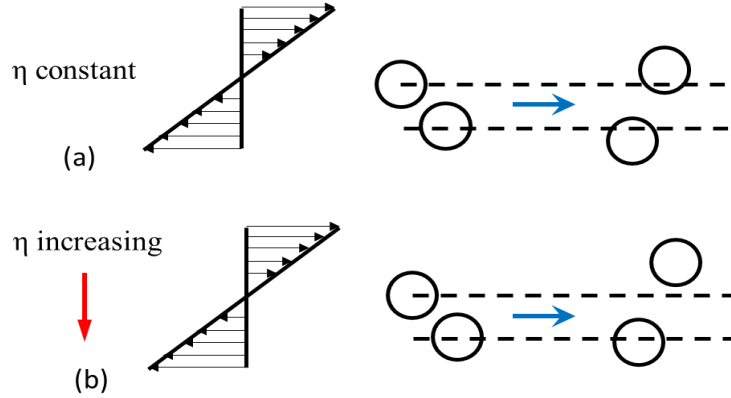interaction frequency. The consequence of these collisions will be particle movement to low shear regions

Figure 4-2: Schematic illustrations of two-body collision in a flow with (a) constant viscosity and (b) spatially varying viscosity (Philips et al., 1992)

In a concentrated suspension, the particles experiencing a shearing motion and the number of impacts received by a specific particle, on average, will scale as $\dot{\gamma}\varphi$, where $\dot{\gamma}$ the magnitude of the local shear rate. The variation in the interaction frequency over a distance of particle radius is given by $a\nabla(\dot{\gamma}\varphi)$ (Philips et al., 1992).

Philip et al. (1992) consider the particle migration velocity in a linear relation to the variation in the interaction frequency and displacement of a for each of these two-body collisions generates an expression for the flux M_c, where B_c is a constant value of order unity.

$$M_c = -B_c a^2 (\varphi^2 \nabla \dot{\gamma} + \varphi \dot{\gamma} \nabla \varphi) \qquad (4-9)$$

The first term $B_c a^2 \varphi^2 \nabla \dot{\gamma}$ indicates that, even in homogeneous suspensions with constant φ, migration will take place if the particles on one side of a specific particle move past it more rapidly than on the other side. This variation increases the number of inter-particle interactions in the region with higher $\dot{\gamma}$. Correspondingly, the second term $B_c a^2 \varphi \dot{\gamma} \nabla \varphi$ of equation 8 expresses that the particle concentration gradient is going to result in a spatial variation in the collisions frequency. The two terms in equation 4-9, will generally

compete with one another, where the first term increases the flux and this rising flux causes a concentration gradient and induces a second flux proportional to $\nabla\varphi$ through the second term.

4.3.1.2.2 « Viscosity varying flux »

In the previous section, the flux described for concentrated suspensions, which was caused by the difference in impact frequencies. In this section, another flux is discussed that the positional variation in viscosity $\eta(\varphi)$ caused by the gradients in particle concentration. The viscosity gradient results in the different amount of resistance experienced by interacting particles.

A quantitative flux value relating to this effect is derived by Leighton and Acrivos (1987). It has been considered that the drift velocity corresponding to the variation in viscosity over a distance of a relates to the overall magnitude of the viscosity, $(a/\eta)\nabla\eta$. Assuming a displacement of a for each interaction and measuring the interaction frequency as $\dot{\gamma}\varphi$, then the consequential migration velocity can be scaled as $\dot{\gamma}\varphi(a^2/\eta)\nabla\eta$. Eventually, multiplying by φ and using equation 4-8, to indicate the gradient of viscosity in terms of $\nabla\varphi$ results in the flux.

$$M_\eta = -B_\eta \dot{\gamma} \varphi^2 \left(\frac{a^2}{\eta}\right)\frac{d\eta}{d\varphi}\nabla\varphi \qquad\qquad (4-10)$$

The particle flux due to the positional variation in the viscosity is expressed by M_η in equation 4-10 and B_η, is a constant of order unity. Based on equation 4-10, shear induced particle migration rates are independent of the viscosity of the suspending fluid.

Empirical constants B_c and B_η were determined from experimental measurements of the concentration profile in Couette (Phillips et al., 1992) and Poiseuille flows (Lyon and Leal, 1998). Since their values were found to be almost identical in both cases, the same values of 0.41 for B_c and 0.62 for B_η were used for all the simulations in this work (Ritz et al., 2000).

4.3.1.2.3 « Conservation equation for concentrated particle suspensions »

A conservation equation for solid particles can be expressed as

$$\frac{\partial \varphi}{\partial t} = -\nabla.\left(M_c + M_\eta\right) \qquad\qquad (4-11)$$

where the left hand side of equation 4-11 is the rate of particle accumulation. In this study, micron size particles are used to investigate the concentration suspensions hydrodynamics where the Brownian diffusive flux can be neglected. The constitutive description for the concentrated suspension can be described with the local volume fraction of solids dependent viscosity and the diffusion equation for describing the particle distribution and the motion of the particles in a flow field. Equations 4-9 to 4-11 result in the diffusion equation for the particle volume fraction, in an Eulerian reference frame:

$$\frac{D\varphi}{Dt} = a^2 B_c \nabla.\left(\varphi^2 \nabla\dot{\gamma} + \varphi\dot{\gamma}\nabla\varphi\right) + a^2 B_\eta \nabla.\left(\dot{\gamma}\varphi^2 \frac{1}{\eta}\frac{\partial\eta}{\partial\varphi}\nabla\varphi\right) \qquad (4-12)$$

Equation 4-12, indicates the constitutive equation for a highly concentrated suspension of mono-modal spheres undergoing non-uniform shear flows. This equation is implemented in the finite volume based CFD platform, OpenFOAM, with the related libraries for applying in the numerical calculation of multiphase systems consist of the concentrated suspensions with the free surface.

Three simulation cases using the implemented algorithm are shown in the next sections.

4.4 « Simulations of Concentrated Suspensions»

In the current study, OpenFOAM is employed as a platform for numerical calculations and code implementation. The implemented algorithm is applied for the simulation of three cases: flow through a cylindrical tube (Poiseuille flow), continuous fiber dip coating, and dip coating of a finite length cylinder. In section 4.4.1 the simulation

outcomes of Poiseuille flow is compared with the results of Phillips et al. (1992). In section 4.4.2 the simulation of continuous fiber in dip coating is presented to show the particle migration in the continuous dip coating process. Finally, in section 4.4.3 the simulation results for the coating thickness for a finite length cylinder is validated with the experimental data for suspensions for a range of particle volume fraction.

4.4.1 « Flow through a Cylindrical Tube »

The implemented algorithm in OpenFOAM is validated against Poiseuille flow through a cylinder tube. The simulation results for Poiseuille flow using the new algorithm are compared with the particle distribution values of Philips et al. (1992) in the radial direction.

The simulation results, using the implemented algorithm for the particle distribution, for a pressure-driven flow is shown in Figure 4-3 for a suspension from the uniform initial state for the particle volume fraction of 0.4.
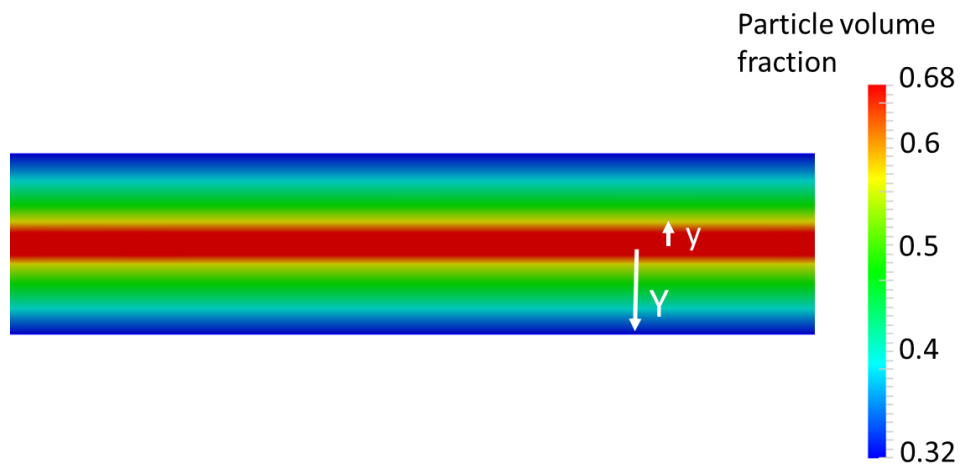
Figure 4-3: particle distribution from the initial concentration state of $\varphi = 0.4$ in the pressure-driven flow

In addition, the volume fraction profile in Figure 4-4 shows a significant variation from wall to the tube center, with φ reaching a maximum of particle volume fraction at $r = 0$. similar to Philips et al. (1992) and Leighton (1988).
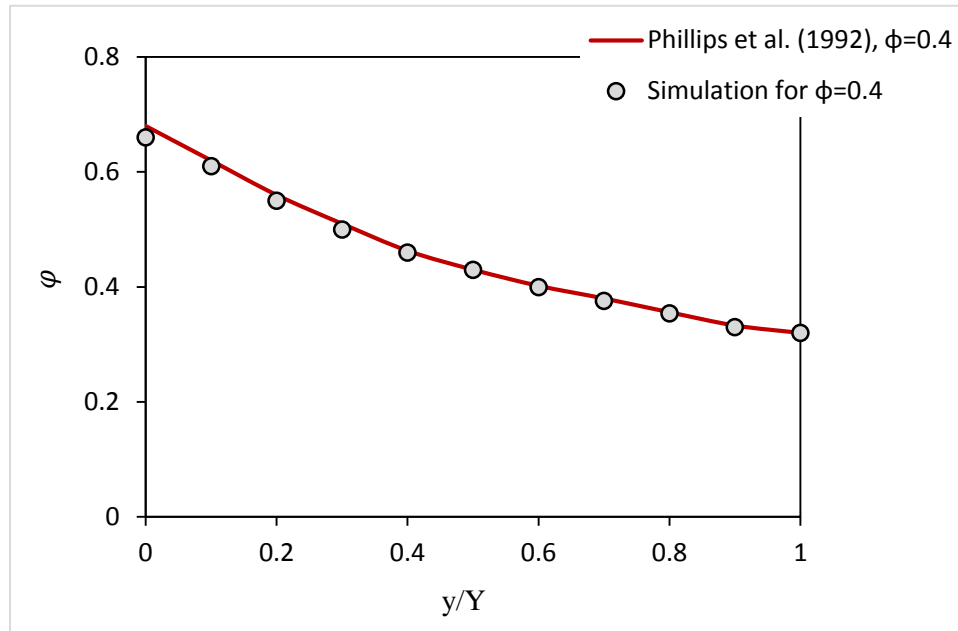
Figure 4-4: Profile of the volume fraction of particles in radial direction in the Poiseuille flow
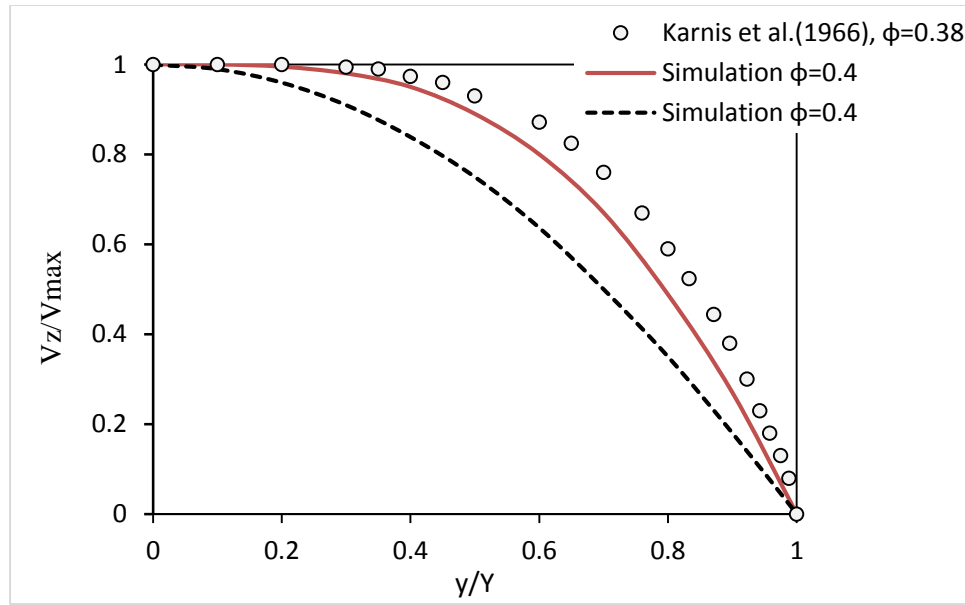
Figure 4-5: Velocity profile in the Poiseuille flow for simulations with particle concentration of $\varphi = 0.4$ without using the diffusive flus model (dashed line) and $\varphi = 0.4$ using diffusive flux model (red line), and experimental data of Karnis et al. (1966) for the particle concentration of $\varphi = 0.38$

The effect of the variation in φ on the velocity profile, shown in Figure 4-5, is to flatten the shape of the profile in the region near the center of the tube relative to the parabolic shape displayed by a homogeneous Newtonian fluid.

The feature of the velocity profile is in qualitative agreement with the flow visualization experiments of Karnis et al. (1966).

4.4.2 « Continuous Fiber Dip Coating »

The simulation of particle distribution in a continuous fiber dip coating is performed using the new implemented algorithm in OpenFOAM for concentrated suspensions.

In continuous fiber dip coating, particle distribution fractionation occurs due to the coating bath fluid hydrodynamic during the withdrawal. Shear rate variation happens in the bath and consequently the volume fraction of particles decreases near each wall and increase near the coating bath base and in the corners of bath.

Decreasing the concentration of particles occur along the flow streams, where shear rate varies. The evolution of this flow field from the uniform initial state leads to particle migration that starts from the bath surface and the movement of flow steams downward from the bath surface while the substrate is being withdrawn changes the concentration of particles in the coating bath. In addition, particle migration in the coating bath is shown in Figure 4-6.

Particle movement and flow field evolution in the bath is shown in Figures 4-6(a) to 4-6(d). The simulation results are for continuous dip coating, using a suspension with an initial uniform state of 0.3 particle volume fraction and a withdrawal velocity of 0.1 m/s. In addition, the liquid phase is shown in Figure 4-7 for the same conditions.
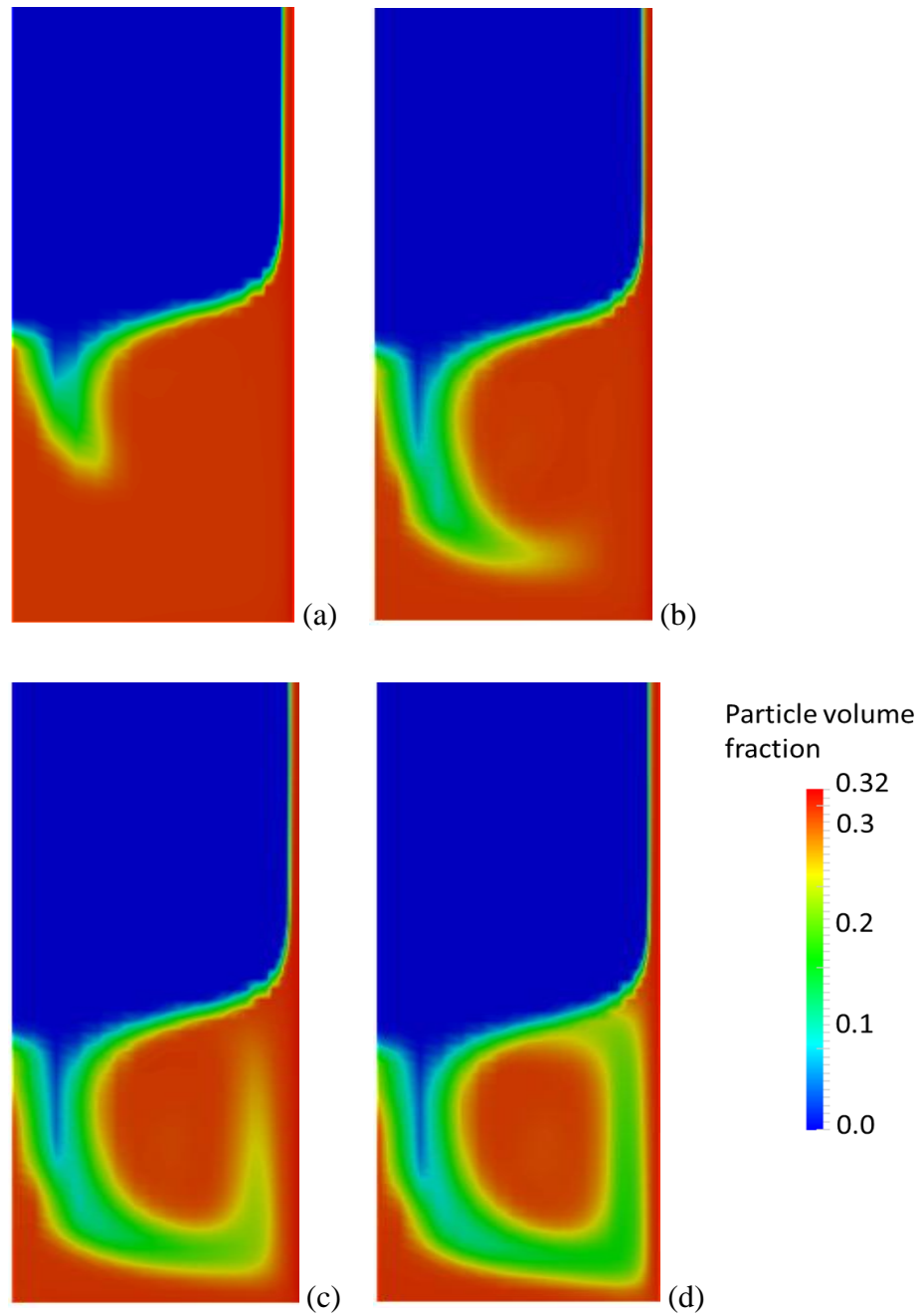
Figure 4-6: Particle movement in the coating bath during the continuous fiber dip coating process at the withdrawal velocity of 0.1 m/s and $R/r = 32$: (a) particle distribution at time = 2s, (b) particle distribution at time = 2.5, (c) time = 3.5s and (d) time = 4s
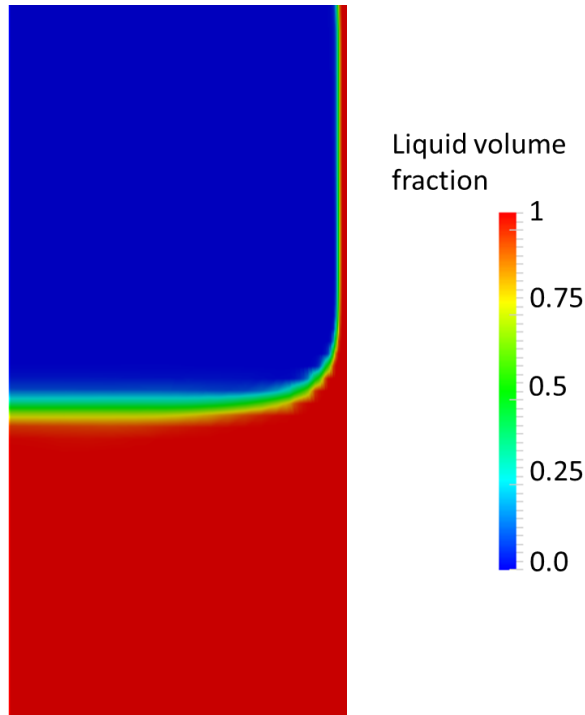
Figure 4-7: Liquid volume fraction (α_1) values for continuous fiber coating with $\varphi = 0.3$ in the coating bath at time $= 4$s, with value of 1 for liquid phase and 0 for gas phase, and values between 0 and 1 containing the interface

As shown in Figure 4-6, in continuous fiber dip coating, particle migration occurs due to the shear rate variation in the coating bath and the variation in the volume fraction of particles affects the coating bath hydrodynamic.

Experimental data are not available for the particle distribution effects in a continuous fiber coating, and thus only simulation results for this case are presented.

Furthermore, particle movement and fractionation process during the flow field evolution can be presented through the flow streams in the bath. The stagnation point that is shown in Figure 4-8, can be considered as a demarcation point of particle volume fraction and defining the initial deposited coating layer.
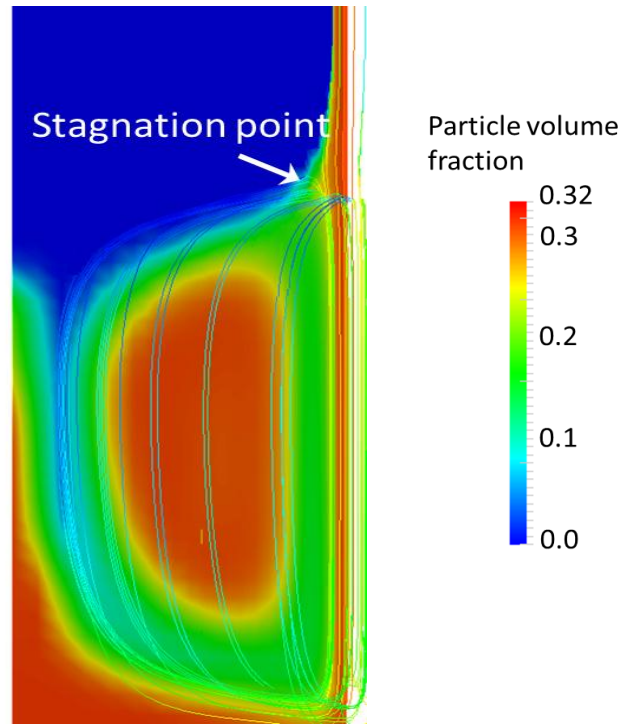
Figure 4-8: Stream lines and the stagnation point in continuous fiber dip coating

4.4.3 « Finite Length Cylinder »

The simulation procedure for coating a finite length cylinder using suspensions of different particle volume fractions is represented in the next subsections. In order to ensure numerical stability of the solution procedure, the calculations are performed using an adaptive time step (www.openfoam.org-2013), which is adjusted at the beginning of the time iteration loop. This adjustment is based on the Courant number, defined as $Co = (u/\Delta x)\Delta t$, where Δt is the time step and Δx is the cell size in the direction of the velocity and for this study the maximum Courant number is set to 0.5.

4.4.3.1   « Grid Generation »

The numerical solution procedure requires the discretization of the problem into a large number of cells points. The geometry is considered as a finite length cylinder withdrawn

from a concentrated suspension. In this work, simulation domains for cylindrical coating baths, considered a tube with radius of 2.54 cm and height of 12 cm. The cylindrical substrate with a radius of 1590 μm was centered in the coating bath and three dimensional meshes have been created for finite volume analysis. Approaching the mesh development consists of two main steps for this coating process. The background mesh of hexahedral cells is generated such that it fills the entire region of the coating bath domain. The background mesh defines the extent of the computational domain and a base level mesh density. The substrate geometry is added to the background mesh. The important feature in generating the background mesh is keeping the cell aspect ratio ~ 1, at least near surfaces where the subsequent substrate boundary is going to be located, which enables acceleration of the convergence of the substrate surface mesh generation and avoids possible failure in the meshing process.

After adding the substrate geometry to the background mesh, the quality of mesh and the element sizes can be controlled on the substrate surface and the areas around the substrate. For accurate results, the mesh around the substrate needs to be refined and the refinement process is performed by splitting the cells at the substrate surface and the mesh around it. The splitting process in different levels around the substrate provides a smooth transition to the background coarse mesh area. An additional 20-30 layers of mesh with the size of 10-20 μm is created in the densified mesh region around the substrate to cover the coating area around the cylindrical substrate. The vertical and horizontal cross section of grid with densified mesh layers around the cylindrical substrate is shown in Figure 4-9.
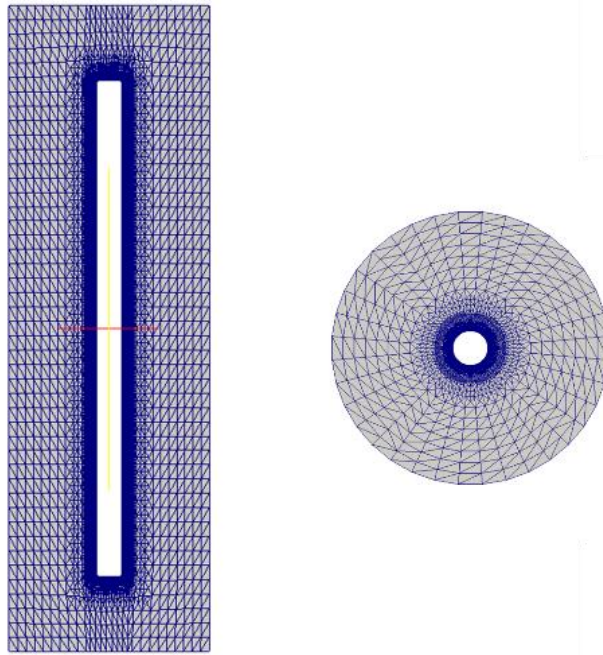
Figure 4-9: Vertical and horizontal cross section of the grid

The mesh density is required to be sufficiently high and with a small cell size, in order to capture all the flow features and coating film thickness. Mesh sensitivity analysis is performed to investigate the grid size effect on the coating thickness results. Three different mesh densities applied in the simulation are shown in Table 4-1.

Table 4-1: Number of cells used for the three different grid sizes

Grid type and size	Fine	Medium	Coarse
	1,430,780 elements	927,696 elements	422,078 elements

The simulation run on the coarse mesh gave a coating thickness estimate below the experimental values with a 38% difference. The coarse grid size makes it difficult to see a clear interface between the two phases, and inaccurate results achieved from coating thickness estimations.

The fine meshing showed a clear distinction between the liquid and air phases in the coating region and the coating thickness prediction was in good agreement with the

112

experimental data shown in section 4.6. However, the computational time was significantly increased and using the fine mesh was not feasible due to time constraints. For instance, running the simulation of finite length cylinder with the withdrawal speed of 0.1 m/s and volume fraction of 0.4 on a coarse mesh took 7 hrs on a 2 dual core processor computer. The processor is an Intel ® Xenon® with 16 CPU-E5520 2.27 GHz using the 64-bit Ubuntu operating system with 12 GB RAM. The same case with the medium size grid took 82 hrs and using the fine size grid the computational time increases to 265 hrs. These computational times vary based on the different withdrawal velocity and particle concentration in the system. Increasing the withdrawal speed or volume fraction of particles decreases the processing and computational time for a simulation.

The coating thickness for the withdrawal velocity of 0.1 m/s and particle concentration of 0.4 for the coarse mesh is 375 μm, for the medium grid size the film thickness prediction is 600 μm and for the fine grid the coating thickness prediction is 615 μm. The reason for the smaller estimate for coating thickness using the coarse mesh, is the thick layer of interface around the cylinder while using the finer mesh size there is a commensurate decrease in the interface layer around the substrate. In addition, the variables such as the pressure and velocity residuals are set to be $< 10^{-8}$, which changes the number of iterations for solving each matrix and the simulation time.

Thus the medium size grid is applied to provide satisfactory flow description for the film thickness prediction. The medium grid size is used throughout this study to minimize the long computational time imposed by the fine grid size, but achieving an acceptable solution. Similar to the fine mesh results, the coating thickness results with medium grid size were in a good agreement with experimental data. Prediction of coating thickness with medium grid size was 2.5% less than the fine mesh results, which is an acceptable range in this study.

This percentage of error is equal to a 10-15 μm difference in the coating thickness , which is comparable to the errors in the experimental measurements.

The substrate used in the coating process is a finite length cylinder in a semi-immersed initial condition in the bath. Withdrawing the finite length substrate from the coating liquid requires application of the dynamic mesh utility in the simulation, where the background mesh follows the moving substrate to capture the coating liquid around the substrate. In this study, applying the dynamic mesh in the simulations moves the grid with the withdrawal speed in the same direction as removal. Mesh elements remain unchanged and the motion of the substrate boundary points is specified.

4.4.4 « Boundary Conditions »

Boundary conditions need to be specified following the discretization of the simulation domain. Boundary conditions are defined for boundaries of coating bath and the cylindrical substrate as shown in Figure 4-10. In the simulations, boundaries are set as: wall of coating vessel, base of coating vessel, coating bath top and substrate. For each boundary the corresponding conditions for pressure, velocity, volume faction of α_1 for interface and volume fraction of φ for the particles are defined.
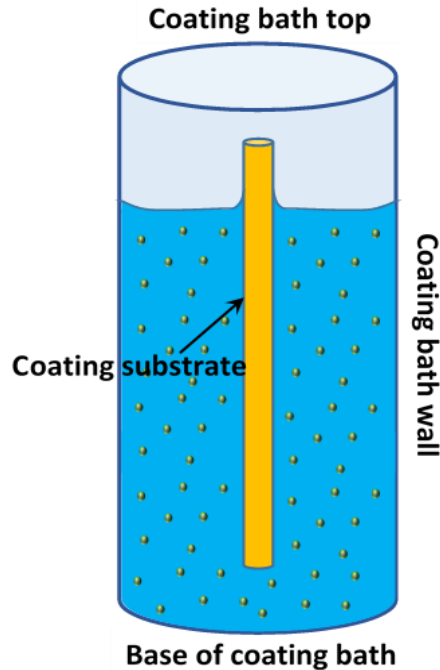
Figure 4-10: Boundaries in the simulation process

a. Wall of coating bath

The zero gradient is set for pressure and volume fraction of particles φ on the coating container wall. The zero gradient for volume fraction of liquid, α_1 with a constant value for contact angle and zero value for velocity are fixed for this boundary.

b. Base of coating bath

The symmetry plane boundary has been set for velocity, pressure and volume fraction of α_1 and the volume fraction of φ. In OpenFOAM (www.openfoam.org, 2013), there is a difference between the symmetry boundary condition and the zero gradient condition. A symmetry plane condition inserts the same values for scalars but for vectors all components parallel to the patch are mirrored whereas the normal components of vectors are set to zero while a zero gradient condition sets the boundary value to the near-wall cell value.

c. Coating bath top

The coating vessel top is the upper part of the simulation domain, which contains the gas phase and is open to the atmosphere. The corresponding boundary condition for the region is total pressure condition with the value of zero. Total pressure boundary condition is defined as $P = P_0 + \frac{1}{2}\rho|u|^2$ where P_0 is the atmospheric pressure and when u changes, P is adjusted accordingly. Pressure-inlet-outlet-velocity (www.openfoam.org, 2013), is the velocity boundary condition, applied for this region and it can be employed, where the pressure is specified and reverse flow is possible or expected. In the inward flow situation, the inflow velocity is set as a zero value and zero gradient velocity condition is applied for the outflow. For the volume fraction of liquid at the interface, α_1, the inlet-outlet boundary condition (www.openfoam.org, 2013) is set. This boundary condition switches u and P between fixed value and zero gradient, depending on the direction of velocity. Having the outflow situation, this boundary condition applies zero gradient for velocity. Besides, in the inflow conditions due to the return flow, this boundary condition sets velocity to a specified value which has been set to zero in this study. The inlet-outlet boundary is set for φ, volume fraction of particles as well.

d. Coating substrate

Boundary for cylindrical substrate is considered with the withdrawal speed condition for velocity, zero gradient for pressure, α_1 and φ.

4.5 « Experimental Validation »

4.5.1 « Preparation of Suspensions »

Food grade mineral oil (FG WO 35 White Mineral Oil, Petro-Canada) is selected as the medium with spherical polystyrene particles (Powder buy the pound). The average radius of the particles is $60 \pm 3\ \mu m$ with minimum of 99.0% in the target size range, which was considered large enough to avoid Brownian motions, yet small enough to keep the homogeneity of suspension and avoid the dispersion segregation during the tests.

Polystyrene particle density is $1050 \ kg/m^3$. Using the Stoke's equation, the settlement time can be estimated for the polystyrene/mineral oil dispersions assuming spherical particles.

$$V = \frac{2}{9} \frac{(\rho_p - \rho)}{\eta_s} g a^2 \qquad\qquad (4-13)$$

Introducing the values for ρ_p as the particle density and ρ as the density of suspending medium, and η_s for the viscosity of suspending medium, the settlement velocity is estimate as $V = 4 \times 10^{-5} \ m/s$. The settling velocity of particles is small compared to the processing time for depositing a coating layer on a substrate with length of 6.5 cm and withdrawal velocities of 5, 10 and 15 cm/s.

4.5.2 « Rheological Tests »

Four different samples of monomodal polystyrene particles in mineral oil were prepared with particle volume fractions of 0.1, 0.2, 0.3 and 0.4. Rheological tests were conducted using the TA 1500ex stress-controlled rheometer with a Couette tool. Concentric cylinder geometries for Couette tool, include a standard cup radius of 15 mm configured with a rotor of radius 14 mm and height of 42 mm.

Before each measurement, the dispersion solution is completely stirred with a glass rod. Measurements for each sample are repeated three times to ensure the accuracy of the rheological quantifications. All rheological measurements are conducted at $22°C$. The rheological data are presented in the range of 0.1-$1000 \ s^{-1}$ for dispersion samples of polystyrene particles in mineral oil. For the rheological tests, 10 measurement points considered in each decade (log scale) with allocating 2 seconds for each measurement point. Measured rheological data for various volume fractions of polystyrene particles in mineral oil is presented in Figure 4-11.
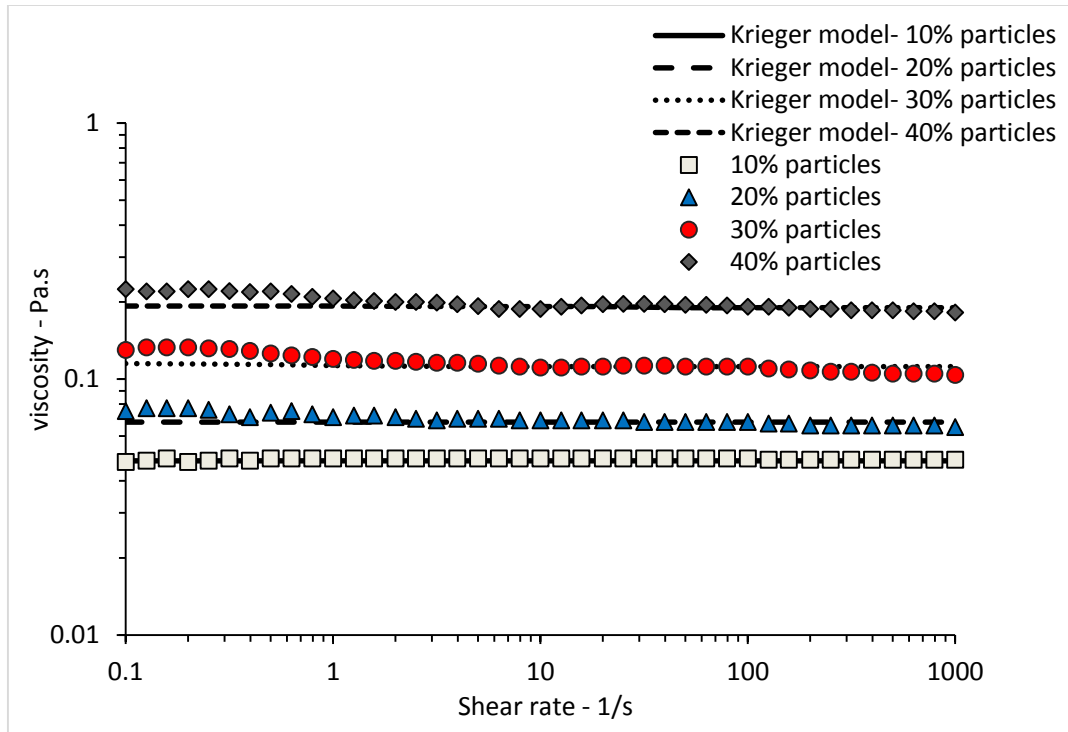
Figure 4-11: Rheological data of polystyrene particles in mineral oil

Based on the rheological measurements and fitting the parameters of equation 4-8 with the experimental data of viscosity, the value for the parameter n is this equation estimated to be 1.86 for these suspensions.

The value for n in this study is close to the value of 1.82 used by Phillips et al. (1992) and the value of 2 for n applied by Maron and Pierce (1956).

The viscosity of mineral oil is determined using a capillary viscometer (Cannon-Fensk Routine, Technical Glass Products) and the surface tension values extracted from the literature, are presented in Table 4-1 (Middleman, 1978; Blake and Shikhmurzaev, 2002).

Table 4-2: Physical properties of mineral oil

Mineral oil	Surface tension, N/m	Viscosity, $Pa.s$	Density, kg/m^3
	0.0285	0.036	875

These values applied in the related viscosity, stress tensor and free surface calculation codes in OpenFOAM.

4.5.3 « Contact Angle Tests »

The contact angle must be applied in the numerical calculations as a semi-immersed substrate used in the study of dip coating process and fluid contact angle to the coating bath wall must be considered. Images from the contact angle during the experimental coating measurements reveals the contact angle remains relatively unchanged while the substrate is being withdrawn and coating liquid level declines gradually in the coating bath. In the current study, a finite length cylinder was withdrawn from the coating vessel and consequently the liquid level drop in the vessel was fairly small.

The static contact angle (θ) between the fluid and an acrylic surface and fluid with brass cylindrical substrate was measured with a contact angle goniometer (Rame-hart model 100) of 17º for brass/mineral oil and 11º for acrylic/mineral oil.

4.5.4 « Coating Thickness »

Coated film thickness is measured at the time the substrate is completely out of the coating vessel. Images are captured using a high speed, high resolution camera, adjusted to capture 25 frames per second (IO industries camera model Flare 4M180-CL with resolution of 2048x2048 pixels).

The camera is positioned at 3, 7 and 10 cm above the bath surface, perpendicular to the cylindrical substrate. A black sheet of paper was placed in the background and light sources provided around the coated film, which helped to ensure a clear view of the deposited film. Film thickness images have been captured by repeating the thickness measurements for eight different images captured for each velocity and individual suspension. Coating images have been captured without taking the parallax effect into account and precision of the measurements for coating layer on the substrate is estimated

to be within ± 10 μm over most of the range based on the coating layer interface thickness with surrounding space. The error in the thickness measurement is estimated magnifying the coating images and measuring the blurred line at the end of coating layer (where the pixels of the image can be seen in a lighter color). Thus, these pixels are considered as the error in the coating thickness.

Different withdrawal velocities were investigated up to 15 cm/s. An acrylic tube with a diameter of 2.54 cm is used as the coating bath in the system to provide the clear view of particles homogeneity in the bath during the experiments. The cylindrical substrate used in this work has a radius of 1590 μm, chosen based on the radius to be small enough for considering the substrate curvature in the same order of magnitude as the coating film thickness and yet large enough to be able to capture the deposited film thickness in a photograph. The radius of bath to the substrate radius ratio is 8 for this study and for this R/r ratio there are bath wall proximity effects on the coating thickness based on the results of chapter 3.

4.6   « Results and Discussion »

For various suspensions prepared with a Newtonian carrier fluid, mineral oil, the simulation and experimental investigations have been performed and coating film thickness was selected as the quantifiable parameter for this investigation.

The particle concentration at every point in the flow domain needs to be calculated, because the viscosity is estimated based on the volume fraction of particles at each point and these viscosity values are applied in the Navier-Stokes equation, which affects the velocity and pressure in the system and the coating layer thickness.

The coating thickness is presented along the substrate length after withdrawal from the coating bath as shown in Figure 4-12. This figure represents the total substrate length which is considered as 6.5 cm and coating thickness measured every 0.5 cm along the cylindrical substrate. The cross section of the coated substrate is shown in Figure 4-12 and the coating thickness measurement along the substrate has been done based on the

order of points along the substrate that are being withdrawn out of the coating bath. Thus, the upper part of substrate is withdrawn first from the bath signed as 0 cm and lower part of substrate indicates point 6.5 cm, as it is shown in Figure 4-12.

The upper part of the cylinder associate with the point 0 cm and lower part of the substrate refers to the point at 6.5 cm.
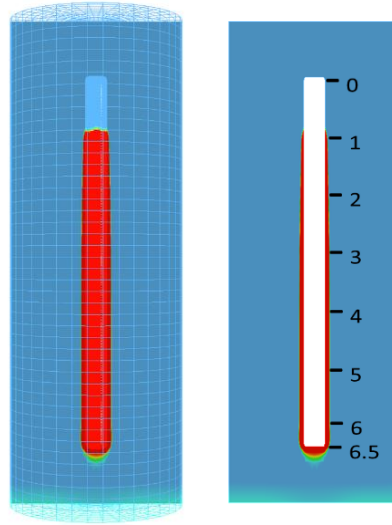

Figure 4-12: The coating thickness is displayed along the substrate length withdrawn from coating bath, the simulation results with associated positions on the cylinder

The experimental and simulated coating film thickness are measured for mineral oil and suspensions with 10, 20, 30 and 40 vol% of polystyrene particles as presented in the Figures 4-13, 4-14 and 4-15 at three different withdrawal speeds. The coating thickness results for mineral oil suspensions at 5, 10 and 15 cm/s are shown in Figures 4-13 to 4-15 respectively, with increasing coating thickness as withdrawal speed and suspension concentration increase. In all coating thickness measurements for suspensions, the substrate radius is 1590 μm and the coating bath diameter is 2.54 cm.

The measurements of coating thickness were done when the total substrate length was out of the coating bath and the lower part of substrate was above the coating bath surface.

A uniform coating layer is observed over most of the substrate and the maximum coating thickness is observed in the lower part of the substrate. During the withdrawal process the coating thickness at the upper part of the substrate gradually thins due to gravity effects.
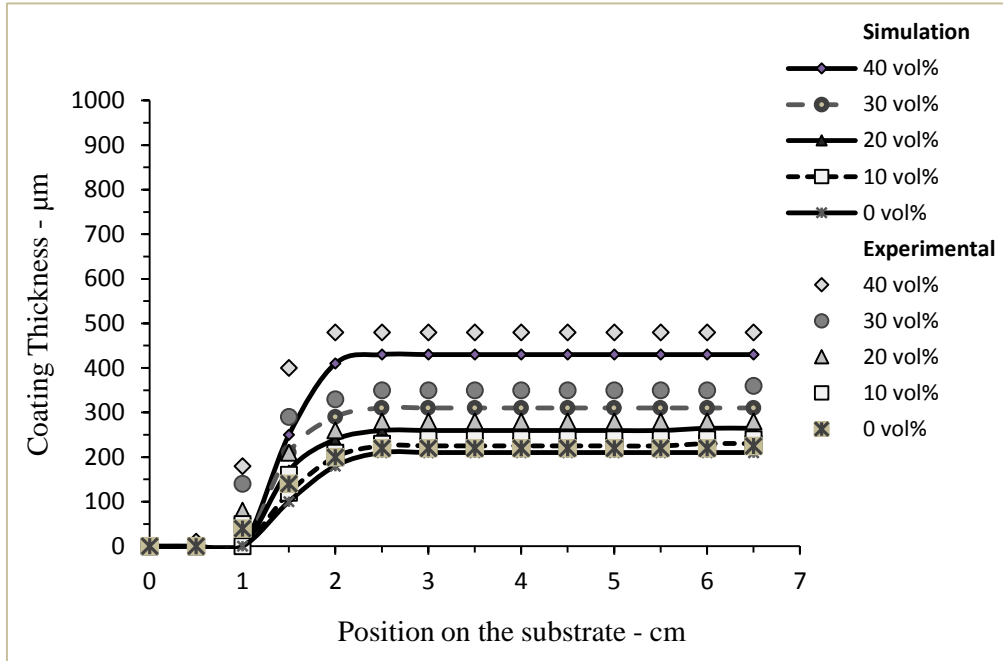

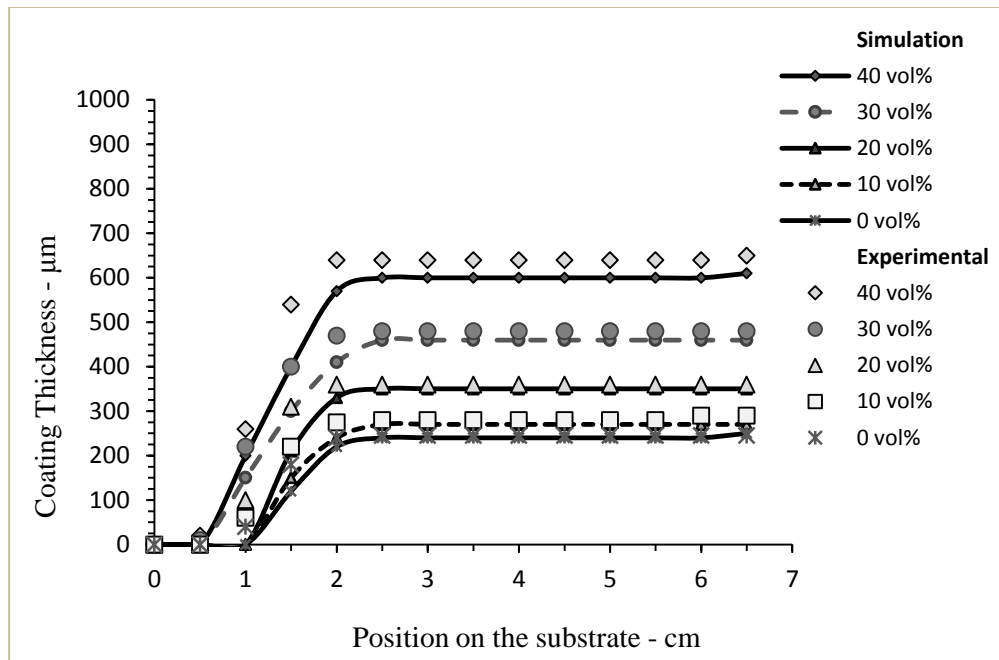**Figure 4-13:** Coating film thickness at speed of 0.05 m/s for mineral oil suspensions

Figure 4-14: Coating film thickness at speed of $0.1\ m/s$ for mineral oil suspensions
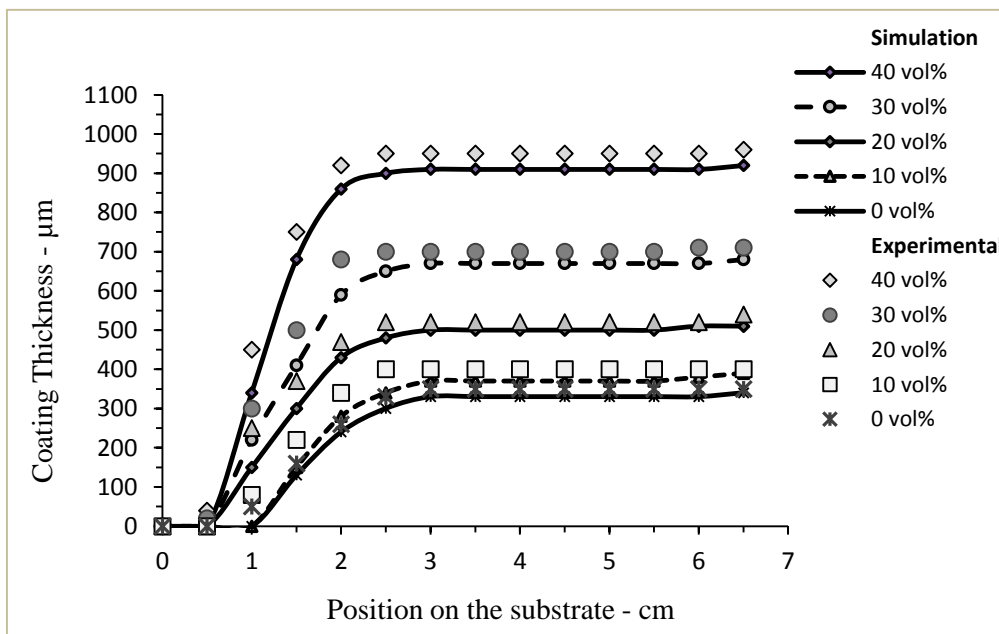

Figure 4-15: Coating film thickness at speed of $0.15\ m/s$ for mineral oil suspensions

The experimental data reflects slightly higher values for the coating layer thickness in comparison with the simulation results. The highest coating thickness can be achieved at a withdrawal velocity of 0.15 m/s for every particular concentration of rigid particles in the coating fluid, which was the maximum speed for the experimental data in this work. The coating layer thickness increases with the solid particle concentration due to higher viscosity.

Furthermore, parametric studies were done to understand the performance of the simulation for higher capillary numbers. The dimensionless capillary number is defined as $Ca = \eta u/\sigma$ plays an important role in dip coating processes. The results for the capillary number effects are displayed in Figure 4-16(a, b, c and d). Increasing the capillary number can be associated with high withdrawal speed or high viscosity of coating fluid increasing the film thickness.

In Figure 4-16 the coating thickness starts from position 1 on the substrate at the capillary numbers less than 0.22, and by increasing the capillary number the gravity effect decrease in the coating process. Thus, for capillary numbers greater than 0.22, the coating layer starts from position 0.5 on the substrate and a uniform layer of coating can be achieved. Figure 4-16(a), represents the capillary numbers effect for the suspensions with 0.1 volume fraction of particles and coating thickness is thinning on the upper part of cylinder at three Ca values of 0.07, 0.15 and 0.22.

As shown in Figure 4-16(b), increasing the volume fraction of particles in the suspension to 0.2, decreases the thinning effect and for two values the Ca of 0.1 and 0.21, the thinning of coating layer occurs at the upper region of substrate. Higher values of Ca can be seen in Figure 4-16(c) and 4-16(d), the coating layer covers the specified length of the substrate and the desired area can be coated by the fluid.
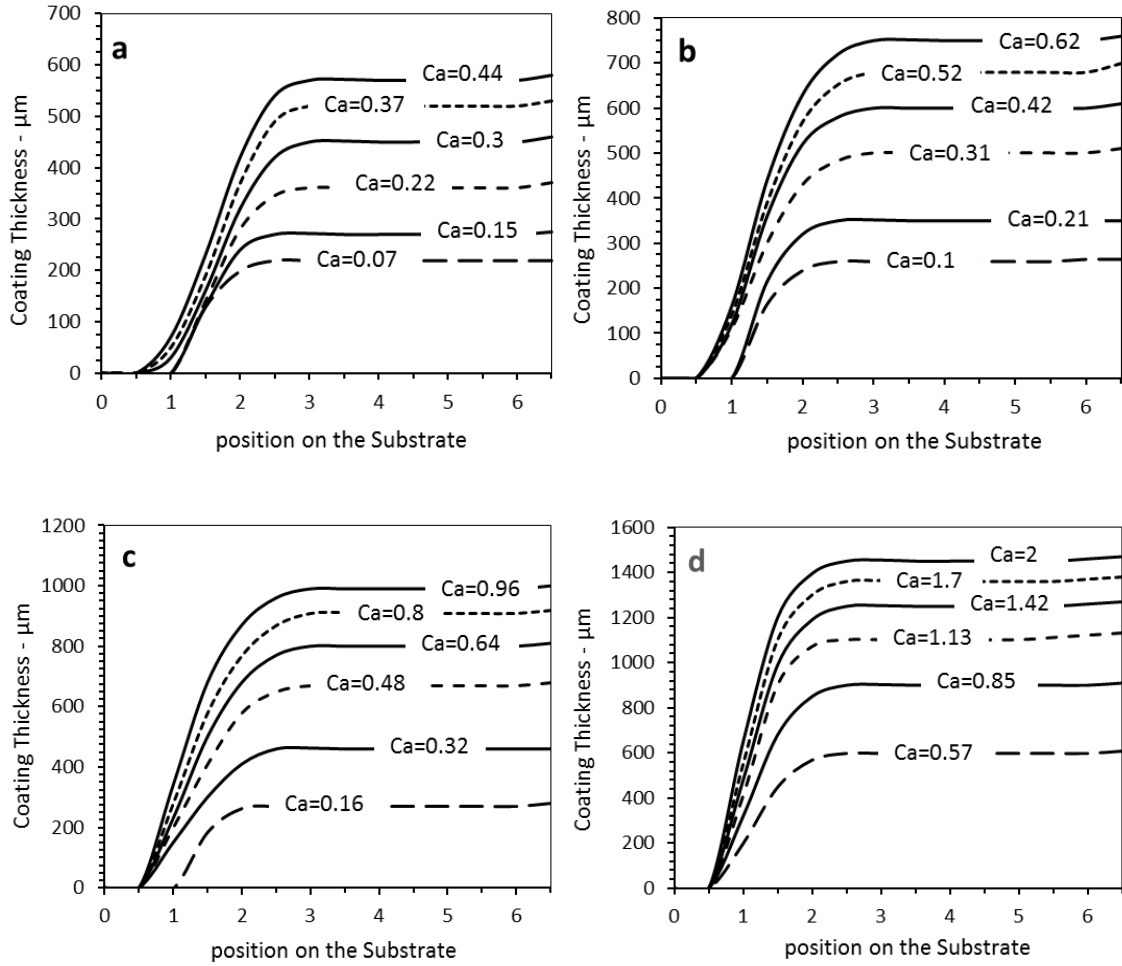
Figure 4-16: Coating profile along the substrate length applying the suspensions with volume fraction of particles 0.1, 0.2, 0.3, and 0.4 shown in a, b, c and d respectively

4.7 « Conclusion »

Dip coating process for a finite length substrate is investigated in this study through simulation and experiment. The simulation results of coating film thickness are validated with the corresponding experimental data for mineral oil suspensions. The solid particles concentration in the coating fluid considered in the range of 10-40% vol, and the coating thickness increases with enhancing the particle volume fraction in the suspension and withdrawal velocity. By increasing the capillary number coating film thinning effects of fluid can be reduced.

125

4.8 « References »

Abbott J. R., Tetlow N., Graham A. L., Altobelli S. A., Fukushima E., Mondy L. A., Stephens T. A., Experimental observations of particle migration in concentrated suspensions: Couette flow, Journal of Rheology, Vol. 35, pp. 773, 1991

Arp P. A., Mason S. G., The kinetics of flowing dispersions, Doublets of rigid spheres (experimental), Journal of Colloid and Interface Science, Vol. 61, pp. 44, 1977

Ashmore J., Shen A. Q., Kavehpour H. P., Stone H. A., McKinley G. H., Coating flows of non-Newtonian fluids: Weakly and Strongly Elastic Limits, Kluwer Academic Publishers, Netherlands, 2007

Averbakh A., Shauly A., Nir A., Semiat R., Slow viscous flows of highly concentrasions, Part 1: Laser-doppler velocimetry in rectangular ducts, International Journal of Multiphase Flow, Vol. 23, pp. 409, 1997

Bird R. B., Armstrong R. C., Hassager O., Dynamics of polymeric liquids, Wiley, New York, Vol. 1, 1987

Blake T. D., Shikhmurzaev Y. D., Dynamic wetting by liquids of different viscosity, Journal of Colloid and Interface Science, Vol. 253, pp. 196, 2002

Brackbill J. U., Kothe D. B., Zemach C., A continuum method for modeling surface tension, Journal of Computational Physics, Vol. 100, pp. 335, 1992

Brad J. F., Bossis G., Stokesian dynamics, Annual Review of Fluid Mechanics, Vol. 20, pp. 111, 1998

Buyevich I. A., Particle distribution in suspension shear flow, Chemical Engineering Science, Vol. 51, pp. 635, 1996

Cho Y. I., Kensey K. R., Effects of the non-Newtonian viscosity of blood on flows in a diseased arterial vessel: part 1: steady flows, Biorheology, Vol. 28, pp. 241, 1991

Colosqui C. E., Morris J. F., Stone H. A., Hydrodynamically driven colloidal assembly in Dip Coating, Physical Review Letters, Vol. 110, pp. 188302-1, 2013

Fang Z., Phan-Thien N., Numerical simulation of particle migration in concentrated suspensions by a finite volume method, Journal of Non-Newtonian Fluid Mechanics, Vol. 58, pp. 67, 1995

Gadala-Maria F., Acrivos A., Shear-induced structure in a concentrated suspension of solid spheres, Journal of Rheology, Vol. 24, pp. 799, 1980

Guttfinger C., Tallmadge J. A., Films of non-Newtonian fluids adhering to flat plates, American Institute of Chemical Engineering Journal, Vol. 11, pp. 403, 1965

Hirt C., Nicholls B., Volume of Fluid (VOF) method for dynamics of free boundaries, Journal of Computational Physics, Vol. 39, pp. 201, 1981

Karnis A., Goldsmith H. L., Mason S. G., Journal of Colloid Interface Science, Vol. 23, pp. 531, 1966

Kistler S. F., Schweizer P. M., Liquid film coating. Chapman and Hill, London, 1997

Krieger I. M., Rheology of monodisperse lattices, Advances in Colloid and Interface Science, Vol. 3, pp. 111, 1972

Ladd A. J., Numerical simulation of particulate suspensions via a discretized Boltzmann equation, Journal of Fluid Mechanics, Part 1, Vol. 271, pp. 285, 1994

Landau L., Levich B., Dragging of a liquid by a moving plate, Acta physicochem. URSS, Vol. 17, pp. 42, 1942

Leighton D., Acrivos A., Viscous resuspension, Chemical Engineering Science, Vol. 41, pp. 1377, 1986

Leighton D., Acrivos A., Measurement of shear-induced self-diffusion in concentrated suspension of spheres, Journal of Fluid Mechanics, Vol. 177, pp. 109, 1987

Leighton D., Acrivos A., The shear-induced migration of particles in concentrated suspensions, Journal of Fluid Mechanics, Vol. 181, pp. 415, 1987

Leighton D., NASA Conf. Proc. 3006, 109, 1988

Leshansky A. M., Brady J. F., Dynamic structure factor study of diffusion in strongly sheared suspensions, Journal of Fluid Mechanics, Vol. 527, pp. 141, 2005

Lyon M. K., Leal L. G., An experimental study of the motion of concentrated suspensions in two dimensional channel flow, part 1, monodisperse systems, Journal of Fluid Mechanics, Vol. 363, pp. 25, 1998

Marchiaro M., Acrivos A., Shear-induced particle diffusivities from numerical Simulations, Journal of Fluid Mechanics, Vol. 443, pp. 101, 2001

Maron S. H., Pierce P. E., Application of Ree-Eyring generalized flow theory to suspensions of spherical particles. Journal of Colloid Science. Vol. 11, pp. 80, 1956

McTigue D. F., Jenkins J. T., Channel flow of a concentrated suspension, In Advances in Micromechanics of Granular Materials, Shen H. H., Satake M., Mehrabadi M., Chang C. S., Campbell C. S. (eds). Elsevier, Amsterdam, 1992

Mewis J., Wagner N. J., Colloidal Suspension Rheology, Cambridge University Press, New York, 2012

Middleman S., High speed wire coating from a bath of viscoelastic liquids, Polymer Engineering Science, Vol. 18, pp. 335, 1978

Mukhopadhyay S., Usha R., Tulapurkara E. G., Numerical study of concentrated fluid–particle suspension flow in a wavy channel, International Journal for Numerical Methods in Fluids, Vol. 59, pp. 1125, 2009

White D. A., Tallmadge J. A., A gravity corrected theory for cylinder withdrawal, American Institute of Chemical Engineering Journal, Vol. 13, pp. 745, 1967

Perktold K., Resch M., Florian H., Pulsatile non-Newtonian flow characteristics in a three-dimensional human carotidartery bifurcation model, Journal of Biomechanical Engineering-Transactions of the ASME, Vol. 113, pp. 464, 1991

Phillips R. J., Armstrong R. C., Brown R. A., Graham A. L., Abbott J. R. A constitutive equation for concentrated suspension that accounts for shear-induced particle migration, Physics of Fluids A, Vol. 4, pp. 30, 1992

Ritz J. B., Caltagirone J. P., A numerical continuous model for hydrodynamics of the fluid particle systems, International Journal of Numerical Methods in Fluids, 1999

Ritz J. B., Bertrand F., Thibault F., Tanguy P. A., Shear-induced particle migration in a short-dwell coater, Chemical Engineering Science, Vol. 55, pp. 4857, 2000

Ro J. S., Homsy G. M., Viscoelastic free surface flows: thin film hydrodynamics of Hele-Shaw and dip coating flows, Journal of Non-Newtonian Fluid Mechanics, Vol. 57, pp. 203, 1995

Rusche H., Computational fluid dynamics of dispersed two phase flows at high phase fractions, Ph.D. thesis, University of London, 2002

Sierou A., Brady J. F., Shear-induced self-diffusion in non-colloidal suspensions, Journal of Fluid Mechanics, Vol. 506, pp. 285, 2004

Spiers R. P., Subbaraman C. V., Wilkinson W. L., Free coating of non-Newtonian liquids onto a vertical surface, Chemical Engineering Science, Vol. 30, pp. 379, 1975

The OpenFOAM® Foundation (www.OpenFOAM.org)

Ubbink O., Issa R. I., A method for capturing sharp fluid interfaces on arbitrary meshes, Journal of Computational Physics, Vol. 153, pp. 26, 1999

Bird R. B., Armstrong R. C., Hassager O., Dynamics of polymeric liquids, Wiley, New York, Vol. 1, 1987

Chapter 5

5 « Conclusions and Recommendations »

In this Chapter the main conclusions of this study are presented; also some recommendations for future work are suggested.

5.1 « Conclusions »

In the current study of dip coating process, a new theory for free coating of cylindrical substrates by withdrawal from a bath of an Ellis fluid has been developed. The developed mathematical model using the Ellis constitutive equation is an extension of previous works for Generalized Newtonian fluids. Good agreement between the theory developed in this study and experimental data, indicates significant role that low shear rates and consequently high value viscosities play in dip coating systems.

OpenFOAM was used for the numerical solution for two phase flow (liquid and gas) in dip coating, which provides significantly better estimation of the coated film thickness compared to analytical models over a wide range of withdrawal velocities up to $6\ m/s$. The simulation results validated for Ca number up to 1.1 for Newtonian fluids and for Ca number up to 60 for non-Newtonian fluids (viscosity of 1 sec-1).

In the numerical simulations for dip coating process at higher withdrawal speeds, three constitutive equations (Newtonian, power-law, Carreau) have been considered for numerical solution of both Newtonian and non-Newtonian fluids and compared to experimental data in the literature, where good agreement is found between the experimental data and the simulation results.

The coating film thickness depends on the coating bath dimension. Based on experimental and simulation results, the wall effect needs to be considered as an extra factor when R/r is less than a plateau value (30 for substrate with radius of 785 μm and 25 for substrate with radius of 1590 μm) and this value decreases with increasing

cylindrical substrate radius. For both Newtonian and non-Newtonian fluids, the final film thickness increases with raising the ratio of R/r, before achieving a plateau.

The results for the substrate with the radius of 785 μm, demonstrates for R/r less than 30, wall effects need to be considered in the coating process and for $R/r > 30$ a plateau coating thickness is reached for film thickness values at constant withdrawal velocity. Similarly, for a substrate radius of 1590 μm, coating thickness increases with increasing R/r up to approximately 25.

In addition, dip coating process for a finite length substrate investigated in the present study to provide the opportunity for assessing the dip coating process in the unsteady-state condition through the simulation and experimental procedures. The simulation results of coating film thickness validate with the corresponding experimental data for mineral oil suspensions. The solid particles concentration in the coating fluid considered in the range of 10-40 vol%, and the coating thickness increases with enhancing the particle volume fraction in the suspension. Results indicate by increasing the capillary number coating film thinning effects of fluid can be reduced.

5.2 « Recommendations »

From the experience obtained after the completion of this thesis the following suggestions are done for future work:

- Most fluids that are being used in the dip coating process reveal non-Newtonian behavior and viscoelastic proprieties are part of the characteristics of these fluids. Applying the viscoelastic characteristic of the coating liquid in the calculation of dip coating can help to have more precise prediction of the hydrodynamics of this coating process which can be done by developing and implementing the viscoelastic models in the OpenFOAM libraries.

- The capability of handling multiphase simulations in OpenFOAM provides a chance to study the multilayer coating processes through the numerical

calculation. In some industrial coating processes, applying multilayer coating is common and the investigation through the numerical simulation can be an approach to understand the fundamentals of these systems as well as troubleshooting of the processes.

- These days tailored coating is a popular method of advanced material production by dip coating and understanding the individual particles behavior in the system facilitates the design and control of the production process for these assemblies. For the study of individual particles interaction in the fluid and investigation on dilute suspensions computational fluid dynamic methods can be merged with discrete element method calculation and CFDEM platform can be used for the numerical estimations and new algorithms development for the cases.

- The developed algorithm for concentrated suspensions with free surface can be used for the simulation of other industrial processes.

- There is an opportunity to study the dip coating process using various geometries as coating substrates, that is provided by the OpenFOAM meshing utilities and better control of coating deposition on the complicated substrates can be achieved by the prediction of coating liquid behavior in the system.

Curriculum Vitae

Name:	**Mahyar Javidi**
Post-secondary Education and Degrees:	Sharif University of Technology Tehran, Iran 2002-2006 B.Sc. Sharif University of Technology Tehran, Iran 2007-2009 M.Sc. The University of Western Ontario London, Ontario, Canada 2010-2015 Ph.D.
Honours and Awards:	Western Graduate Research Scholarship (WGRS) 2010-2015 Ranked 7th in Gas & Petroleum Engineering National Exam Iran, University Entrance Exam 2007 M.Sc. Ranked 33th in Chemical Engineering National Exam Iran, University Entrance Exam 2007 M.Sc. Ranked within the top 0.1% of participants National Exam Iran, University Entrance Exam 2007 M.Sc.
Related Work Experience	Teaching Assistant The University of Western Ontario 2010-2014

Publications:
M. Javidi, A. N. Hrymak, Numerical simulation of the dip coating process with wall effects on the coating film thickness, Journal of Coatings Technology and Research, Vol. 12, Issue 5, pp 843-853, 2015

Conference Proceedings: (presenter underlined)
M. Javidi, A. N. Hrymak, Simulation of concentrated suspension in free surface processes, AICHE, Salt Lake City, USA, 2015

M. Javidi, A. N. Hrymak, Simulation of concentrated suspension in thin film processes, CICHE, Calgary, CA, 2015

M. Javidi, A. N. Hrymak, Numerical simulation of three dimensional free coating process with wall effect study, ISCST, San Diego, USA, 2014

M. Javidi, A. N. Hrymak, Simulation of dip coating process with OpenFOAM software, ECS, Mons, Belgium, 2013

M. Javidi, A. N. Hrymak, Withdrawal of a cylinder from an Ellis fluid, ISCST, Atlanta, USA, 2012

M. Javidi, A. N. Hrymak, Modeling of free-withdrawal coating with UV curing TiO2 filled resins, PPS, Marrakech, Morocco, 2011